LINKING HYDRODYNAMIC AND BIOLOGICAL PROCESSES IN A SHALLOW AND MICRO TIDAL ESTUARY: THE CASE OF FANGAR BAY (EBRO DELTA)

by

Marta Balsells Fdez.-Pedrera

Tesis Doctoral por compendio de publicaciones

Barcelona, 2021

DOCTORADO EN OCEANOGRAFIA

VINCULACIÓN DE LOS PROCESOS HIDRODINÁMICOS Y BIOLÓGICOS EN UN ESTUARIO SOMERO Y MICROMAREAL: EL CASO DE LA BAHÍA DE FANGAR (DELTA DEL EBRO).

Doctoral thesis by compendium of publications presented by Marta Balsells F-Pedrera to opt for the title of doctor by the Catalonia University of Technology (UPC). The thesis has been carried out at the Department of Hydraulic, Maritime and Environmental Engineering, within the PhD programme in Marine Sciences.

DIRECTORES:

Manuel Espino

Manel Grifoll

Approved by _____

Chairperson of Supervisory Committee

_____

Barcelona, 2021

A la meva mare…ja som doctores marona!

A mi marido, por recorrer conmigo el último y más difícil tramo.

"Venid a Mí los que estáis cansados y agobiados, y Yo os aliviaré"

Mt 11,25-30

ABSTRACT

This thesis analyses the relationships between hydrodynamics (and their forcings) and biological variables in Fangar Bay based on *in situ* observations, numerical models, and satellite data. Fangar Bay is a relatively small, shallow, microtidal bay and is of vital importance for the biodiversity of the region and the local economy as it is the site of both aquaculture and nautical leisure activities.

From a hydrodynamic point of view, Fangar Bay is predominantly influenced by wind and freshwater flows, presenting problems of water renewal, as well as high temperatures in summer that affect the bivalve cultures present in the bay. To analyse the hydrodynamics, the ROMS (Regional Ocean Modeling System) numerical model and measurements from two field campaigns were used to obtain data on currents, sea level, wind, salinity, and temperature in the water column. During calm periods, the observed currents show a complex water circulation in the inner part of the estuary due to its shallow depth and a positive estuarine circulation at the estuary mouth. Numerical experiments have investigated the local wind-induced water circulation. For intense wind conditions in the bay, an axially symmetric transverse structure is produced with outflow in the central channel axis and inflow in the shallow lateral zones. These numerical results explain the water circulation observed during wind episodes where the water column tends to homogenise rapidly.

The effect of wind on the evolution of surface Chlorophyll *a* (Chl *a*) concentration was then investigated with field data and satellite images. The analysis revealed that strong wind events from both NW (off-shore, up-wind)

and SE-E (on-shore, down-wind) cause an increase in the surface Chl *a* concentration. The mechanisms responsible are horizontal dispersion of nutrients from freshwater channels and vertical mixing (also linked to stratification breakdown) that presumably resuspends Chl *a* and/or incorporates nutrients throughout the water column. On the other hand, the breeze is not able to break the stratification, so Chl *a* concentration does not change significantly during these episodes. In conclusion, the mixing produced by the strong winds favours an accumulation of Chl *a* in the bay while the stratification associated with the estuarine circulation tends to reduce this accumulation.

To complete the observational analysis of the primary production distribution in the bay, numerical simulations have been carried out with a NPZD numerical model coupled to ROMS. The numerical results show that wind has a major effect on the distribution of nutrients from the discharge channels and consequently on the distribution of phytoplankton within the bay. Idealised simulations show that phytoplankton biomass tend to redistribute throughout the water column (due to broken stratification) when strong NW and E-SE winds blow.

Although the results of this thesis have allowed a deeper understanding of the relationship between hydrodynamic and biological processes, there are still aspects that need to be explored, such as the effect of bottom resuspension or the relationship between processes at different time scales. The implementation of more complex numerical models, analysis of high-resolution satellite images, and more intensive data acquisition campaigns in space and time can be a starting point for future studies.

RESUMEN

Esta tesis analiza las relaciones entre la hidrodinámica (y sus forzamientos) y variables biológicas en la bahía del Fangar a partir de observaciones *in situ*, modelos numéricos y datos satélite. La bahía del Fangar es una bahía relativamente pequeña, somera y micro mareal y es de vital importancia para la biodiversidad de la región y la economía local ya que en ella se practican tanto actividades de acuicultura como de ocio náutico.

Desde un punto de vista hidrodinámico, la bahía del Fangar está predominantemente influenciada por el viento y los flujos de agua dulce presentando problemas de renovación del agua, así como altas temperaturas en verano que llegan a afectar a los cultivos de bivalvos presentes en ella. Para analizar la hidrodinámica se ha utilizado el modelo numérico ROMS (Regional Ocean Modeling System) y medidas de dos campañas de campo donde se obtuvieron datos de corrientes, nivel del mar, viento y salinidad y temperatura en la columna del agua. Durante los períodos de calma, las corrientes observadas muestran una circulación de agua compleja en la parte interior del estuario debido a su poca profundidad y una circulación estuárica positiva en la bocana. Los experimentos numéricos realizados han permitido investigar la circulación de agua inducida por el viento local. Para condiciones intensas de viento en la bahía, se produce una estructura transversal axialmente simétrica con flujo de salida en el eje del canal central y entrada en las zonas laterales poco profundas. Estos resultados numéricos explican la circulación de agua observada durante episodios de viento donde la columna de agua tiende a homogeneizarse rápidamente.

Posteriormente se investigó el efecto del viento en la evolución de la concentración de Clorofila *a* (Chl *a*) en superficie con datos de campo e imágenes satélite. El análisis reveló que episodios de viento intensos tanto del NW (*off-shore, up-wind*) como SE-E (*on-shore, down-wind*) provoca un aumento en la concentración de Chl *a* superficial. Los mecanismos responsables son la dispersión horizontal de nutrientes proveniente de los canales de agua dulce y la mezcla vertical (también vinculada a la rotura de la estratificación) que presumiblemente resuspende Chl *a* y / o incorpora nutrientes en toda la columna de agua. Por otro lado, la brisa no es capaz de romper la estratificación, por lo que la concentración de Clorofila *a* no cambia significativamente durante estos episodios. En conclusión, la mezcla producida por los fuertes vientos favorece una acumulación de Chl *a* en la bahía mientras que la estratificación asociada a la circulación estuárica tiende a reducir dicha acumulación.

Para completar el análisis observacional de la distribución de producción primaria en la bahía se han realizado simulaciones numéricas con un modelo numérico NPZD acoplado al ROMS. Los resultados numéricos muestran como el viento tiene un efecto primordial en la distribución de nutrientes provenientes de los canales de descarga y en consecuencia sobre la distribución de la biomasa de fitoplancton en el interior de la bahía. Las simulaciones idealizadas demuestran que la biomasa de fitoplancton tiende a redistribuirse en toda la columna de agua (debido a la rotura de la estratificación) cuando soplan vientos intensos del NW y del E-SE.

Aunque los resultados de la tesis han permitido profundizar en el conocimiento de la relación de los procesos hidrodinámicos y biológicos aún existen aspectos por explorar como el efecto de la resuspensión por fondo o

la relación entre procesos a diferente escala temporal. La implementación de modelos numéricos más complejos, análisis de imágenes satélite de alta resolución y campañas de adquisición de datos más intensas en espacio y tiempo puede ser un punto de partida para futuros estudios.

X

RESUM

Aquesta tesi analitza les relació entre la hidrodinàmica (i els seus forçaments) i les variables biològiques a la badia del Fangar, a partir d'observacions in situ, models numèrics i dades satèl·lit. La badia del Fangar es una badia relativament petita, somera i micro mareal, i es de vital importància per a la biodiversitat de la regió i la economia local, ja que en ella es practiquen tant activitats d'aqüicultura com d'oci nàutic.

Des de el punt de vista hidrodinàmic, la badia del Fangar està predominantment influenciada pel vent i pels fluxes d'aigua dolça, presentant problemes de renovació de l'aigua, així com altes temperatures a l'estiu, que arriben a afectar als cultius de bivals presents en ella. Per analitzar la hidrodinàmica s'ha utilitzat el model numèric ROMS (Regional Ocean Modeling System) i mesures de dues campanyes de camp on es van obtenir dades de corrents, nivell del mar, vent i salinitat i temperatura en la columna d'aigua. Duran els períodes de calma, les corrents observades mostren una circulació de l'aigua complexa a la part interior de l'estuari degut a la poca profunditat i una circulació estuàrica positiva a la bocana. Els experiments numèrics realitzats han permès investigar la circulació de l'aigua induïda pel vent local. Per a condicions intenses de vent a la badia, es produeix una estructura transversal axialment simètrica amb un fluxe de sortida en el eix del canal central i un fluxe d'entrada a les zones laterals poc profundes. Aquests resultats numèrics expliquen la circulació de l'aigua observada durant els episodis de ven ton la columna d'aigua tendeix a homogeneïtzar-se ràpidament.

Posteriorment, es va investigar l'efecte del vent en l'evolució de la concentració de clorofil·la a (Chl *a*) en superfície amb dades de camp i

imatges satèl·lit. L'anàlisi va revelar que els episodis de vent intensos tant del NW (Off-shore, up-wind) com del SE-E (on-shore, down-wind) provoca un augment en la concentració de Chl *a* superficial. Els mecanismes responsables son la dispersió horitzontal dels nutrients procedents del canals d'aigua dolça i la barreja vertical (també vinculada a la ruptura de l'estratificació) que presumiblement resuspèn la Chl *a* i/o incorpora nutrients en tota la columna d'aigua. Per altre banda, la brisa marina no es capaç de trencar l'estratificació, per tant la concertació de Chl *a* no canvia significativament durant aquests episodis. En conclusió, la barreja produïda pels forts vents afavoreixen una acumulació de Chl *a* dins la badia mentre que l'estratificació associada a la circulació estuàrica tendeix a reduir aquesta acumulació.

Per completa l'anàlisi observacional de la distribució de la producció primària dins la badia s'han realitzat simulacions numèriques amb el model numèric NPZD acoblat al ROMS. Els resultats numèrics mostren com el vent te un efecte primordial en la distribució de nutrients dels canals de descàrrega i en conseqüència sobre la distribució de la biomassa del fitoplàncton en el interior de la badia. Les simulacions idealitzades demostren que la biomassa de fitoplàncton tendeix a redistribuir-se en tota la columna d'aigua (degut a la ruptura de l'estratificació) quan bufen vents intensos del NW i del E-SE.

Encara que els resultats de la tesi han permès profunditzar en el coneixement de la relació dels processos hidrodinàmics i biològics, encara queden aspectes per explorar com l'efecte de la resuspensió del fons o la relació entre els processos a diferents escales temporals. La implementació de models numèrics més complexos, anàlisi d'imatges satèl·lit d'alta

resolució i campanyes d'adquisició de dades més intenses en espai i temps poden ser un punt de partida per a futurs estudis.

ACKNOWLEDGMENTS

A Margarita Fernández, por creer en mí, por los datos proporcionados y por ayudarme con la parte biológica de este trabajo.

A mis compañeros de la Barceloneta. Empezamos muchos, acabamos pocos. Por vuestra compañía, simpatía, las comidas, las charlas, las risas, los cafés…tantas cosas compartidas en el día a día.

A mis amigos. Simplemente por estar ahí y distraerme.

A la meva família, especialment a la marona, per recolzar-me sempre i estar passi el que passi. Pels anys d'esforços que, amb constància, sempre donen resultats.

Y para terminar a mi marido, Rafa. Llegaste a mi vida y la transformaste. El apoyo, cariño, fuerza, consuelo que he recibido de tu persona no son de este mundo. Gracias por tanto, gracias por todo. Te amo.

PUBLICATIONS

Publications associated with the core of the thesis

F-Pedrera Balsells M, Grifoll M, Espino M, Cerralbo P, Sánchez-Arcilla A. Wind-Driven Hydrodynamics in the Shallow, Micro-Tidal Estuary at the Fangar Bay (Ebro Delta, NW Mediterranean Sea). Applied Sciences. 2020; 10(19):6952. https://doi.org/10.3390/app10196952

F-Pedrera Balsells, M.; Grifoll, M.; Fernández-Tejedor, M.; Espino, M. Short-Term Response of Chlorophyll a Concentration Due to Intense Wind and Freshwater Peak Episodes in Estuaries: The Case of Fangar Bay (Ebro Delta). Water 2021, 13, 701. https://doi.org/10.3390/w13050701

F-Pedrera Balsells, M.; Grifoll, M.; Fernández-Tejedor, M.; Espino, M. Mestres, M. and Sánchez-Arcilla, A. Biological response to hydrodynamic factors in estuarine-coastal systems: a numerical analysis in a micro-tidal bay. Submitted.

Other publications

F.-Pedrera Balsells, M.; Mestres, M.; Fernández, M.; Cerralbo, P.; Espino, M.; Grifoll, M., and Sanchez-Arcilla, A., 2020. Assessing nature based solutions for managing coastal bays. In: Malvárez, G. and Navas, F. (eds.), Global Coastal Issues of 2020. Journal of Coastal Research, Special Issue No. 95, pp. 1083–1087. Coconut Creek (Florida), ISSN 0749-0208.

Cerralbo, P., F.-Pedrera Balsells, M., Mestres, M., Fernandez, M., Espino, M., Grifoll, M., and Sanchez-Arcilla, A.: Use of a hydrodynamic model for the

management of water renovation in a coastal system, Ocean Sci., 15, 215–226, https://doi.org/10.5194/os-15-215-2019, 2019.

Conference contributions

F-Pedrera Balsells, M., Cerralbo, P., Espino, M., Mestres, M., Sánchez-Arcilla A., and González-Marco, D. Water exchange processes in a mediterranean coastal bay (Fangar, Ebro Delta). EOF 2018, V Encuentro de Oceanografía Física. Vigo, Spain. Oral presentation.

F-Pedrera Balsells, M., Grifoll, M., Espino, M., Cerralbo, P. Sub-tidal hydrodynamic wind response in a small and shallow coastal bay: the Fangar bay case (Ebro Delta). MONGOOS 2019 - Mediterranean Oceanographic Network of the Global Oceanographic Observing System. Workshop on Modelling and Observations in the Coastal Mediterranean Sea: Physical and Biogeochemical Processes. Trieste, Italy. Oral presentation.

F-Pedrera Balsells, M., Grifoll, M., Mestres, M., Liste, M., Espino, M. and Sanchez-Arcilla, A. Hydrodynamic response in small, micro-tidal and shallow estuaries: the Fangar case (Ebro Delta, NW Mediterranean Sea). ISMS 2020 - VII International Symposium on Marine Sciences. Barcelona, Spain.

F-Pedrera Balsells, M., Grifoll, M., Fernández-Tejedor, M., Manuel Espino, M., Agustín Sánchez-Arcilla, A. Influence of the hydrodynamics in spatio-temporal variability of clorophyll *a* in a small-scale and micro-tidal bay: Fangar Bay case (Ebro Delta). EGU2021- European Geoscience Union General Assembly 2021. Oral presentation.

F-Pedrera Balsells, M., Grifoll, M., Espino, M. Fernández-Tejedor, M. and Sánchez-Arcilla, A. Wind-driven hydrodynamics in the shallow, micro-tidal

estuary at the Fangar Bay (Ebro Delta, NW Mediterranean Sea). EOF 2021 - VI Expanding Ocean Frontiers conference. Barcelona, Spain. Oral presentation.

F-Pedrera Balsells, M., Mestres, M., Fernández-Tejedor, M., Cerralbo, P., Espino, M., Grifoll, M., Sánchez-Arcilla, A. Assessing Nature Based Solutions for managing coastal bays. ICS 2021 - International Coastal Symposium 2021. Sevilla, Spain. Oral presentation.

TABLE OF CONTENTS

LIST OF FIGURES

LIST OF TABLES

1. Introduction and Objectives

C h a p t e r   1

INTRODUCTION

1. Coastal Areas, Estuaries, and Primary Production Dynamics

Bays and estuarine areas are among the most vulnerable and productive coastal areas from an ecological and socio-economic standpoint, as recognized in recent literature (Gao et al., 2019; Umgiesser et al., 2020). These ecotones are increasingly threatened, particularly in the past half century, by anthropogenic pressures, coastal urban environments, and their associated massive discharge of pollutants (Cardoso et al., 2008). Within coastal areas, estuaries are one of the most productive marine ecosystems and provide a rich source of natural resources. They are areas of transition between land and sea, where rivers enter the sea and a mixture of fresh and salt water occurs (Dyer, 1973). Estuaries are enriched with nutrients from river flow and land drainage, but their high productivity from a biological point of view, is also result of the retention of nutrients within the estuary. This is due to the pattern of water circulation that is established when less dense freshwater overlaps with heavier salt water (Lalli & Parsons, 1993). These areas are of great economic importance because a large number of activities take place there such as aquaculture, navigation, water sports, etc. They are also used as a

source of sand extraction and suffer coastal structure development in the framework of coastal engineering projects.

Currently, the most accepted definition of an estuary is that proposed by Cameron & Pritchard (1963): "an estuary is a semi-enclosed coastal body of water which has a free connection with the open sea and within which sea water is measurably diluted with freshwater derived from land".
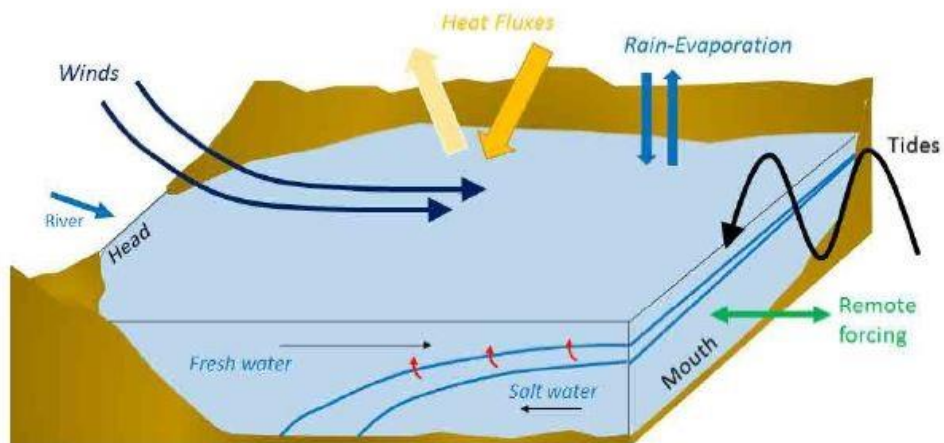
Figure 1. Conceptual scheme of the estuarine circulation and the main physical process. Source: Cerralbo et al. (2015).

There are many ways to classify estuaries. One the most accepted was suggested by Valle-Levinson (2012), based on Pinet (2003). They classify them according to their stratification, that is to say, according to their competition between tidal forcing and buoyancy forcing. They can be distinguished as:

a) <u>Salt-wedge estuary</u>: The freshwater volume of the river is much larger than the tidal volume, or the tides are simply not significant. The freshwater flows over the seawater in a thin layer. All mixing is restricted to a thin transition layer between the freshwater at the top and the saltwater wedge at the bottom.

b) <u>Partially mixed estuary</u>: When the tide is of the order of the freshwater volume or slightly larger, the estuary will be partially mixed. These estuaries support the strongest longitudinal density gradients because of the active mixing, albeit not sufficiently energetic to homogenize the basin.

c) <u>Well-mixed estuary:</u> The freshwater volume is negligible compared to the tidal volume. Locally, complete mixing of the water column between the surface and the bottom is obtained, eliminating all vertical stratification.
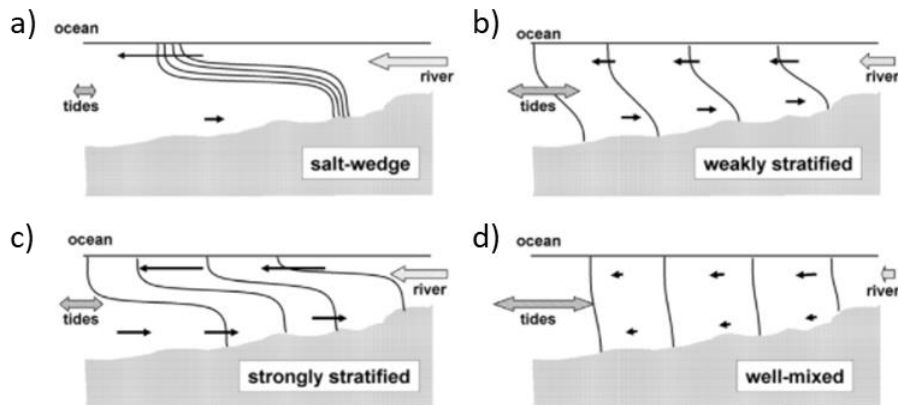
Figure 2. Classification of estuaries based on vertical structure of salinity: a) salt wedge, b) weakly stratified, c) strongly stratified, and d) well mixed. Source: Valle-Levinson (2010).

However, not all estuaries fall into this classification. There may be variations or even that during one season or specific events, they behave like one and during another season like another, as they are highly changeable environments due to the contributions of fresh water, as well as meteorology and oceanography. Estuaries and coastal bays used to be areas of large short-term variability due to environmental factors such as local wind, freshwater inputs, tides, etc. The water depth, which used to be shallow, makes the estuary water circulation vary in respect to forcings such as wind. In this sense, in terms of water circulation, there are many differences between shallow estuaries (Noble et al., 1996) and deeper estuaries (Wong & Valle-Levinson, 2002).

In terms of primary productivity, the estuaries and coastal bays can be classified according to the predominant physical mechanisms and the main drivers of phytoplankton biomass. Considering the temporal variability of environmental factors that may dominate the estuary dynamics, the phytoplankton distribution also changes over time. The first classification considers an increase in phytoplankton biomass from the landward to the seaward end (Jiang et al., 2020). This can often be attributed to an increasing source from the shore, an increasing sink landward, or more favourable growth conditions seaward. This is common in estuaries and bays open to coastal upwelling areas, for example, the Rias Baixas of Galicia (Spain) (Reguera et al.,1993) and Tomales Bay or the Eastern Scheldt (The Netherlands) (Jiang et al., 2020), where algal blooms generated are transported to the bays through multiple physical mechanisms of tidal, gravitational, and wind-driven circulation. In these cases, the tides are dominant. Another example of phytoplankton biomass increasing towards the sea, but dominated by freshwater inputs, would be the Chilika lagoon (India). In this lagoon, phytoplankton are light-limited due to the huge fluvial sediment load, and towards seaward direction, the transparency of the water leads to an increase in Chl *a* concentrations (Srichandan et al., 2015).

Another classification would be the opposite case, decreasing phytoplankton biomass in the seaward direction. The causes of this phenomenon is the result of tributary importation, lack of zooplankton grazing, or the nutrient gradient provided by the river plume that controls phytoplankton distribution (Gomez et al., 2018; Jiang & Xia,

2018). A typical example is the Scheldt River and Scheldt estuary (France), a eutrophic and turbid estuary with salinity ranging between 0 and 30. Several studies found that Chl *a* concentration is higher in the freshwater areas of the bay and decreases as salinity increases (Soetaert et al., 2006).

In many estuaries with substantial freshwater input, a Chl *a* Maximum Zone (CMZ) occurs in the middle area, as would be the case in the Chesapeake Bay (EEUU) (Jiang & Xia, 2017). This would be another factor that determines the classification of an estuary from a biological point of view. Near the discharge point there is maximum water turbidity, so phytoplankton are limited by light, but in the middle areas the CMZ appears, where conditions are optimal for phytoplankton growth. The CMZ is a combined consequence of optimal light conditions and terrestrial nutrient abundance. The location and coverage of the CMZ changes with river discharge and climate (Fisher et al., 1988; Miller & Harding, 2007).

The degree of grazing of certain species can also affect the phytoplankton biomass present in an estuary. This would be the case in the Hudson River (NY, EEUU), with a high nutrient rate but low Chl *a* concentration. This is due to the introduction of the invasive zebra mussel (*Dreissena polymorpha*) in the 1990s. Grazing by this species and transport losses have been two dominant sink terms that maintain a low phytoplankton stock throughout the estuarine catchment (Strayer et al., 2008). Such grazing may also create an uneven distribution of phytoplankton biomass throughout the estuary as the dominant sink (or

source) factor is not always evenly distributed and does not always follow consistent gradients. This would be the case in the Baie des Veys estuary (France), where benthic grazing by cultivated oysters
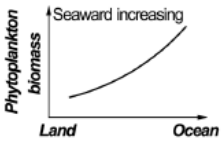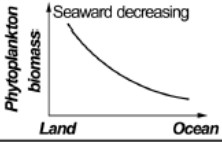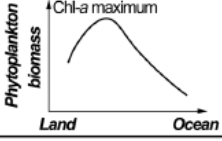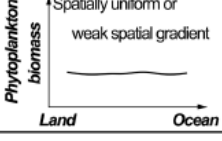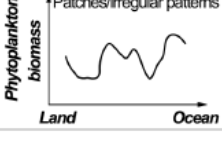
Common spatial gradients	Example ecosystems and references	Flushing mechanisms	Main drivers of phytoplankton biomass
Seaward increasing	(1) Oosterschelde, the Netherlands (this study)	Tide dominated	Grazing loss and tidal import
	(2) Rías Baixas of Galicia, Spain (Figueiras et al., 2002); Willapa Bay, USA (Hickey and Banas, 2003; Banas et al., 2007)	Tide dominated	Tidal import
	(3) Chilika Lagoon, India (Srichandan et al., 2015)	River dominated	Light limitation
Seaward decreasing	(1) Westerschelde Estuary, the Netherlands and Belgium (Kromkamp and Peene, 1995; Krompkamp et al., 1995; Muylaert et al., 2005; Soetaert et al., 1994, 2006)	River and tides, or river dominated	Salinity stress, grazing loss, and transport
	(2) Chesapeake Bay outflow plume, USA (Jiang and Xia, 2018); Mississippi River plume, USA (Gomez et al., 2018)	River and tides	Nutrient limitation
Chl-a maximum	(1) Chesapeake Bay, USA (Jiang and Xia, 2017); Delaware Bay, USA (Fisher et al., 1988); York River, USA (Sin et al., 1999); Neuse-Pamlico Estuary, USA (Valdes-Weaver et al., 2006); Logan River and Moreton Bay, Australia (O'Donohue and Dennison, 1997)	River and tides, or river dominated	Upper reach limited by light or transport loss; lower reach limited by nutrients
Spatially uniform or weak spatial gradient	(1) San Francisco Bay, USA, after 1987 (Cloern et al., 2017; Kimmerer and Thompson, 2014)	River and tides	Grazing loss
	(2) Hudson River estuary, USA (Fisher et al., 1988; Howarth et al., 2000; Strayer et al., 2008)	River dominated	Transport and grazing loss
Patches/irregular patterns	(1) Baie des Veys Estuary, France (Grangeré et al., 2010)	River and tides	Grazing loss
	(2) Krka Estuary, Croatia (Ahel et al., 1996)	River dominated	Point-source nutrient input
	(3) St. Lucia Estuary, South Africa (van der Molen and Perissinotto, 2011)	River dominated	DIN:DIP ratio, salinity, temperature, and irradiance

Figure 3. Common spatial patterns of phytoplankton biomass in estuarine-coastal systems. Source: Jiang et al. (2020).

results in an area of low Chl *a* concentrations over the oyster bed, and this patch of low Chl *a* is imposed onto a seaward decreasing Chl *a*

gradient, forming an irregular spatial pattern (Grangeré et al., 2010). This spatial irregularity may also be due to other factors, such as pollutant discharge. In the Krka estuary (Croatia), a discharge of raw sewage acts as a point source of DIN (Dissolved Inorganic Nitrogen), increasing phytoplankton production downstream. Without the point source, phytoplankton appear to decrease seaward (Ahel et al., 1996).

All these classifications can be summarized in Figure 3, suggested by Jiang et al. (2020). In any case, the understanding of hydrodynamics is a key factor in the analysis of primary production as estuaries are very shallow coastal areas that are strongly influenced by physical factors.

2. Study area

2.1.Ebro Delta

The Ebro River is the second largest river in the Iberian Peninsula and forms a deltaic system in the southern area of Catalonia, on the Spanish western Mediterranean coast, which extends around 25 kilometres offshore and forms two enclosed bays (Fangar to the north and Alfacs to the south). The Ebro valley was a closed basin until its opening to the Mediterranean Sea ca. 5.3 M years ago (transition between the Miocene and Pliocene). During the 20th and 21st centuries there had been a relative stabilization of the deltaic morphology, largely caused by the hydrological modifications carried out by man in the basin.

Nowadays we can distinguish three types of sedimentary environments in the Ebro Delta: the deltaic plain, the coastal environments, and the marine environments (Curcó, 2006).

➢ The deltaic plain comprises most of the emerged lands and includes two types of sedimentary environments: river environments and lake and marsh environments. The former are represented by the river channels and the natural specks that surround them (dykes), formed by soils of medium granulometry and for silt. The lacustrine and marshy environments are located in the regular or permanently flooded wetlands.

➢ Coastal and transitional environments are sedimentary environments with fluvial influence in which there is a more or less

intense retreat of sediments by marine agents (waves and storms). These environments are basically represented by the deltaic front, formed by the crescent-shaped sand bars and associated with the deltaic progression. The materials which form them have a fairly homogeneous granulometry, basically sandy. The beaches, the coastal bars, and the arrows are holo-marine coastal formations, originating from the deltaic river front, which are removed by the sea, or from erosion of the ancient deltaic lobes.

➢ Marine environments can be classified into bay, beach, and platform environments.

• The beach environment develops in the bodies of sea water that are confined by the coastal fringe, even though they are connected in accordance with the open sea by the permanent rivers.

• The pro-delta environment is located in coastal submerged environments and constitutes the transition between fluvial-marine and marine sediments. It is mainly made up of terrestrial materials with a significant content of organic matter of terrestrial origin.

• The continental shelf environment is located in the open sea, at a depth of more than 100 m, and is a relict sedimentary environment associated with the last post-glacial eustatic descents.

All aquatic ecosystems of the delta are influenced by water coming from rice fields. About 65% of the delta's area is dedicated to rice cultivation. From April to October, a quantity of 45 $m^3 \cdot s^{-1}$ of river water is diverted to the irrigation canals for continuous irrigation (Ibàñez et al., 1997). The river water is rich in nutrients (Ibàñez et al., 1995), but farmers add large amounts of fertilizer to enhance rice production, as well as several types of pesticides, mainly during spring and early summer (Ibàñez et al., 1997). Water coming from the rice fields is carried by drainage canals to the sea through the bays.

2.2. Fangar Bay

This study focuses on Fangar Bay. This area receives freshwater discharges from the irrigation channels of rice fields from the left side of the Delta, which reaches about 25 km offshore and forms two semi-enclosed bays, Fangar to the north and Alfacs to the south. Of these, Fangar Bay is the smallest, extending over 12 km^2, with a length of about 6 km, a maximum width of 2 km, and a volume of water around 16 x 10^6 m^3 (Camp & Delgado, 1987). The average depth is 2 m, with a maximum of 4 m (see bathymetry in Figure 4). Its connection with the open sea is oriented to the NW, and is approximately 1 km wide (Garcia et al., 1984), although it is currently narrowing because of the accumulation of sediment from the beach located to the north (Archetti et al., 2010).

The freshwater contribution is regulated by rice cultivation throughout the year. Open channels occur from April to December receiving a seasonal mean flow of 7.23 $m^3 \cdot s^{-1}$ throughout these months

(*Automatic Water Quality Information System, SAICA Project, 2013. Available online: https://www.saica.co.za/* (accessed on 30 January 2020)). This flow is distributed irregularly throughout the year, with maximum values in the months of April to November. Negligible freshwater flow occurs from December to March when the channels are closed (Perez & Camp, 1986). This flow is distributed in two main freshwater discharges in Fangar Bay: one in the Illa de Mar harbour (inside the bay, 'IM' in Figure 4) and the other, Bassa de les Olles, located in the bay mouth ('BO' in Figure 4). Additional freshwater discharges along the coastline are expected because freshwater inputs are regulated by gravity according to sea level. Finally, a substantial contribution from groundwater inputs is expected within the bay (Camp & Delgado, 1987; Jou, et al., 2019). In both cases, the expected freshwater flow is smaller than the water pumping stations mentioned above.
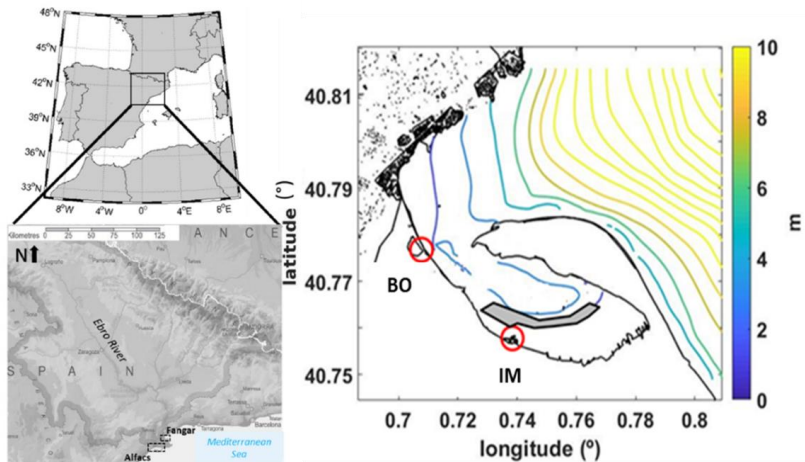
Figure 4. Location of Fangar Bay. The shaded area is the location of the mussel's farms. The red circles mark the two main freshwater discharge points. The coloured lines show the bathymetry of the bay.

2.2.1. Fangar Climatology

The Ebro Delta area is characterized by a mild and humid climate with hot temperatures in summer and mild winters. The Fangar area is influenced by the presence of S/SE sea breezes – which do not exceed 6 m·s^{-1} during the summer and spring seasons – and strong winds from the N and W of more than 12 m·s^{-1} in autumn and winter (Bolaños et al., 2009; Grifoll et al., 2016). The most frequent wind throughout the year is the NW wind, locally known as the Mistral, which is characterized by strong gusts of cold and dry wind (Garcia & Ballester, 1984). NW winds are associated with the general weather pattern and occur throughout the year but have maximal strength and persistence during the cooler months. In addition, the E and NE winds are responsible for rain events and increasing local mean sea level at the coast (Muñoz, 1990), which can also be quite intense (~10 m·s^{-1}).

The air temperature is characterized by a mild environment, with a limted range of variations between summer and winter. In summer, the temperature ranges from 24 –27 °C, and in winter it is between 10–15 °C.

As for rainfall in this area, there are generally two seasons when it rains more heavily, being from September to November and from April to June (Muñoz, 1990).

2.2.2. Fangar Hydrography

In the bibliography, we found studies on the distribution and variations of temperature, salinity, dissolved oxygen, and pigments in the surface water of Fangar Bay at different levels. (Lopez & Arté, 1973). These authors established maximum surface temperatures from February to September (spring/summer months) and minimum temperatures at the bottom, and conversely during the months of October to January (winter months) (Camp & Delgado, 1987; Lopez & Arté, 1973). In the case of salinity, they recorded minimum concentrations throughout the year at the surface and maximum concentrations at the bottom, increasing gradually with depth. They also observed that, during the warmer months, temperature and salinity are inversely related while during the winter months they are proportional to each other. As for oxygen, Lopez & Arté (1973) observed that its concentration is always higher than 70% in the whole column, however, years later, Delgado & Camp (1987) concluded that the concentration varies between day and night (ranging from 50% to 180%).

Several studies have shown that the waters of the bay typically behave like a positive estuary, with more static periods and other periods of great dynamism (Camp & Delgado, 1987; Varas Schiavi, 2012) depending on freshwater inputs, meteorological, and oceanographic factors. The surface waters are affected by freshwater inputs from the drainage channels on the left side of the delta, as they have characteristics closer to continental waters rather than marine

waters (Archetti et al., 2010). According to Camp & Delgado (1987) the vertical profiles of temperature and salinity showed a situation of almost permanent stratification. However, it has subsequently been seen that there are situations of vertical mixing that tend to make the water in the whole column more uniform. Caused mainly by strong N-NW winds, which produce abrupt changes in the characteristics of the bay in the short term, such as decreases in temperature and increases in salinity due to evaporation, influencing the biology of the organisms living in the bay (Varas Schiavi, 2012).

Studies of the permanence of freshwater in Fangar Bay have also been carried out based on calculations made in Alfacs Bay over the years. The first integrated data for the whole bay tells us that the renewal time in Fangar is 10 times less than in Alfacs (i.e., 1–2 days), calculated on the basis of the average flows of the outflow channels and an average salinity of the external water (Camp & Delgado, 1987). Subsequently, Llebot et al. (2011) using a hydrodynamic model to conclude that the residence times of the water in Fangar Bay were 5 times lower than in Alfacs, taking into account that the freshwater inflows are of the same order of magnitude in both bays, and that the times in Alfacs are 10 days for open channels and 25 days for closed channels. Therefore, in Fangar Bay, the times would be 2 days for open channels and 5 days for closed channels. On the other hand, Varas Schiavi (2012), in his doctoral thesis, focuses more on this small bay and establishes residence times ranging from 3 to 6 days when meteorological or tidal influences are minimal, based on

estimates of flow rates and/or irrigation volumes mentioned by other authors.

2.2.3. Fangar Ecology

In 1986, Perez & Camp carried out a study on marine phanerogams in the delta bays and found that they are an important factor to the input of organic matter into the bay system. The vast majority of nutrients come from the freshwaters of the drainage channels, specifically for Fangar Bay, that has annual figures of 200 Tm of nitrogen and 10 Tm of phosphorous (Delgado & Camp, 1987). Due to the low residence time of the waters of this bay, a large part of these nutrients pass into the sea without being assimilated by the phytoplankton present in the bay (Delgado & Camp, 1987). The ecological carrying capacity in one third of the bay is known to be close to the threshold of acceptability for this type of water and ecosystem ($\leq$ 4 according to the AMBI index) (Archetti et al., 2010) because a large amount of organic matter is constantly deposited in it, which causes a displacement and modification in the balance of the ecosystem characteristics of the area. Nutrient concentration, salinity, and sediment type can affect the segregation of the different species present. Nitrogen was initially known to act as a limiting factor in the development of phytoplankton (Delgado & Camp, 1987). However, later studies showed that not only nitrogen is limiting, but that phosphorus also plays an important role in the development of these species (Llebot et al., 2010, 2011; Varas Schiavi, 2012).

The morpho-sedimentary dynamics of the bay regulates the sediment distribution pattern (Archetti et al., 2010). There is evidence that sediment supplies significant amounts of nutrients to the water column (Delgado & Camp, 1987) and that part of the particulate organic matter carried by the water accumulates in them.

The concentration of phytoplankton has also been studied. A total of 124 surface phytoplankton species were identified, 10 of which were typical of freshwater (Lopez & Arté, 1973). However, there is no established trend in the distribution of phytoplankton biomass (Llebot et al., 2011). Fangar Bay is an area of high productivity due to the fact that the annual average of chlorophyll is 9 times higher than that of the Catalan coasts, being 2.47 mg·m^{-3} (Lopez & Arté, 1973). High phytoplankton biomass levels may be due to particular environmental and ecological conditions, such as high nutrient loads from canals, combined with high water residence time (Llebot et al., 2011).

3. Motivation

Fangar Bay is an easily accessible area that can act as a natural laboratory. It has its own characteristics that make it interesting on several levels, both physical and biological. In turn, it can represent other bays in the world with similar characteristics.

This area has not been intensively analysed in comparison with the other bay in the Ebro delta, Alfacs Bay, due to its distance from major urban centres and because it is smaller than the aforementioned bay. However, it is an area of high aquaculture productivity (cultivation of oysters and mussels) (Ramón et al., 2007a; Varas Schiavi, 2012) due to its own characteristics such as its shallow depth, relatively calm waters and shelter from coastal circulation, freshwater inputs from the rice fields on the left bank of the Delta (Camp & Delgado, 1987). It has a capacity of between 74 and 84 rafts, with an approximate production of 50 tonnes per nursery, depending on the area and year (Varas Schiavi, 2012). In recent years, changes in land use, such as the regulation of the flow of the river Ebro, rising sea levels, variations in land use, and water management (use of pesticides, nutrients, or elimination of the 'poma' snail) have led to concern on the part of the entities that manage and exploit the bay's resources about the decline in the productivity of inland waters.

Even though there are several studies on this bay, most of them just skim the surface of the situation in the bay and are, additionally, quite old. We know that the characteristics of the water have changed in recent years. There are certain problems in this bay related to low

water renewal, such as water heating during the summer months, blooms of toxic algae that affect mussel farming, water pollution due to the discharge of fertilisers from the rice fields…. This situation of low water renewal is aggravated by the closure of the mouth due to the accumulation of sediment due to two factors: one is a natural process since, due to coastal dynamics, sediment accumulates at the tip of the 'Banya del Fangar'. While the other is an anthropogenic process since every summer the Arenal beach, in 'La Ampolla', is filled in by sand from quarries and other areas, as well as the hydrodynamics of the area cause sediment to travel and accumulate on the south coast of the bay as we can see in Figure 1. Hence the interest in carrying out this thesis, where we are going to study the current situation of the bay in depth and model specific scenarios using numerical models in order to design tools that allow the good management of the bay and the best productivity of its aquaculture activities.

4. Objetives

The main objective of this thesis is to investigate the relationship between hydrodynamics and the evolution of biological variables in a small-scale, shallow, micro-tidal bay such as Fangar Bay. Aside from the main objective, four specific (or secondary) objectives are:

1. Description of the water circulation of the bay based on observations from intensive field campaign

2. Characterisation of the bay from a meteor-hydrodynamic point of view using numerical modelling

3. Description of the primary production of the bay and its evolution at wind and freshwater variables using *in situ* observations and satellite images

4. Development of a conceptual model supported by numerical modelling relating the physical and biological processes of the bay

2.Wind-Driven Hydrodynamics in the Shallow, Micro-Tidal Estuary at the Fangar Bay (Ebro Delta, NW Mediterranean Sea)

C h a p t e r   2

WIND-DRIVEN HYDRODYNAMICS IN THE SHALLOW, MICRO-TIDAL ESTUARY AT THE FANGAR BAY (EBRO DELTA, NW MEDITERRANEAN SEA)

Abstract

This chapter investigates water circulation in small-scale (~10 km^2), shallow (less than 4 m) and micro-tidal estuaries. The research characterizes the hydrodynamic wind response in these domains using field data from Fangar Bay (Ebro Delta) jointly with three-dimensional numerical experiments in an idealized domain. During calm periods, field data in Fangar Bay show complex water circulation in the inner part of the estuary owing to its shallow depths and positive estuarine circulation in the mouth. Numerical experiments are conducted to investigate wind-induced water circulation due to laterally varying bathymetry. For intense up-bay wind conditions (wind intensities greater than 9 m·s^{-1}), an axially symmetric transverse structure occurs with outflow in the central channel axis and inflow in the lateral shallow areas. These numerical results explain the water circulation observed in Fangar Bay during strong wind episodes, highlighting the role of the bathymetry in a small-scale environment. During these episodes, the water column tends to homogenize rapidly in Fangar Bay, breaking the stratification and

disrupting estuarine circulation, consistent with other observations in similar domains.

1. Introduction

Water circulation induced by local wind effects can contribute to the water exchange between an estuary and the adjacent open sea (Rockwell Geyer & MacCready, 2014). Seminal investigations presented by Csanady (1973) described how wind stress applied at the surface of a basin of variable depth sets up a circulation pattern characterized by coastal currents in the direction of the wind, with return flow occurring over the deeper regions. Narváez & Valle-Levinson (2008) showed that the observed transverse partition of the subtidal circulation is consistent with that driven by local wind in a channel with lateral depth variations. Wong & Valle-Levinson (2002) showed how the impact of the wind-induced coastal sea level at the entrance of an inlet exerts a huge impact on the subtidal variability within the interior of the bay. The influence of wind can also have effects on salinity structure or resuspension events in shallow estuaries estuaries (Cerralbo et al., 2015; Geyer, 1997; Llebot et al., 2014; Grifoll et al., 2019). These studies indicate that spatial scales and water depth determine the flow response to wind forcing. Moreover, Noble et al. (1996) determined that both river and wind-driven flow patterns change as a function of water depth in a shallow estuary (below 4 m). In this case, for wind-driven flows the critical parameter is the degree of stratification in the lower bay. However, the particular role that plays the geometry and the bathymetry in wind response in a small-scale bay is still not clear. An illustrative contribution presented by Sanay & Valle-Levinson (2005) reflects the role of the bathymetry in the water contribution for larger and deeper basins than that mentioned in this study. Numerical experiments reveal a wind-induced water circulation dominated by an axially symmetric

transverse structure due to laterally varying bathymetry. So, the investigation at very small-scales (order of few km) and shallow depths (few meters) still presents some challenges that may be addressed by complementing observational and numerical efforts. The short time scales expected due to the shallowness, the role that plays the geometry (for instance the mouth width) and the link between bathymetry and water circulation are challenging questions to describe properly small-scale bays under micro-tidal conditions.

Contributions focusing on coastal bays and estuaries conclude that they are regions with complex hydrodynamics due to multiple forcing (Cerralbo et al., 2015; Llebot et al., 2014; Noble et al., 1996). In some cases, wind stress competes with baroclinicity to determine the hydrodynamics. However, the astronomic tide (Valle-Levinson et al., 2001), seiches (Cerralbo et al., 2014), water run-off, the bathymetry or the effect of rotation (Sanay & Valle-Levinson, 2005) are variables that may not be neglected in the analysis of the local wind influence on this type of water bodies. In these cases, the combination on observational and numerical efforts have allowed obtaining substantial new knowledge on water circulation and termohaline structure.

This chapter investigates the relationship between wind and hydrodynamics of small-scale, shallow and micro-tidal estuary. The research combines *in situ* data using the case study of Fangar Bay, located in the Ebro delta, NW Mediterranean Sea, and the implementation of numerical experiments in idealized geometries. These simulations should figure out the impact of the bathymetry on wind-driven water circulation. The complexity of the flow observed have suggested to focus,

at this first stage, on the effect of the bathymetry in the wind-driven circulation. Fangar Bay presents problems of water renewal, high water temperatures, anoxia and permanence of pollutants in the water. All these problems affect the oyster and mussel crops present in the bay that need a sustained water renewal for their growth and development (Ochoa et al., 2012). Several intensive field campaigns have been carried out to characterize the bay hydrodynamics as a first step for a subsequent water renewal analysis. In this sense, Fangar Bay is a good example to investigate the hydrodynamics of small-scale and shallow scale bays under micro-tidal conditions.

2. Materials and Methods

2.1. Field campaigns in Fangar Bay

The observational data corresponded to two field campaigns (each of around two months) from 25 July to 5 September 2017 (FANGAR-I) and from 5 October to 16 November 2017 (FANGAR-II), hence summer and autumn, respectively. The data set consisted of two Acoustic Doppler Current Profilers (ADCPs, from NORTEK, model AQUADOPP 2MHz) (mooring points M and B in Figure 5), with the velocity and the direction of the water currents obtained every 10 minutes in 25 cm layers distributed from the bottom to the surface. Moreover, the systems were equipped with pressure systems and a temperature sensor (Vaisala PTB110 and HMP40). A set of CTD (Conductivity, Temperature and Depth, model SeaBird 19plus) campaigns were conducted. During FANGAR-I, 16 CTD campaigns were carried from 11 July to 5 September (two campaigns per week). During FANGAR-II, only two surveys were undertaken, one at the beginning of the campaign (18 October) and the other at the end (16 November). For each of the CTD campaigns, twenty points were chosen, including both the inner and the outside sections of the bay, where temperature and salinity were measured (see black dots in Figure 5).
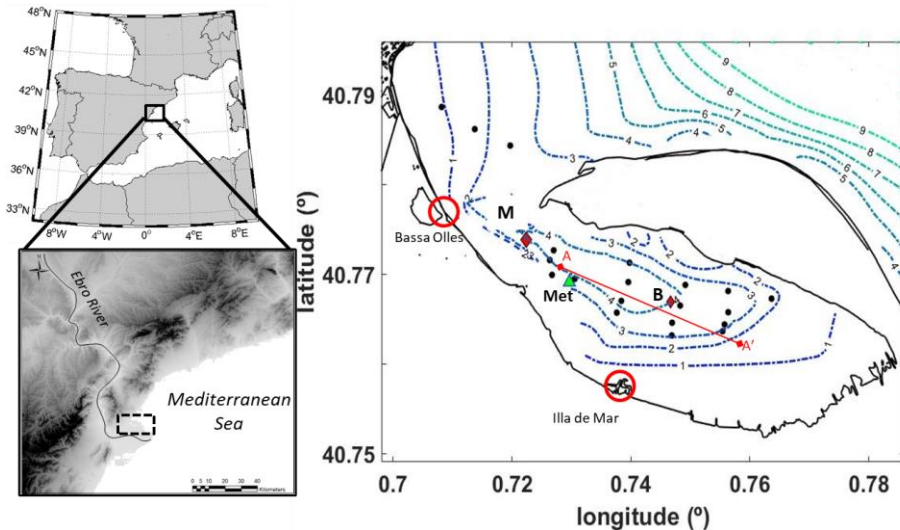
Figure 5. Location of the study area. The red circles show the two main points of freshwater discharges (Bassa de les Olles and Illa de Mar), the red diamonds show the points of measurement during the field campaigns (M: Mouth; B: Bay) and the green triangle shows the location of the meteorological station during FANGAR-II (Met). The black point shows the CTD profiles, the blue lines show the bathymetry and the red line (A-A') shows the longitudinal section presented in Figure 14.

During FANGAR-I, data from Servei Meteorologic de Catalunya (MeteoCat, http://www.meteo.cat/) of the Illa de Buda, located about 12 km from Fangar Bay, were used. This station records wind data every 30 min. During FANGAR-II, a meteorological station (with temperature and humidity sensor, air pressure and acoustic wind sensor) was mounted on a mussel raft near the mouth (Met in Figure 5) to measure wind, atmospheric pressure, air temperature and humidity every 10 min. The measurement periods and instruments are summarized in Table 1.

Table 1. Data acquisition instruments and observational periods (year 2017) shown in Figure 1.

Name (ID)	Observations	Period	Data interval (min)
Meteo station (Met) (wind Sonic/Vaisala HMP40/Vaisala PTB110)	Wind, atmospheric pressure	19 Oct – 16 Nov	10
Illa de Buda station (wind Sonic/ Vaisala HMP40/Vaisala PTB110)	Wind, atmospheric pressure	25 July – 5 Sept	30
ADCP mouth (M) (Nortek Aquadopp 2MHz)	Currents, sea level, waves, bottom temperature	25 July – 5 Sept _____ 5 Oct – 16 Nov	10
ADCP inner bay (B) (Nortek Aquadopp 2MHz)	Currents, sea level, waves, bottom temperature	25 July – 5 Sept _____ 5 Oct – 16 Nov	10
CTD (SeaBird 19plus)	Temperature, salinity	11 July – 5 Sept _____ 18 Oct and 16 Nov	- -

2.2. Numerical modelling

A series of numerical experiments were conducted using the Regional Ocean Model System (ROMS) to analyse the hydrodynamic wind response in small and shallow estuaries. The ROMS numerical model is a 3D, free-surface, terrain-following numerical model that solves the Reynolds-Averaged Navier-Stokes equations using hydrostatic and Boussinesq assumptions (Shchepetkin & McWilliams, 2005). ROMS uses the Arakawa-C differentiation scheme to discretize the horizontal grid in curvilinear orthogonal coordinates and finite difference approximations on vertical stretched coordinates (Haidvogel et al., 2007). The numerical details of ROMS are described extensively in Shchepetkin & McWilliams (2005). This model has been used and validated in similar bays and estuaries, such as Alfacs Bay located south of the Ebro Delta (e.g. (Cerralbo et al., 2014, 2015, 2019)). The domain used is inspired in Fangar Bay and consists in an idealized domain due to the difficulty of achieving good bathymetry. The domain consists of a regular 37x27 grid with a horizontal resolution of about 70 m (Figure 6a) and 10 sigma levels in the vertical direction (the bottom layer being the first and the surface layer the tenth, Figure 6b). The model boundary is located 10 points away of the mouth entrance to avoid boundary noise (faster than show in the Figure 6a). The 2D variables were accommodated with the Chapman and Flather algorithms (Carter & Merrifield, 2007), whereas a clamped boundary condition is imposed on the 3D variables. The same model configuration has been used and validated in the bay located south of the Delta, the Alfacs Bay (Cerralbo et al., 2015).
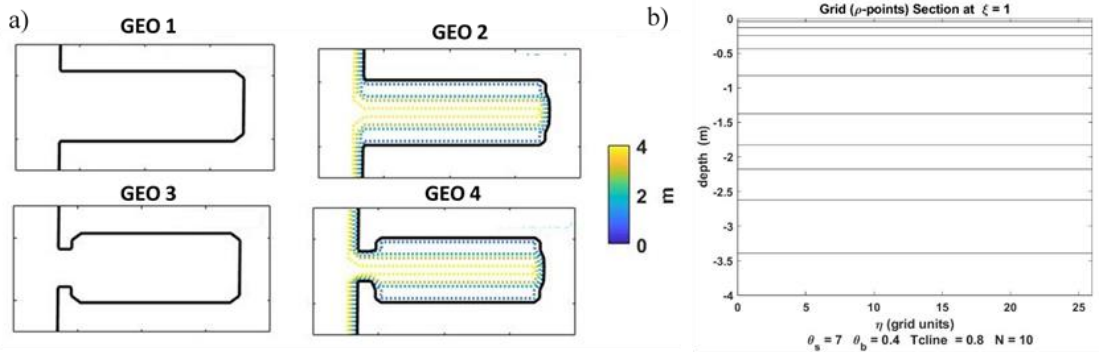
Figure 6. a) Geometry and bathymetry for the four configurations used in the numerical experiments. GEO 1 and GEO 3 have 4 m of water depth. b) sigma layers used in the numerical model. The geometrical parameters are included following the stretching formulation described in Cerralbo et al (2015).

Figure 6a presents the different geometries used for the numerical experiments. We modelled a simple case, regarding the water body as a channel 2.5 km long and 1.9 km wide, to simplify the response of the wind to the idealized bathymetry similar to that of the Fangar Bay. First was homogeneous depth of 4 m (GEO 1). Second was variable bathymetry (v-shape channel with 1m to the sides up to 4 m in the central part, GEO 2). The same experiment was then conducted, but reducing the mouth of the channel to simulate the narrow entrance of the Fangar Bay (GEO 3). Finally, it was simulated to include variable bathymetry (GEO 4). Experiments were conducted up-bay wind and down-bay wind according to the axis of the estuary (wind spatially homogenous). An additional simulation took into account the Coriolis effect for GEO 1 to verify the influence of the Earth's rotation. All simulations are summarized in Table

2. Constant temperature (20ºC) and salinity (36) conditions were applied. Freshwater inputs were deactivated in order to observe the behaviour of the currents only as a function of wind and bathymetry. The bottom boundary layer was parameterized with a logarithmic profile using a characteristic bottom roughness height of 0.002 m. The turbulence closure scheme for the vertical mixing was the generic length scale (GLS) tuned to behave as a k-ε (Warner et al, 2005). Horizontal harmonic mixing of momentum was defined with constant values of 5 $m^2 \cdot s^{-1}$. Long-term simulations (around 2 months each) were performed in order to analyze the wind response avoiding spurious velocities. The wind is constant throughout the simulation. According to the results less 24 hours of the spin-up is observed in the numerical results. The numerical results used are 16 days after the start of the simulation to avoid spurious velocities.

Table 2. Summary of the different simulations used in ROMS.

Simulation name	Geometry	Wind direction	Intensity wind ($m \cdot s^{-1}$)	Coriolis
SIMU 1	GEO 1	Up-bay wind	12	No
SIMU 2	GEO 2	Up-bay wind	12	No
SIMU 3	GEO 2	Up-bay wind	6	No
SIMU 4	GEO 2	Down-bay wind	12	No
SIMU 5	GEO 3	Up-bay wind	12	No

SIMU 6	GEO 4	Up-bay wind	12	No
SIMU 7	GEO 4	Down-bay wind	12	No
SIMU 8	GEO 1	Up-bay wind	12	Yes

3. Results

3.1. Meteorological description of Fangar Bay

Wind roses for both field campaigns are shown in Figure 7. During FANGAR-I the predominant winds were southerly and easterly, associated with sea breezes, whereas during FANGAR-II the predominant and strongest winds were from the NW (i.e. an upward wind direction considering the axis of the estuary). Note the presence of NW winds in both campaigns.
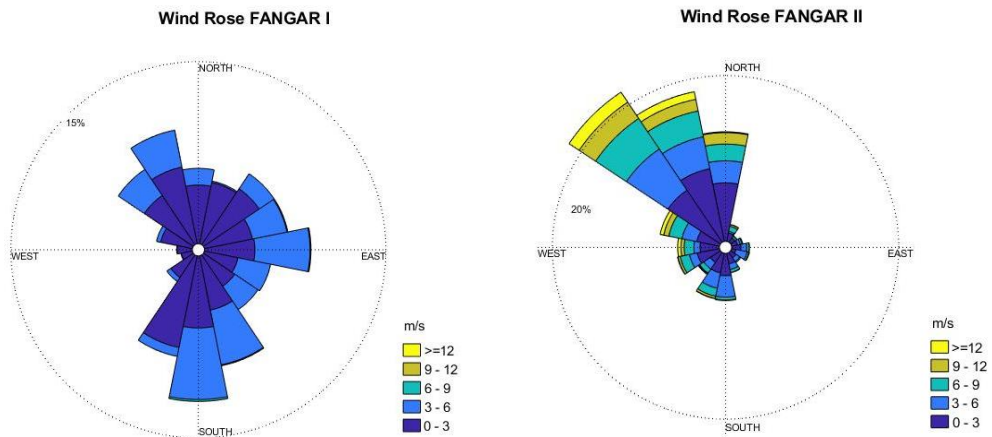
Figure 7. Wind roses of mean velocity for FANGAR-I (left) and FANGAR-II (right) during both campaigns. Wind intensities are grouped by intervals of 3 $m \cdot s^{-1}$.

Figure 8 shows the time series of the wind and air temperature measured at the corresponding meteorological station. During summer (FANGAR-I), the sea breeze was characterized by daily southerlies with a wind intensity of 6 $m \cdot s^{-1}$. Furthermore, two episodes of NW winds were

distinguished during FANGAR-I – from 6 to 12 August (henceforth called episode E1) and from 29 August to 3 September (henceforth called E2) – as well as in FANGAR-II from 21 to 23 October (henceforth called E3) and from 5 November until the end of the campaign (henceforth called E4). These NW episodes could also be identified alongside the air temperature drops in Figure 8 superimposed at daily variability during both field campaigns.
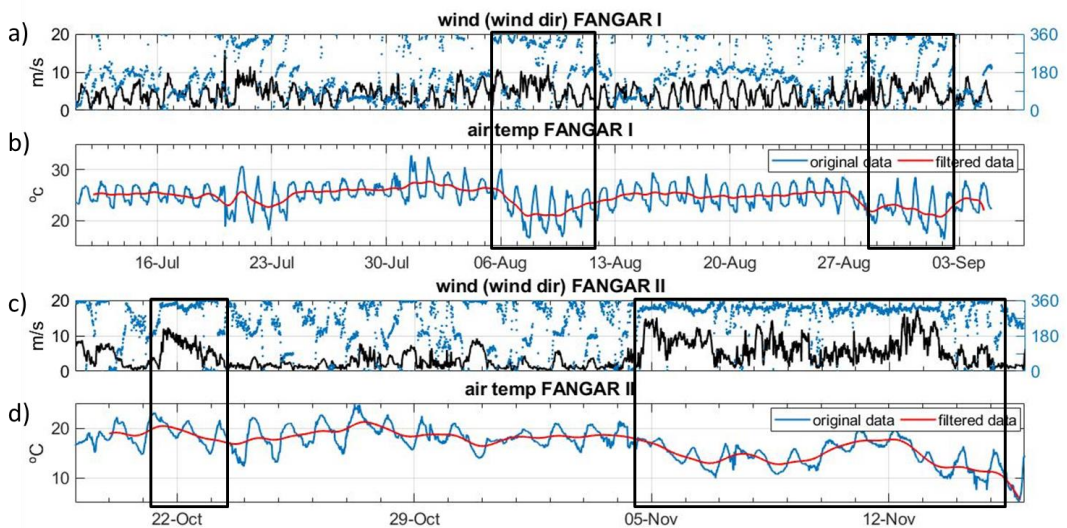
Figure 8. Wind direction and intensity from FANGAR- I (a) and FANGAR-II (c). Air temperature for FANGAR-I (b) and FANGAR-II (d). Air temperature is filtered to exclude daily variability. The black box shows the periods with falling air temperatures during NW winds.

3.2. Hydrodynamic description of Fangar Bay

A dispersion diagram of the water currents (surface and bottom) measured by the ADCPs in each campaign is shown in Figure 9. The

diagram shows how in the mouth (M station) the flow was aligned following the longitudinal axis of the bay. By contrast, in the B position the flow did not show a prevalent pattern, the water circulation being more complex. In addition, Figure 9 demonstrates how the water flow in the mouth was larger than in the inner bay. The maximum water currents measured in the mouth were 0.5 m·s^{-1} in FANGAR-I and FANGAR-II, but below 0.02 m·s^{-1} in both campaigns within the bay. Furthermore, the surface and the bottom signal showed similar patterns across the campaigns.
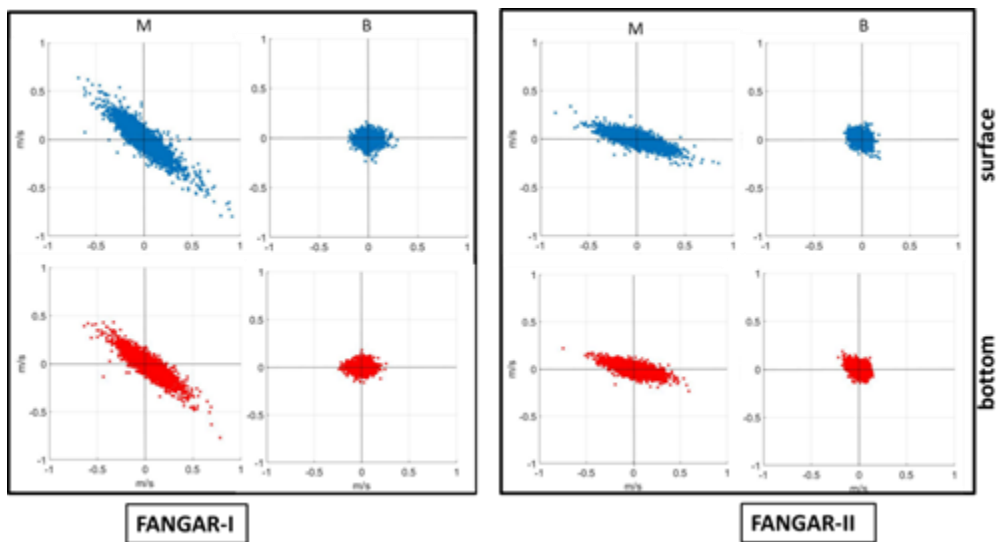
Figure 9. Dispersion diagram for FANGAR-I (box on the left) and FANGAR-II (box on the right), in blue the surface water circulation and in red the bottom water circulation. The first column of panel corresponds to the measurements in the mouth (M) and the second column to those within the bay (B).

Regarding the flow alignment shown in the dispersion diagram (see Figure 9), the water current observations were rotated following the alongshore (longitudinal axis of the bay with positive inward) and cross-shore alignment. The rotation angle was equal to 35º for FANGAR-I and 15º for FANGAR-II (north clockwise negative) according to the flow alignment of the dispersion diagram. Discrepancies in the rotation angles probably owed to differences in the mooring location of the ADCPs. Figure 10 shows the alongshore time-averaged currents for each measurement layer of the ADCPs. The resultant profiles in the water column revealed a predominant two-layer structure during FANGAR-I (Figure 10a), indicating that estuarine circulation was the surface current leaving the bay (negative values), while bottom currents were entering (positive values). During FANGAR-II, the water circulation pattern was similar to FANGAR-I, aside from differences in surface values (above 1 m depth, Figure 10b) when averaging the whole period. However, after differentiating calm wind or sea breeze periods with those of the NW winds (i.e. E3 and E4), distinctions became evident. Indeed, during such periods the profile corresponded to the positive estuarine circulation pattern, normal behaviour in this type of geometry (Figure 10c), whereas when considering only the NW wind episodes that lasted the entirety of November, the water currents were negative (leaving the bay, Figure 10d) in almost all water column broking down the positive estuarine circulation.
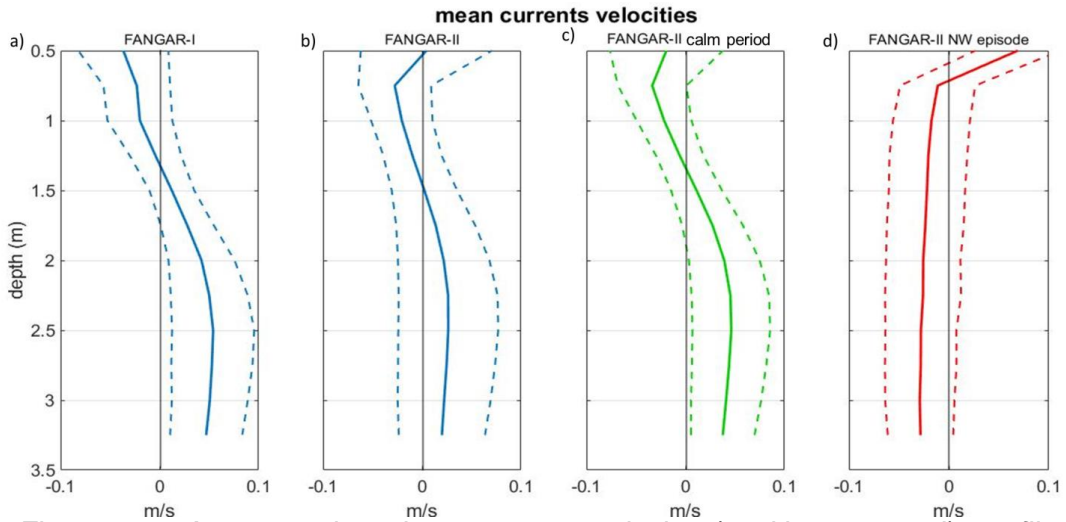
Figure 10. Average alongshore current velocity (positive outward) profile (continuous line) and standard deviation (dashed lines) for the mouth in FANGAR-I (a) and in FANGAR-II (b); c and d show the mean profile during FANGAR-II for the calm period (c) and the NW wind period (d).

Figure 11 shows the spectral analysis of the alongshore current in the mouth and in the inner bay. High-frequency peaks corresponding to the tidal ranges and typical resonance periods are shown. The seiching band using the Merian formula ($2L/n\sqrt{gH}$) approximately corresponded to periods of two hours in the fundamental mode (considering a characteristic length of about 6 km). These values are consistent with other locations in semi-closed bays (Cerralbo et al., 2014; Niedda & Greppi, 2007).
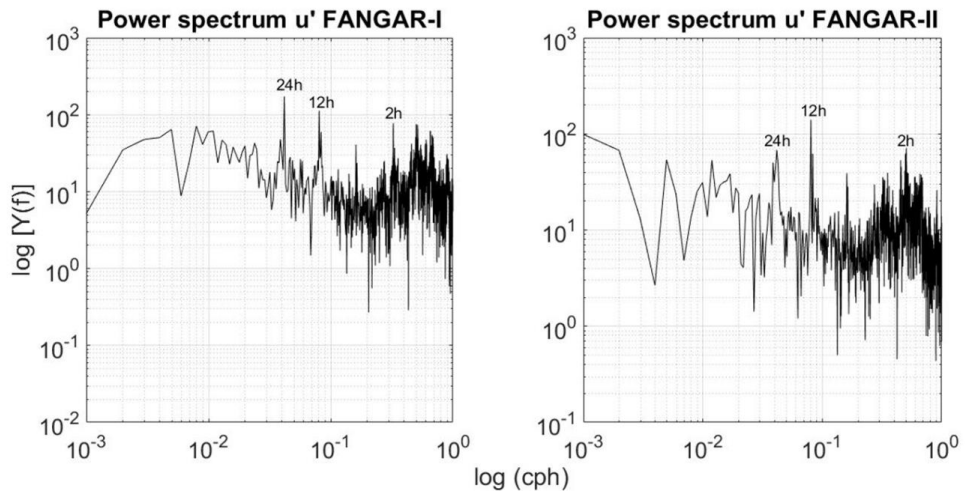
Figure 11. Spectral analysis of the signal of the alongshore current in the mouth for FANGAR-I (left) and FANGAR-II (right)

In order to conduct an episodic analysis, the time series were filtered using a 30h Lanczos (Duchon, 1979) to focus on the low-frequency signal. Figure 12 and Figure 13 show the rotated and filtered components of water currents jointly with wind, temperature and mean flow. Additional measurements of T and S are also shown in Figure 12, with Figure 12d-e and Figure 13c-e presenting the estuarine circulation mentioned previously, whereby the surface water flows out from the bay (negative and blue colour) while the bottom water circulation enters (positive and red colour). These periods were characterized by a strong stratification. This was due to the fact that the irrigation channels during FANGAR-I were open, contributing to the discharge of fresh water into the bay (Figure 12c). The same occurred at the beginning of FANGAR-II. Marked with a black box are the episodes of NW winds in Figure 12. Note that during these episodes, both temperature and salinity were homogenized (Figure 12b-c) and there was a change from positive

estuarine circulation to homogeneous currents in the water column. Moreover, a substantial drop in sea bottom temperature occurred (Figure 12f), notably during episodes E1 and E2 in Figure 12, and during events E3 and E4 in Figure 13. Note that during NW wind episodes, the currents were opposite to the wind direction in both locations (i.e. M and B). Figure 12g and Figure 13g shows the average flow through the mouth. It can be seen that during the NW episodes the net flow is outflow in the central area of the channel, while in the rest of the period occurs the opposite.

The water temperature observations during FANGAR-I exhibited variations of between 23ºC and 29ºC (Figure 12b and f). The maximum temperature was reached on 4 August after the ambient temperatures reached 30ºC (Figure 12). However, just two days later on 6 August, the water temperature dropped drastically to 23ºC, indicating a difference of 6ºC. This event coincided with the presence of the NW winds, as can be seen in Figure 12. Once the wind stopped, the temperatures rapidly increased again, reaching 28ºC, as can be seen in Figure 12b-f. As noted in the previous paragraph, during episodes E1 and E2, the wind events started on 6 and 27 August, respectively. For both episodes, the temperatures began to drop from those dates and persisted during the subsequent days when the wind died down (Figure 12b-f). This temperature decrease was associated with a cold NW wind, alongside the likely contribution of an open sea entrance (i.e. colder) through the mouth, indicated by the reduction in water temperature observed a few days later, when the wind stopped.
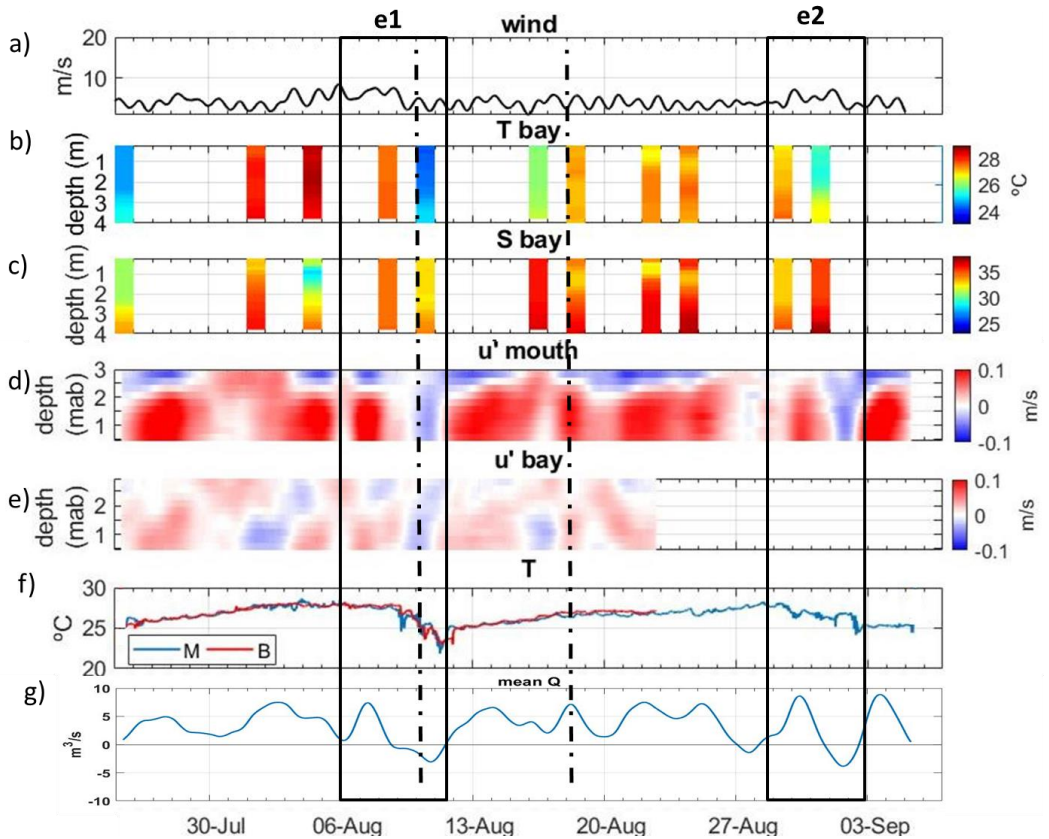
Figure 12. From top to bottom, wind speed (a), time series of temperature at a central point of the bay (b), time series of salinity at a central point of the bay (c), alongshore currents in mouth (d), alongshore currents in the bay (e), and bottom temperature (f) in mouth (blue) and bay (red), mean flow (positive inflow) in the mouth (g). The black boxes show the NW events. The dotted lines mark the days of the vertical sections shown in Figure 14.

During FANGAR-II, the water temperature was lower than FANGAR-I because the ambient temperature decreased (i.e. autumn season) (Figure 13a). Throughout FANGAR-II, water temperatures between 11°C and 25°C were recorded. The campaign began with water temperatures of 22°C, until 19 October saw a small decline in the sea

45

bottom water temperature (20ºC) (Figure 13f). This could be associated with E3, when another drop in the water temperature occurred, falling to 18ºC. Once the NW wind stopped, the water temperatures rose slightly again to 20ºC, until 5 November when there was another episode of NW winds (E4). Note that before this event the
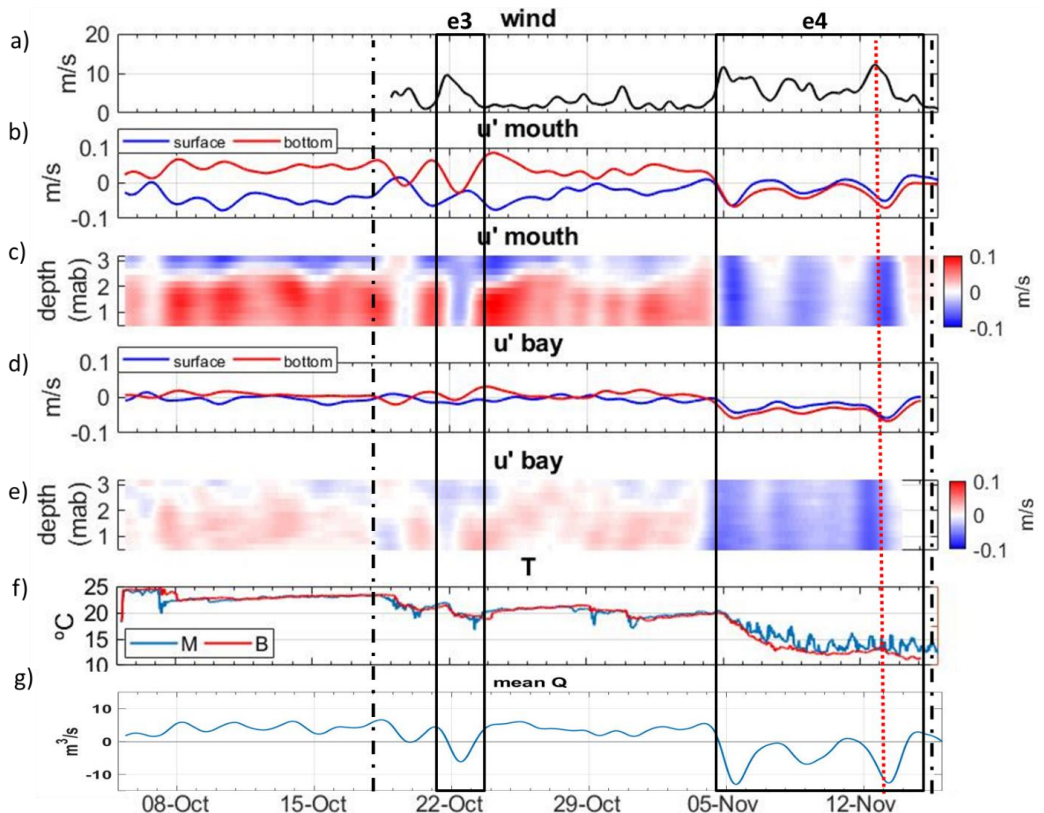
Figure 13. From top to bottom, wind speed (a), alongshore currents in the mouth (b), Hovmöller diagram in the mouth for the alongshore currents (c), alongshore currents in the bay (d) and Hovmöller diagram in the bay for the alongshore currents (e), and bottom temperature (f) in the mouth (blue) and the bay (red), mean flow (positive inflow) in the mouth (g). The black boxes show the NW events. The dotted lines mark the days of the vertical sections shown in Figure 14.

water temperatures in the bay and in the mouth were similar, whereas from 5 November there were oscillations of about 4ºC in the data from the mouth, as can be seen in Figure 13f. This is due the diurnal cycle of heat fluxes (day/night) during those days.

Figure 14 shows a vertical section of the bay area (A-A', Figure 5) for four different situations. Sections a and b depict a situation prior to NW winds during FANGAR-I and during FANGAR-II, respectively. In these cases, a low vertical gradient in temperature could be observed (0.5ºC). Focusing on salinity, there was an evident gradient, with less salty surface waters (freshwater contributions, 31-33 for Figure 14a, 32-34 for Figure 14b) and deeper, saltier waters characteristic of ocean waters (37 for Figure 14a, 38 for Figure 14b). Figure 14c and d show the T/S values during or immediately after NW episodes (i.e. E1 and E4). There was a clear horizontal gradient for both temperature and salinity in Figure 14c (i.e. a decreasing gradient as it enters the inner part of the bay), while in Figure 14d the salinity was homogenized in the water column and the temperature also decreased towards the inner part of the bay.
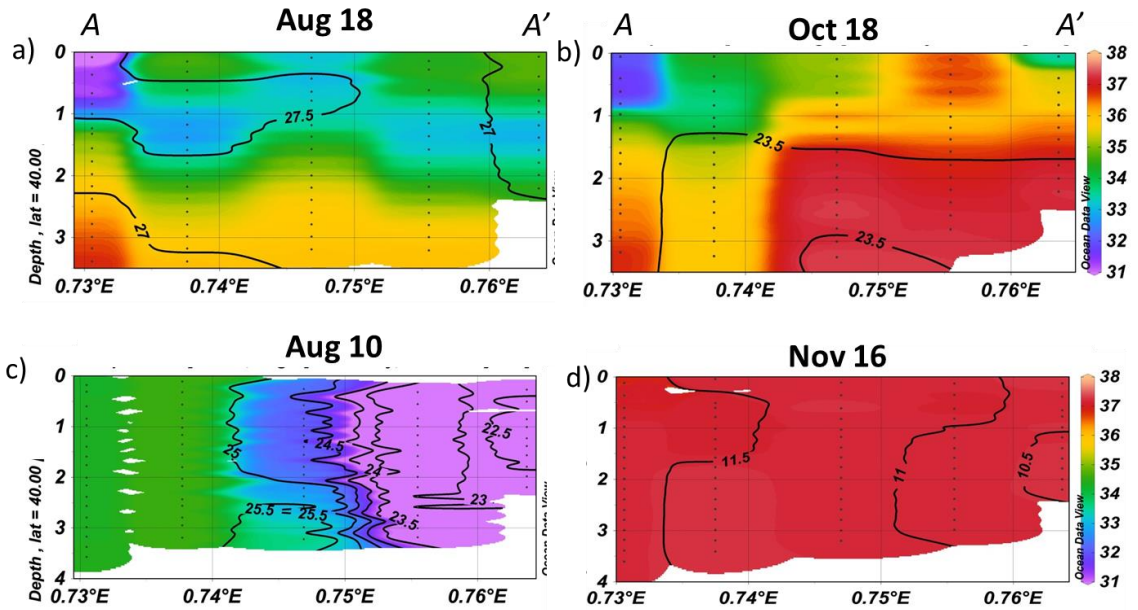
Figure 14. Vertical transect of a) stratification summer situation, b) stratification autumn situation, c) situation during episode E1, d) situation during episode E4. The colour bar shows salinity values; black lines show temperature values.

3.3. Numerical Experiments

Figure 15 shows the results of the numerical model in terms of surface and bottom water currents, with no more variables than the force of the wind pushing the water. SIMU 1 (up-bay wind) indicated an expected water circulation pattern for the homogeneous flow (surface water following the wind direction and return flow at the bottom). However, when a varying bathymetry was considered (SIMU 2), the surface flow in the central axis reduced significantly in comparison to the shallower shore where the bottom friction is very relevant due to its shallowness. Tests have been made with different bottom roughness and it was found that the magnitude varies but the circulation pattern does not. In this case, an

outward flow was observed in the central axis of the estuary in the bottom layers, opposite to the direction of the wind, as noted in the observations of the campaigns in the previous section. A homogeneous upward flow is observed at the shore. This pattern was reproduced for upward and smaller winds (SIMU 3). For the case down-bay wind, the picture differed significantly: downward flow towards the shore and upward flow in the axis and the bottom layers (SIMU 4). Therefore, the numerical experiments revealed transversal variability in flow direction due to the bathymetry. SIMU 5, 6 and 7 reproduced the previous cases but a stretching at the bay entrance is added. In this case, the pictures do not significantly differ in relation of the upward/downward flow in the shore/central axis for bottom layers in relation to the open mouth. The Coriolis effect was negligible in idealized cases when comparing SIMU 1 and SIMU 8. Finally, sensitivity test of the bottom friction parametrization has not shown relevant influence on the water circulation patterns affecting mainly the water speed.
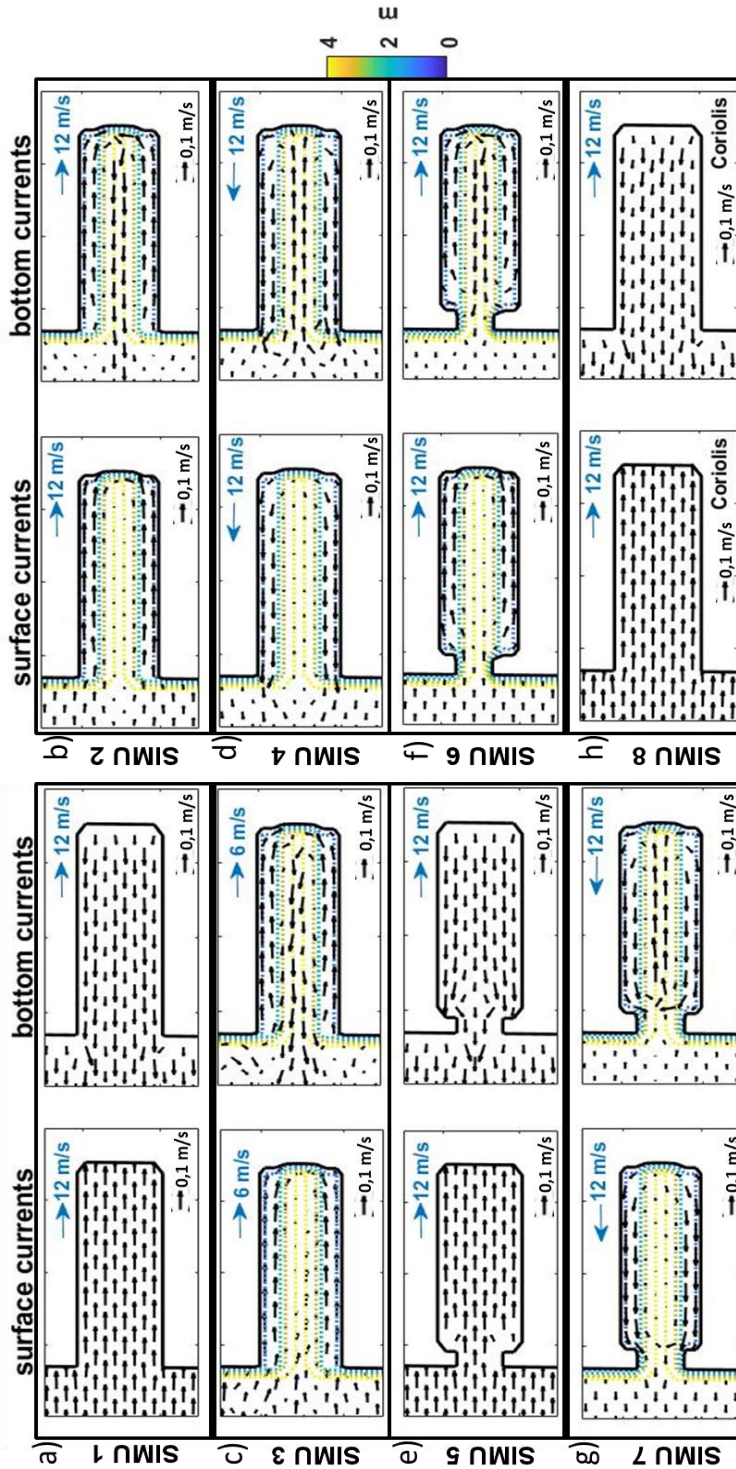
Figure 15. Representation of the simulations: a) SIMU 1, surface and bottom; b) SIMU 2, surface and bottom; c) SIMU 3, surface and bottom; d) SIMU 4, surface and bottom; e) SIMU 5, surface and bottom; f) SIMU 6, surface and bottom; g) SIMU 7, surface and bottom; h) SIMU 8, surface and bottom. Blue arrows show the wind direction with the intensity wind and black arrows show the water current intensity.

Focusing on the impact of the wind on water circulation in the bay entrance, the transversal barotropic velocities are shown in Figure 16. This figure shows how the laterally variable bathymetry induces axially symmetric transverse structure (see inshore velocities near the boundaries and offshore in the central section of the bay entrance for SIMU 2; note that barotropic velocities for SIMU 1 its near to zero). Opposite water circulation pattern occurs for downwind simulation (SIMU 4). Bay mouth stretching (SIMU 6) has a similar pattern than SIMU 4 but increasing the spatial gradients between inflow and outflow (not shown). In this case, the magnitude of the transversal barotropic velocity is lower, reducing also the flow exchange expected between the bay and the open sea if the width mouth is reduced.
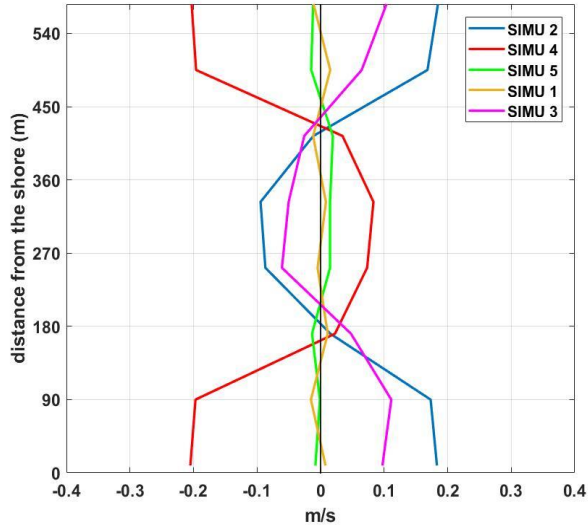
Figure 16. Barotropic velocities (negative outflow) in the entrance section for selected simulations

4. Discussion

Local winds have the predominant influence on water circulation in small, shallow and micro-tidal estuaries and coastal bays. Such influence may lead to complex water circulation patterns due to bathymetric and geometric effects. For instance, Geyer (1997) has found that geometric constrictions restrict wind-induced circulation, resulting in strong fronts between well-mixed reaches in two small Cape Cod (USA) estuaries. Scully et al. (2005) proposed appeared during NW strong wind periods: up-estuary wind weakens and even reverses the shear and reduces the stratification. Li & Li (2011) suggested that wind mixing may dominate over wind straining under typical wind forcing conditions in Chesapeake Bay. More recently, Xie & Li (2018) tried to explain the apparent contradiction between these two studies and revealed opposite responses of the upper and lower bay regions to axial winds. Furthermore, Coogan et al. (2019) have identified substantial transverse variability in Mobile Bay (USA), including the influence of the bathymetric effects previously postulated by Noble et al. (1996). Shallow depths accentuate the wind's influence, sometimes leading to complex water circulation according to observational investigations where the considerable variability of time series is observed (Cerralbo et al. 2019; Llebot et al., 2014; Noble et al., 1996). Llebot et al. (2014) have suggested that the origin of high variability of water currents corresponds to wind variability which is more effective in shallow depths in comparison to deep waters. For instance, the sea breeze represents a sequence covering a wide range of wind directions and intensities. Fangar Bay provides a good example of such estuaries (i.e. shallow and micro-tidal), where the bathymetry and the geometry are

relevant, as well as being a small-scale bay, which accentuates the action of the wind. The data analysis conducted here, based on two intensive field campaigns, revealed a differentiated pattern in terms of the function of the location (mouth or inner part of the estuary) and the wind conditions (calm or intense). During calm conditions, estuarine circulation linked with strongly stratified conditions were identified in the mouth, associated with strongly stratified conditions. In the inner part, stratification in the water column also occurred, but water circulation did not show a clear pattern. Mixing in the water column occurs during intense wind with substantial modifications in temperature and salinity profiles as will be analyzed later. Particularly during up-bay wind episodes, outward flow conditions were observed in the mouth.

The numerical experiments revealed an axially symmetric transverse structure due to laterally varying bathymetry: up-bay flow occurs in the lateral shoals and down-bay flow in the central channel for up-estuary wind pulses. Consequently, the numerical model's results supported the observed divergence between wind and water flow direction in the center of the mouth in Fangar Bay. This combination of observations and a numerical model confirm that there is a strong transverse variability on water flow when bathymetric effects are considered. Comparing the SIMU 1 and SIMU 2 numerical experiments provides an illustrative example of the influence of bathymetry (see *Figure 15*). These results are consistent with Alekseenko et al. (2013) for a coastal lagoon in the Mediterranean Sea (opposite flow in comparison to wind direction in a central part of the lagoon). Moreover, Sanay & Valle-Levinson (2005) and Narváez & Valle-Levinson (2008) found similar results for large bays than the one cited in this paper, highlighting the

value of numerical experiments seeking the fundamental role played by bathymetry in estuarine circulation. Complementing these contributions, we also focused on geometric stretching in the mouth as well as up-bay wind effects using a numerical model in idealized conditions. The geometric stretching appeared to have a limited effect on water circulation, modulating the water exchange in the mouth (see SIMU 6 vs. SIMU 2). This reduction in the mouth width accords with Geyer (1997), who has suggested that constrictions block wind-induced flushing and affect along-estuary salinity gradients. The mixing mechanism in very-shallow bays due strong winds has been illustrated by Llebot et al. (2014) in a similar domain than Fangar Bay. During these episodes pycnocline is tilted and becomes nearly vertical. In this cases, mixing is fast and largely driven by shear, and the interface becomes less defined. Numerical experiments based on our simple geometric model, including density variability, are suggested for further experiments focusing on the relationship between bathymetry variability and the evolution of the hydrographic structure. Remote winds may also produce water currents which flow against the local wind within the estuary. This behavior has been observed in Delaware or Chesapeake estuaries for low frequencies and is caused by a coastal Ekman set up due to remote wind effect (Garvine, 1985; Wong & Valle-Levinson, 2002). The remote wind effect seems not relevant due to the small scale and depth of the Fangar Bay, being the local frictional effects prevailing such as will be discussed in the next paragraph. Also, energetic wind events in Ebro delta (i.e north-easterlies and north-westerlies winds) tends to affect a substantial percentage of the continental shelf being the wind spatial variability small (Ràfols et al., 2017). However, the implementation of a nested numerical

model using real configuration may solve the remote wind effect in Fangar Bay.

Observations in Fangar Bay indicated that the water circulation was complex during calm periods: current velocities were very small and lacked a clear pattern (see Figure 9, Figure 12 and Figure 13), consistent with other contributions mentioned above. Momentum balance can facilitate analysis of the mechanism governing water circulation (Ràfols et al., 2017). In very shallow domains, the bottom frictional term (τ^B) in depth-averaged momentum balance equations (i.e. $\tau^B/\rho H$) may prove relevant (i.e. H^{-1} relation), indicating a substantial effect on water fluctuations. This means that local bathymetric disturbances may have a relevant role in modifying the flow. Similar findings were attained by Noble et al. (1996), observing how a complex, non-linear residual force leads to a stratified estuary in the case of Mobile (USA). These studies reveal that during calm or weak wind periods, being shallow and narrow areas, estuarine circulation is weak and occurs at the expense of frictional parameters, rendering a stable circulation pattern non-existent.

Although water circulation in the inner Fangar Bay proved chaotic and complex, periods of wind intensity of up 9 m·s^{-1} substantially modified water circulation within the Bay's basin. The effects of the energetic NW winds (up-bay wind) on the hydrodynamics could be clearly observed in the results. The observational results in Fangar Bay revealed that mixing occurred when the wind was equal to 10 m·s^{-1} (Beaufort scale 5), as seen in Figure 14c-d. Weaver et al. (2016) similarly observed that only a constant high-magnitude wind was capable of flushing the Indian River Lagoon, while Coogan et al. (2019) noted that in Mobile Bay, winds of 10–

15 m·s⁻¹ could break the strong stratification and completely mix the water column until strong river discharges re-stratified the water again. Furthermore, Geyer (1997) obtained data from two estuaries on Cape Cod (USA) where weak circulation during onshore winds was altered by wind force, inhibiting circulation in the estuary. Mixing was even observed during summer, when temperatures reached 28ºC (Figure 12f). Persistent warm conditions in Fangar Bay have been associated with increases in mussel mortality and oyster growth (Ramón et al., 2007b). The fact that the NW winds cool the water, as observed in the Figure 12 and Figure 13, in a relatively short time aid aquaculture activity. Increased warm periods in recent years represent a significant economic threat to both aquaculture producers in the bay and authorities in the area.

Wind forcing in shallow waters generates stress and introduces turbulence directly to the water column. The data analysis in Fangar Bay revealed that when the rice channels were opened during calm periods, freshwater inflow predominated and stratification was observed in the water column. Homogenization of the water column occurred during strong NW winds (up-bay wind) episodes. The same was true in periods of closed channels, when stratification was less intense. The large-scale response to wind forced may be characterized using the Wedderburn number (Llebot et al., 2014; Shintani et al., 2010), estimated according to the stabilization effect of the stratification and the destabilization effect of the wind:

$$W = (\Delta \rho g H^2)/L \tau_W \qquad\qquad (1)$$

where τ_w = wind stress along the channel, L = length of the channel, $\Delta\rho$ = density change over L, H = channel depth and g = gravitational acceleration. For a wind of 12 m·s⁻¹, W was equal to 0.68 (i.e. W<1), so the wind produced a rapid, shear-driven mixture as the pycnocline tilted to become almost vertical, with the consequent development of horizontal density gradients (see Figure 14). In the case of weak winds (6 m·s⁻¹), the result was W equal to 2.75 (W>>1), so in this case the pycnocline deepened slowly due to stirring. In the observations presented here, it was seen that the episodes of wind at Beaufort scale 5 came from the NW with intensities of between 10-12 m·s⁻¹, leading to mixing. However, being a small-scale and shallow bay, winds greater than 9 m·s⁻¹ may have been able to homogenize the water column. This could clearly be observed during episode E1, when winds rapidly passed from 5 to 10 m·s⁻¹ and were able to stimulate mixing. When there were breezes (weaker winds, ≤ 6 m·s⁻¹), the bay remained stratified. These results agreed with the calculations of the Wedderdurn number, confirming that a moderately strong wind produces bay-wide mixing, due to the shallowness of the basin (4 m). For deeper depths (for example 10 m), the wind necessary to stimulate shear-driven mixing would be about 25 m·s⁻¹ (i.e. a wind of level 10 on the Beaufort scale). In larger bays, it is not possible for the entire water column to be mixed due to the greater role played by earth rotation and strong density gradients (Narváez & Valle-Levinson, 2008; Sanay & Valle-Levinson, 2005).

The Wedderburn number assumes that the wind is constant and blows from a longer cut-off (T_c). T_c was the length of time needed for the effects of the boundaries to propagate to the open end of the estuary (Llebot, 2010):

$$T_c = \frac{L}{\sqrt{g'h}} \tag{2}$$

where L was the length of the basin, $g' = g\Delta\rho/\rho_0$ was the reduced gravity, $\Delta\rho$ represented the top-bottom density difference, ρ_0 was a reference water density and *h* was the average depth. The relaxation times of the horizontal density gradients (cut-off times) for density differences of ~3 kg·m^{-3}, whose average depth was 2 m, were about 7 h. This means that a wind blowing during this time causes bay-wide water mixing. Therefore, in Fangar Bay, winds from the NW that usually blow for more than one day will cause mixing. The sea breeze, which is of lower intensity and blows for a shorter period than the cut-off period (T_c), is not capable of causing this mixing, as can be seen in Figure 12 and Figure 13. After the wind ceases, the system reverts to its original state, with horizontal isopycnals. The time scale necessary to bring the system back to its original state could be calculated as (Llebot, 2010):

$$T_r = \frac{UL}{g'H} \tag{3}$$

where *H* was the depth of the estuary and *U* was the longitudinal velocity generated during the relaxation process, calculated in turn as:

$$U=\sqrt{g'H} \tag{4}$$

Given that *L* was small, the order of magnitude was of just a few hours. Specifically, for Fangar Bay, T_r ranges of five to nine hours implied very short relaxation periods in comparison to larger domains. A visual

inspection suggested a time lag between wind decay and the apparition of estuarine circulation in Fangar Bay of this order of magnitude (see Figure 12).

The water renewal has a relevant influence on water quality within the bay. A simple assessment of the residence time may be computed dividing the volume of water by the flow rate that comes out of the bay (calculated from the velocities in Figure 16). In these cases, we obtain residence times of 4 days for SIMU 2 and 4, and 1 day for SIMU 1 and 5 and respectively. The rest of the simulations are in the same order of magnitude. From the observed change flow (Figure 12 and Figure 13) the average residence time is estimated in 4 days. The study carried out by F-Pedrera Balsells et al. (2020) compute the residence times in the bay in more detail and some possible modifications to help in the bay management.

Empirical orthogonal functions (EOF) estimated for the alongshore water current directions from the entire vertical profile were used to identify the modal variability in the water current measurements (Figure 17a-d). EOFs allow multivariable data to be decomposed into its main components. Along-axis EOF analysis depicted the prevalence of the first component in both periods: 58/76% (Mouth/Bay) in FANGAR-I and 80/90% (Mouth/Bay) in FANGAR-II. During weak wind or calm periods (i.e. most of the time in FANGAR-I), the main components of the EOF analysis showed crossing-zero (suggesting stratification) with baroclinic conditions (see Figure 17a-c). However, during periods of intense winds, as was true of FANGAR-II, the first component revealed a mixing situation, seen especially at the inner bay B point, with barotropic flows.
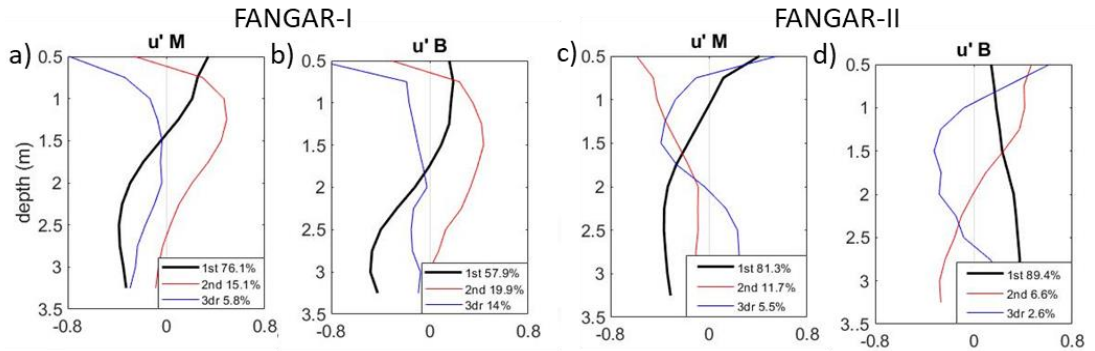
Figure 17. EOF analysis for low-frequency filtered data during FANGAR-I (a and b) and FANGAR-II (b and c) along-shore currents. The legend shows the corresponding percentage of the explained variability.

Rotational effects in small bays and estuaries were expected to be small. Using the geometry of Fangar Bay, the Kelvin number was estimated, which considers the characteristic width of the estuary and the internal radius of deformation (Bolaños et al., 2013):

$$K_e = B/R_{in} \qquad\qquad (5)$$

where R_{in} was equal to $(g'H)^{(1/2)}/f$, g' = reduced gravity, H = channel depth and f = Coriolis force. Rotational effects play a secondary role on the basin circulation when $K_e < 1$, and they can be considered negligible when $K_e << 1$. In the case of Fangar Bay, which is only 2 km wide and 4 m deep, $K_e = 0.39$ (<<1) suggesting that the Coriolis effect is of little importance in terms of water circulation. This was supported by a comparison of SIMU 1 and SIMU 8 (*Figure 15*a and h), where the differences in water currents were negligible.

Questions remain open from observational analysis, in particular the hydrodynamic response during downwind and the spatial variability of the currents. From a numerical point of view, numerical modelling effort may include the bottom roughness sensitivity test, longitudinal and vertical density variations, sea-level oscillations, effect density gradients and baroclinic process due to river discharge sources. The numerical model implemented here is focused on solving the bathymetric effect which affect the wind-driven water circulation due to its shallowness under idealized perspective. So, realistic model implementation is a challenge to evaluate some remaining questions addressed before.

5. Conclusions

The dynamics in small-scale, shallow and micro-tidal estuaries were found to be characterized by very complex circulation in the inner part because of the effectiveness of local wind forcing, as well as a tendency towards stratification due to freshwater inputs that break down in episodes of intense wind lasting a few hours ($O\sim10^1$ h). Once the winds stop blowing, the system returns to its original state with $O\sim10^1$ h, so they are systems with very short relaxation periods. During these episodes of intense winds, bathymetry effects may produce an axially symmetrical transverse structure with outflow on the axis of the central channel, opposite to the wind direction, alongside inflow in shallow lateral areas. Furthermore, being a small-scale bay (2 km wide) and very shallow (average depth 2 m) these winds are capable of mixing all the water inside the bay, and being a narrow domain, the rotation effect is negligible. According to the data obtained from field campaigns and numerical idealized experiments in Fangar Bay, we suggest that a small-scale and shallow bay can be defined as being of 20 km^2 area and about 4 m depth, respectively.

3. Short-term response of Chlorophyll *a* concentration due to intense wind and freshwater peak episodes in estuaries: the case of Fangar Bay (Ebro Delta)

C h a p t e r   3

SHORT-TERM RESPONSE OF CHLOROPHYLL *A* CONCENTRATION DUE TO INTENSE WIND AND FRESHWATER PEAK EPISODES IN ESTUARIES: THE CASE OF FANGAR BAY (EBRO DELTA)

Abstract

Estuaries and coastal bays are areas of large spatio-temporal variability in physical and biological variables due to environmental factors such as local wind, light availability, freshwater inputs or tides. This chapter focuses on the effect of strong wind events and freshwater peaks on short-term chlorophyll *a* concentration distribution in a small-scale and micro-tidal bay such as Fangar Bay (Ebro Delta, northwestern Mediterranean). The hydrodynamics of this bay are primarily driven by local wind episodes modulated by stratification in the water column. Results based on field-campaign observations and Sentinel-2 images reveals that intense wind episodes from both NW (offshore) and SE-E (onshore) cause an increase in the concentration of surface Chl *a* concentration. The responsible mechanisms are the horizontal mixing and the bottom resuspension (linked also to the breakage of the stratification) that presumably resuspends Chl *a* containing biomass (*i.e.* micropyhtobentos) and/or incorporates nutrients in the water column. On the other hand, sea-breeze is not capable of breaking up the stratification so the chlorophyll *a*

concentration does not change significantly during these episodes. It has been concluded that the mixing produced by the strong winds favours an accumulation of Chl *a* concentration, while the stratification, that causes a positive estuarine circulation, reduces this accumulation. However, the spatial-temporal variability of the Chl *a* concentration in small-scale estuaries and coastal bays is quite complex due to the many factors involved and deserve further intensive field campaigns and additional numerical modelling efforts.

Keywords: estuary; Fangar Bay; field measurements; chlorophyll a; physical processes; biological processes; wind; small-scale bay; micro-tidal bay; Sentinel-2.

1. Introduction

Estuaries and bays with an intensive shellfish activity require substantial knowledge on the distribution and concentration of the phytoplankton for a proper management of this production including the growth and harvesting cycles and eventual relocation strategies. In this sense, the biological habitat and the ecosystem characteristics is highly influenced by the physical and morphologic dynamics. Estuaries and coastal environments are characterized by complex hydrodynamics with a high temporal variability in water circulation due to the joint effect of wind, tides, freshwater inflow and other episodic events (Geyer, 1997, F-Pedrera Balsells, Grifoll, et al., 2020; Sanay & Valle-Levinson, 2005; Valle-Levinson et al., 2001). In a small-scale, shallow coastal bay (few meters water depth) such as Fangar Bay in the Ebro Delta (NW Mediterranean Sea), the concentration of Chl *a* concentration shows high variability on a seasonal scale rather than inter-annual scale (Llebot et al., 2011). A maximum peak can be observed during summer and autumn months: from July to November high concentrations have been observed in comparison to low concentrations during February and May (Llebot et al., 2011). Spatial variations also has been observed in Fangar Bay where maximum concentrations were found in the bay mouth and minimum concentrations in the inner bay (Soriano-González et al., 2019). However, due to the small-scale and shallowness of the bay, the temporal scale of the dispersion process is small so the concentration of phytoplankton is quickly homogenised (Ramón et al., 2007a). The link of the Chl *a* concentration and the water circulation has been investigated in Soriano-González et al. (2019), where they explained that the highest concentrations of Chl *a*

occur when the estuarine circulation weakens and decreases after rain events.. However, from an episodic event point of view still some questions remain open. For instance, what is the Chl *a* concentration distribution response to energetic wind episodes? and what about in case of an eventual increasing of the freshwater flow?

These seasonal changes in coastal waters have already been addressed. The seasonal cycle of phytoplankton in open waters near the Ebro Delta is characterized (as in other areas of the Mediterranean) by an increase in the Chl *a* concentration from late autumn, with the weakening and breakdown of the thermocline, culminating in a winter bloom of phytoplankton in January-February (D'Ortenzio, d'Alcalà, 2009; Llebot et al., 2011; Morales-Blake, 2006). These seasonal effects within the bay can be associated with biological factors, such as the availability of nutrients due to the entry of freshwater or the activity of filter feeders (Llebot et al., 2011). In the Ebro Delta bays (i.e. Alfacs at south hemi-delta and Fangar at north hemi-delta), the freshwater discharge plays an important role through man-controlled irrigation channels, as well as contributions from aquifers, being an important source of nutrients in coastal areas (Jou et al., 2019), both inorganic and organic. However, this is not a determining factor since it can happen that when irrigation channels are closed, higher Chl *a* concentrations are reached in comparison to the open channel period (Soriano-González et al., 2019). In consequence, there are many physical and biological processes that can affect the distribution of phytoplankton in coastal waters and estuaries (Artigas et al., 2014; Demers et al., 1979; Geyer et al., 2018; Masson & Peña, 2009) that require intensive field campaigns and long data sets for a robust

analysis. The aim of this contribution is to analyse this distribution in Fangar Bay (as example of a semi-enclosed environment), focusing on the relationship that can exist between the concentration of Chl *a* concentration and energetic wind episodes using *in situ* and satellite data.

The chapter is organized as follows: Section 2 presents a detailed description of two field campaigns carried out in Fangar Bay, and the collection process of Chl *a* concentration data (*in situ* data and the acquisition of satellite images from Sentinel-2). Then, Section 3 (Results) presents the Chl *a* concentration variability according to the different wind episodes, showing both *in situ* and satellite data. Section 4 discusses the presumable mechanisms of variability in Chl *a* concentration related to wind-driven currents and the stratification in the water column in the context of the spatio-temporal process in estuaries and coastal bay. And finally, Section 5 summarizes the main conclusions.

2. Materials and Methods

Recalling what was explained in the previous chapter, Fangar Bay (Figure 18) is a small-scale and micro-tidal bay (tidal range < 2m), which accentuates the action of the wind, and stratified most of the year. This stratification is due to the freshwater flows rather than the contribution of atmospheric heat fluxes. There is a strong transverse variability on water flow due to the bathymetry and the complex geometry. Particularly during prevalent up-bay wind episodes (NW winds), up-bay flow occurs in the lateral shoals and down-bay flow in the central channel for up-estuary wind pulses. The water circulation is complex during calm periods: current velocities are very small and lacked a clear pattern, and a strong stratification is present due to freshwater inputs from the drainage channels (F-Pedrera Balsells et al., 2020a).
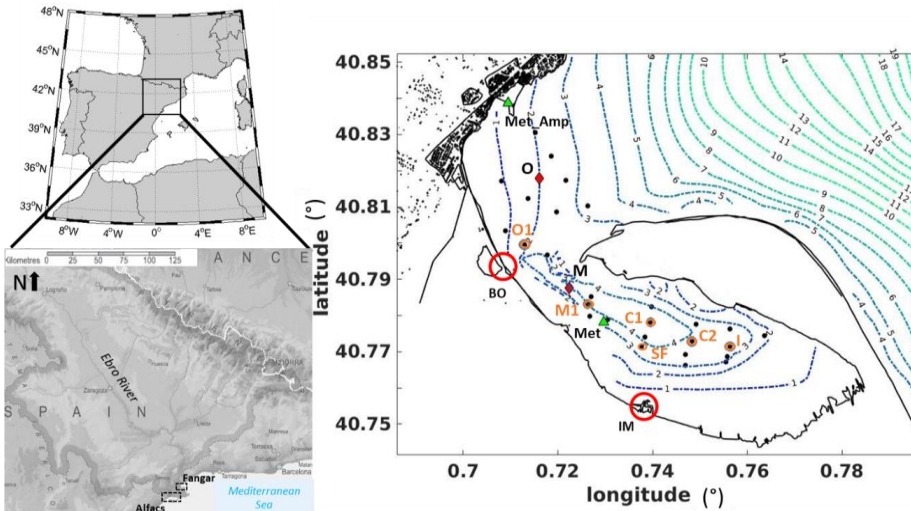
Figure 18. Location of the study area. The red circles show the two main points of freshwater discharges (Bassa de les Olles (BO) and Illa de Mar

(IM)), the red diamonds show the two mooring locations during the field campaigns (M: Mouth; O: Out of the bay) and the green triangle shows the location of the meteorological station (Met and Met_Amp). The black point shows the CTD profile, the black points surrounded by an orange circle are the Chl a water sampling stations and the blue lines show the bathymetry.

2.1. Field campaigns in Fangar Bay

The observational data corresponded to two field campaigns (the first one of one month and the second one around two months) from 26 October to 28 November 2018 (FANGAR-III) and from 5 July to 6 September 2019 (FANGAR-IV), hence autumn and summer, respectively. The data set consisted of two Acoustic Doppler Current Profilers (ADCPs) (mooring points M and O in Figure 18), with the velocity and the direction of the water currents obtained every 10 minutes in 25 cm layers distributed from the bottom to the surface. Moreover, the systems were equipped with pressure systems and a temperature sensor (Vaisala HMP40) and whith an Optical Backscattering Sensor (OBS 3+, Campbell Scientific) that measured water turbidity. A set of Seabird Model 19 CTD (Conductivity, Temperature and Depth) surveys were conducted, one per week during the mooring periods. For each of the CTD campaigns, twenty-seven points were chosen, including both the inner and the outside sections of the bay, where temperature and salinity were measured (see black dots in Figure 18). Similar meteo-oceanographic data and CTD surveys were analysed in detail in F-Pedrera Balsells et al. (2020a) to investigate the water circulation response at the wind forcing within the bay.

During the first campaign, FANGAR-III, two meteorological stations were installed on 16 October, one in the port of La Ampolla (Met_Amp in Figure 18) and the other in the interior of the bay (Met in Figure 18), on top of one of the mussel rafts, near the mouth. During the second campaign, FANGAR-IV, only one meteorological station was installed on 25 June, inside the bay, on the mussel rafts (Met in Figure 18). These stations measure wind, air pressure, air temperature and humidity every 10 minutes. The measurement periods and instruments are summarized in Table 3.

Table 3. Data acquisition instruments and observational periods (years 2018-2019) shown in Figure 18.

Name (ID)	Observations	Period	Data interval (min)
Meteo station	Wind, atmospheric pressure	19 Oct – 28 Nov 2018 25 June – 6 Sept 2019	10
ADCP and OBS mouth (M)	Currents, sea level, waves, bottom temperature, turbidity	26 Oct – 28 Nov 2018 5 July – 6 Sept 2019	10
ADCP and OBS outside bay (O)	Currents, sea level, waves, bottom temperature, turbidity	26 Oct – 28 Nov 2018 5 July – 6 Sept 2019	10
CTD	Temperature, salinity	Nov 2018/ 4 July – 4 Sept 2019	-
Bottle samples	Chl *a*	Oct – Nov 2018 year 2019	-

2.2. Chlorophyll field data collection

Seawater samples were obtained using a silicone hose in order to obtain integrated water samples. For FANGAR-III, samples were collected at an inner point of the bay (C2, Figure 18) and at an outer point (O1, Figure 18), once a week. However, during FANGAR-IV, samples were collected monthly at 6 sampling stations (orange points (O1, M1, C1, C2, I, SF) in Figure 18), both inside and outside the bay. The samples (1L) were maintained in the dark inside a cool box until arrival to the laboratory 1-4 hours after conducting the sampling. At arrival to the laboratory, the samples were immediately filtered through Whatman glass fiber filter grade GF/F (47 mm diameter) under low vacuum. The filters were maintained at -80 °C until analysis. For the analysis the filters were immersed in 10 ml acetone 90 %, ultrasound was applied for 5 minutes, and the tubes were maintained 24 h in the dark at 4 °C. After this time the tubes containing the filters were centrifuged (4000 rpm) during 10 minutes at 4 °C and the supernatant was analysed in a Turner Trilogy fluorimeter equipped with 7200-046-W for the method of Chlorophyll *a* Extracted - Non-Acidification (Welschmeyer, 1994).

2.3. Chlorophyll satellite data collection

The satellite images used were Sentinel-2A and Sentinel-2B, level 1-C, for the period of the campaigns. Sentinel-2A was launched on 23 June 2015 while Sentinel-2B was launched on 07 March 2017. Both are part of a European fleet of satellites aiming to deliver core data to the European Commission's Copernicus program. L1C images

(i.e. not cloud covered) were downloaded from Copernicus Open Access Hub (https://scihub.copernicus.eu/). This level of processing includes radiometric and geometric corrections including ortho-rectification and spatial registration on a global reference system with sub-pixel accuracy.

The Copernicus Sentinel-2 mission comprises a constellation of two polar-orbiting satellites placed in the same sun-synchronous orbit, phased at 180° to each other. The satellites carry a single optical instrument payload, the MultiSpectral Imager (MSI). The MSI samples 13 spectral bands in the visible-near infrared (VNIR) and short wave infrared (SWIR) spectral range at 3 different spatial resolutions (10, 20, 60 m). It aims at monitoring variability in land surface conditions, and its wide swath width (290 km) and high revisit time (10 days at the equator with one satellite, and 5 days with 2 satellites under cloud-free conditions which results in 2-3 days at mid-latitudes) will support monitoring of Earth's surface changes. The coverage limits are from between latitudes 56° south and 84° north (ESA, 2015). Chlorophyll a concentration is computed automatically by the Sentinel Application Platform (SNAP) (https://step.esa.int/main/toolboxes/snap/) programme already tested in Soriano-González et al. (2019). The algorithm (NDCI, Normal Difference Chlorophyll Index developed by Mishra, S. & Mishra, D. (2012) and their corresponding neural networks are split into 2 parts: *i*) retrieval of water leaving reflectance (Rw) from Top of Atmosphere (TOA) reflectances (Rtoa), and *ii*) retrieval of inherent optical properties (IOPs) from water leaving reflectance Rw. The second part can also be used in conjunction with the standard atmospheric correction. All absorptions were normalized to the absorption at 443 nm; the

absorption or scattering coefficients at this wavelength are the output of the IOP neural network. The MSI sensor has had an atmospheric correction applied to it with a C2RCC processor (Case 2 Regional CoastColour) (Brockmann et al., 2016) to obtain the Chl *a* images. C2RCC processor is a multi-mission ocean colour processor, applicable to Sentinel-2 MSI, relied on a large database of radiative transfer simulations, inverted by neural networks (Brockmann et al., 2016). These neural networks do not have a specification for the Ebro Delta. However, as seen in the work done by Soriano-González et al. (2019), the algorithm used is a feasible, although not definitive, solution in this area.

3. Results

3.1. NW wind episode

The time series of the wind measured at the corresponding meteorological station are shown in Figure 19a and Figure 20a. During FANGAR-III, three episodes of NW winds were distinguished: 29-30 October, 9-10 November and 27-29 November (identified as E1, E2 and E3 respectively). The intensity of the wind during these episodes is between 10 - 20 $m·s^{-1}$. During FANGAR-IV, four episodes of NW winds were distinguished: 9-10 July (E4), 15-16 July (E5), 27-29 July (E6) and 12-13 August (E7). During these episodes the wind intensity was lower than during the previous campaign (no more than 10 $m·s^{-1}$). Only the E6 episode exceeded 10 $m·s^{-1}$.

NW cold winds cause cooling of the water in the bay (Garcia & Ballester, 1984), as well as a mixing of the water column. In Figure 19b and Figure 20b it can see how the NW wind causes a cooling in the air temperature, causing the water to cool down in turn (Figure 19c and Figure 20c). In addition, in Figure 19d and Figure 20d it can be seen how the currents become outflow (blue colour) in all the water column. This is corroborated with the flow, calculated from the integration of the currents of the water column, which becomes negative (Figure 19e and Figure 20e). This is also consistent with a vertical mixing of the water column due to the momentum transferred by the wind (F-Pedrera Balsells et al., 2020). During both campaigns, turbidity data was collected with an OBS 3+. However, during the FANGAR-IV campaign
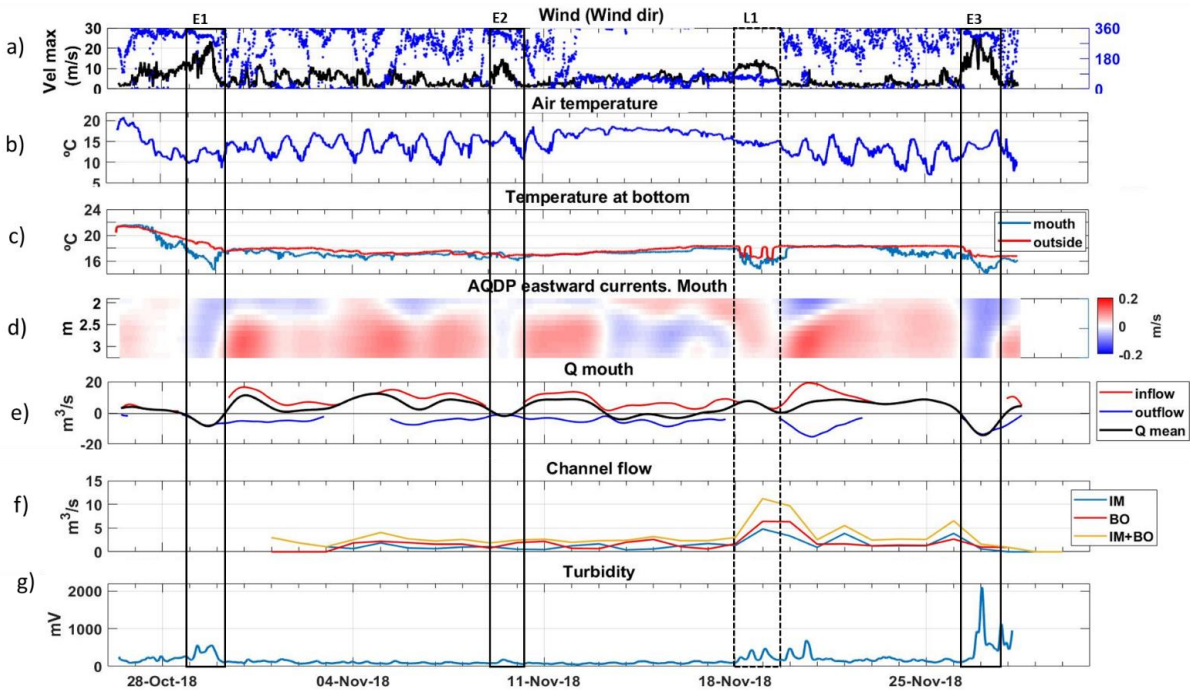
Figure 19. From top to bottom, wind speed (a), air temperature (b), bottom water temperature (c) alongshore currents in mouth (d), inflow (positive) and outflow (negative) of bay (e), flow of the discharge channels (f), turbidity (g). The black boxes show the events of the NW and the dotted black boxes show the events of the E, during FANGAR-III.

data recorded show not feasible values being not useful for the analysis. The data collected by the OBS during FANGAR-III, shows increases in turbidity during the NW episodes, marked in the Figure 19g with black boxes. It means, during NW wind episodes (i.e. E1 to E7), the water circulation is characterized by outflow through the central channel and inflow in the lateral shoals. In addition, during episodes E1 to E3 an increase in turbidity was also observed (see Figure 19g).
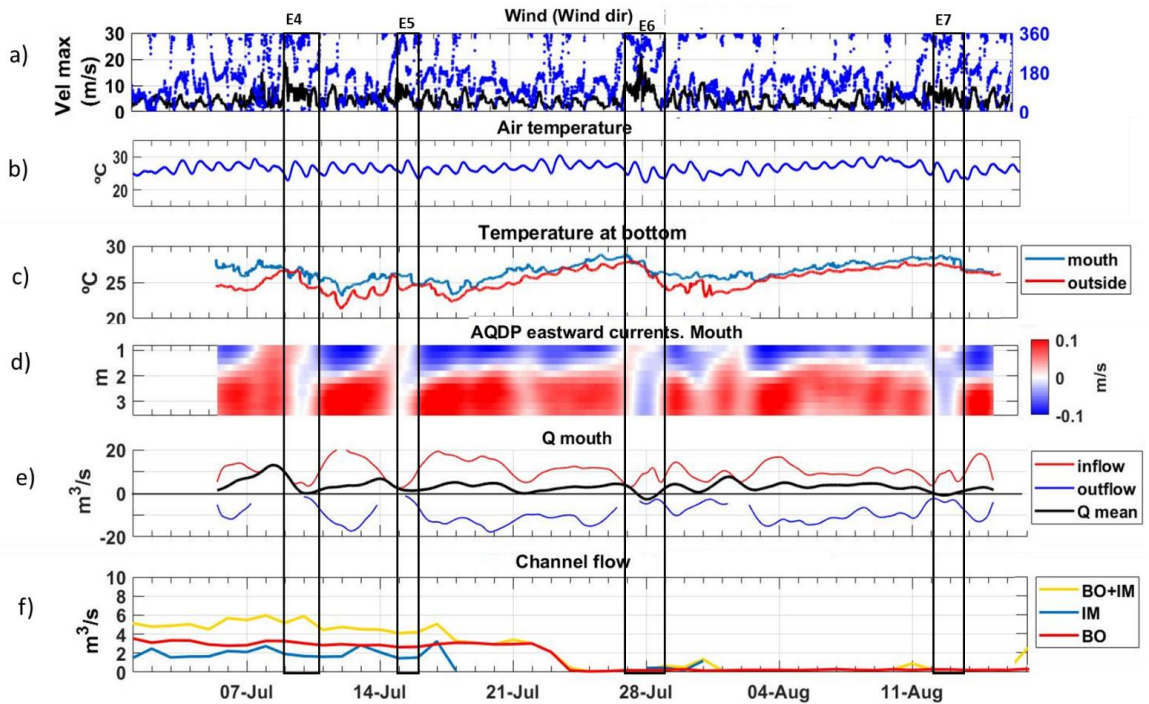
Figure 20. From top to bottom, wind speed (a), air temperature (b), bottom water temperature (c) alongshore currents in mouth (d), inflow and outflow of the mouth (e), flow of the discharge channels (f). The black boxes show the events of the NW during FANGAR-IV.

Chl *a* concentrations during strong NW wind episodes can also be observed using Sentinel-2 images (Figure 21). During the FANGAR-III period, fewer satellite images were available, and those that were available, some of them are of low quality due to the presence of clouds that make satellite observation difficult or due to sun glitter. The images from the FANGAR-IV period were clearer and more meaningful. These images also show increases in Chl *a* concentrations (approx. 5 - 8 mg·m^{-3}) during these wind episodes, and a decay after these episodes.
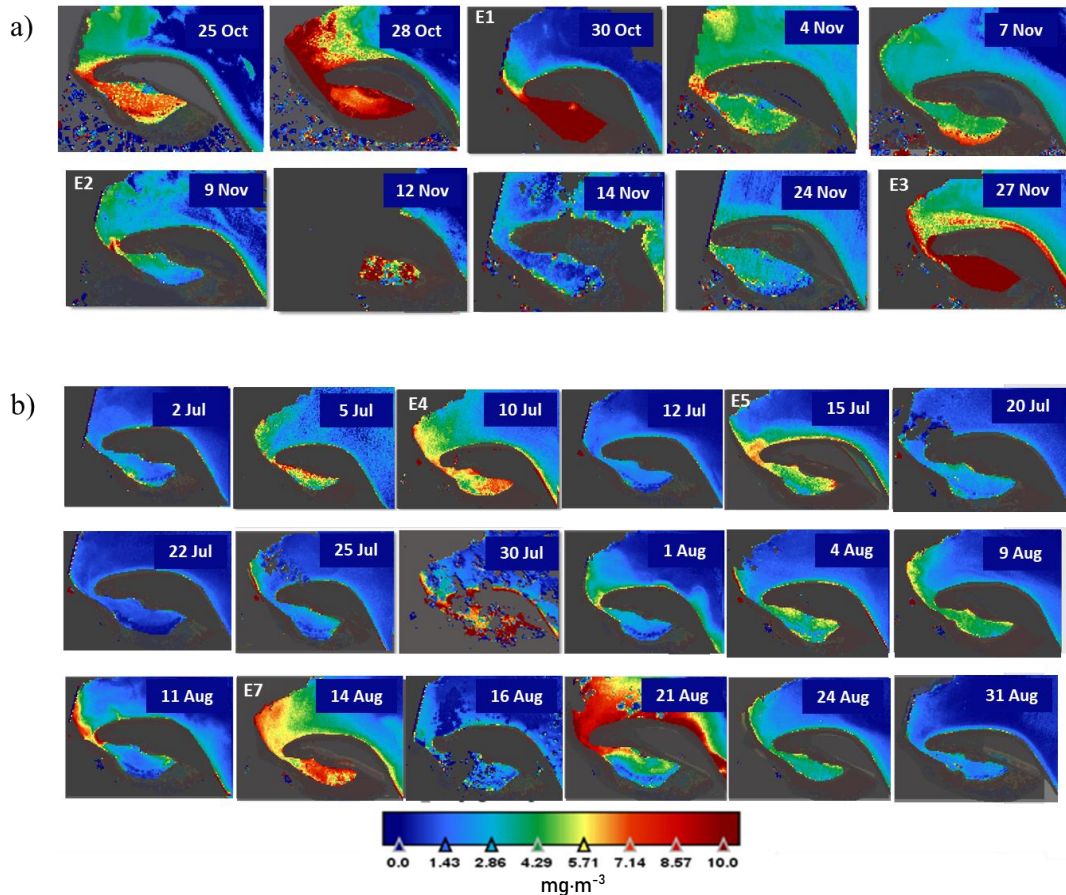
Figure 21. *Sentinel-2 images during FANGAR-III (a) and during FANGAR-IV (b). The wind episodes are marked in each corresponding image with white letters. Episodes L1 and E6 do not match with any satellite image, so they are not represented in the figure.*

Figure 22 shows the evolution of Chl *a* concentration during the field campaign. The episodes of NW winds are shown with boxes of dashed line. In general, during all NW wind events, the concentration of Chl *a* concentration tends to increase, over 6 mg·m^{-3}. For instance,

values of Chl *a* concentration during E1 reveal larger values in comparison to precedent data. Discrepancies in Chl *a* concentration during E2 are observed likely associated to short episode and less intensity in comparison to E1 or E3. This figure also shows that the satellite tends to overestimate (in the case of FANGAR-III) or underestimate (in the case of FANGAR-IV) the data *in situ*, but the temporal evolution of satellite data tends to follow the data collected during the filed campaign. However, note that the lack of high frequency observations suggests a non-conclusive inter-comparison between both data sets. The picture during the summer field campaign also show an increase of Chl *a* concentration during the NW episodes and a subsequent dropping of Chl *a* concentration when the wind calms down. The increase in the E4 and E5 episodes was lower than in the other episodes (< 6 mg·m^{-3}), but the previous concentrations were around 3 mg·m^{-3}, so the increase is clear. The E6 and E7 episodes show peaks similar to the episodes of the previous campaign (over 6 mg·m^{-3}). The vertical mixing response at strong wind events may be characterized by the Wedderburn number, $W=(\Delta\rho g H^2)/L\tau_W$ (F-

Pedrera Balsells et al., 2020a; Shintani et al., 2010) which evaluates the stabilization effect of the vertical stratification versus the destabilization effect of the wind. In Fangar Bay case, strong NW-NE winds (>10 m·s^{-1}) corresponds to W is equal to 0.98 (i.e. W < 1), so the wind produces rapid, shear-driven mixing as the pycnocline tilted until it became almost vertical (F-Pedrera Balsells et al., 2020a). Note that there is a large difference between *in situ* and satellite data for the E6 event. This is also observed for the E1 episode. Some possibilities of these differences are explained in the discussion section. Just after all

these Chl *a* concentration peaks a sharp decrease in Chl *a* concentration can be observed (values of around 2 mg·m⁻³ in the FANGAR-III campaign, and 4 mg·m⁻³ in the FANGAR-IV campaign). Finally, comparing both campaigns autumn Chl *a* concentration show larger mean values in comparison to summer, however peak values during NW wind episodes show similar values (for instance 6.96 mg·m⁻³ during E3 and 7.06 mg·m⁻³ during E6).
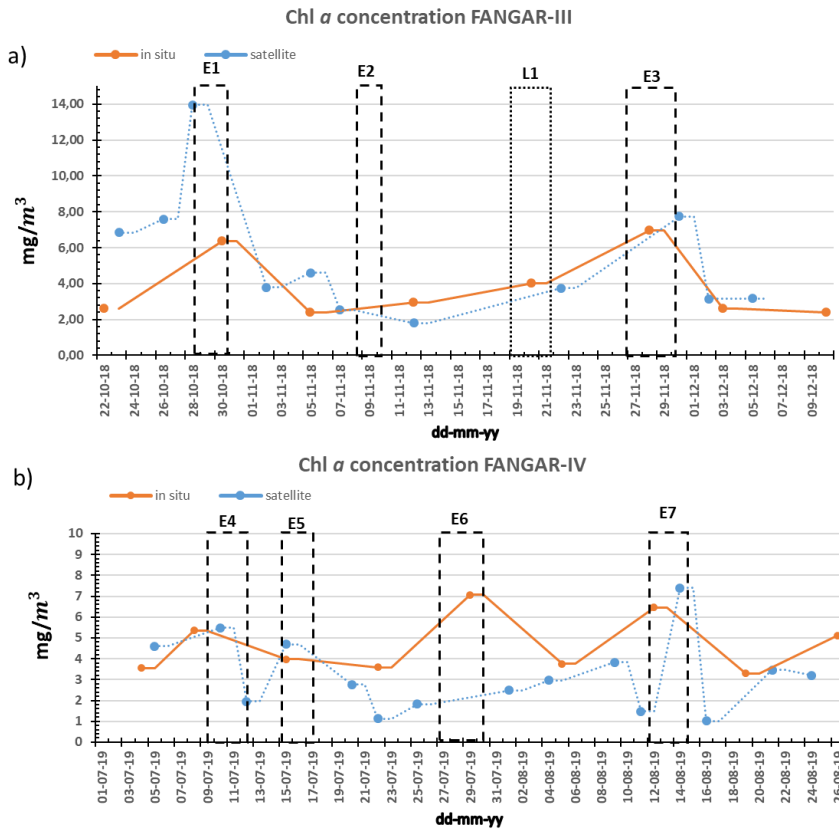
Figure 22. Time series of Chl a *concentration in situ and satellite images, at central point in the bay for FANGAR-III (a) and FANGAR-IV (b). The boxes with dashed line mark the episodes of the NW wind while the dotted box marks the episodes of the E-SE wind.*

3.2. E-SE wind episode

An easterlies wind episode, from 13 November to 20 November of 2018, is observed in Figure 19a (marked as dotted black box). An inversion of the positive estuarine circulation (i.e. outflow near surface and inflow near the bottom) (Figure 19d) is observed during this wind episode. Specifically, from 18 to 20 November (L1), wind intensity period (> 10 m·s^{-1}) is associated to an inflow in the central channel of the mouth. This wind also caused a decrease in the water temperature as can be seen in the Figure 20c. Figure 22 shows *in situ* data measurement during this wind episode. A significant increase in Chl *a* concentration is observed (4 mg·m^{-3}), and also for satellite data (3.9 mg·m^{-3}) followed for a dropping of Chl *a* concentration in the subsequent days. The water circulation (Figure 19d) also show a uniform pattern in the water depth (positive inflow), similar to NW winds episodes, suggesting vertical mixing occurs in the water column (no CTD surveys are available during this period). A small increase in bottom turbidity is also observed during this episode (Figure 19g). During the L1 episode there were no satellite images so we cannot compare it with the data *in situ*.

3.3. Breeze episode

During both campaigns, the sea breeze was characterized by daily southerlies with a wind intensity of 6 m·s^{-1}, as can be seen in the Figure 19 (unmarked events). The water temperature during FANGAR-III ranged from 14°C to 21.5°C (Figure 20c), with an average of about 18°C, both in the mouth and in the outer of the bay. During FANGAR-IV

the water temperature range was between 21°C and 29°C (Figure 20c), with an average of 26°C. According to CTD surveys, the wind is not able to mix the water column during the sea breeze as can be seen from the average salinity profiles (Figure 23), so strong stratification prevails due to freshwater inputs. In Figure 21 and Figure 22, in opposite to the NW wind episodes, during calm periods (breezes) low concentrations are observed (< 4 mg·m^{-3}). The Wedderburn number for the sea breeze episodes (winds about 6 m·s^{-1}) is equal to 2.75 (W >> 1), so that in this case the pycnocline deepened slowly (see Figure 23) due to stirring (F-Pedrera Balsells et al., 2020a).
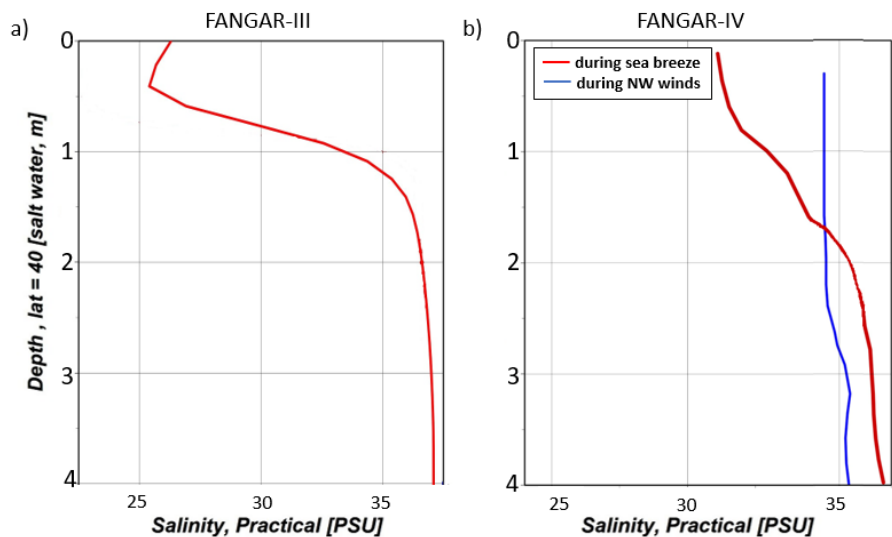
Figure 23. Average salinity profiles from FANGAR-III (a) and from FANGAR-IV (b) from CTD surveys.

3.4. Freshwater inputs

During both campaigns the irrigation channels were open (Figure 19f and Figure 20f), so the supply of nutrients was comparable. The flow rate was approximately 6 $m^3 \cdot s^{-1}$ in both periods. During FANGAR-III two peaks of freshwater input can be seen, from 19 to 22 November, and during 26 November (Figure 19f). These peaks originated from increased pumping of water. This coincides with the L1 episode, which causes more water entering to the bay. To prevent salt water from entering the channels, rice farmers increase the volume of water pumped. During FANGAR-IV, freshwater inputs are observed during the first half of the campaign. After that, there is no data available for the IM point and the contribution of BO is reduced to almost zero (Figure 20f).

The temporal variability of Chl *a* concentration with freshwater discharges does not show a significant correlation: R = 0.107 ($\rho < 0.05$). The nutrient inputs that are discharged by the irrigation channels were presumably constant over time. This fact does not allow us to check if there is a correlation between freshwater discharges and Chl *a* concentration events since during the field campaigns the channels were always opened.

4. Discussion

Previous research in coastal bays and estuaries suggests that the typical temporal dynamics of Chl *a* concentration exhibit a seasonal cycle (Artigas et al., 2014; de Madariaga, 1995; Llebot et al., 2011; Pinckney et al., 1998). In the case of Ebro Delta Bays (i.e. Alfacs and Fangar) the seasonal cycle is dominated by the nutrient inflow from the irrigation channels which reduce its water volume from January to March/April (Artigas et al., 2014). However, the impact on Chl *a* concentration at short term periods, such as wind episodes remains unexplored probably due to the lack of spatio-temporal resolution of the data set. Results from FANGAR field campaigns (III and IV), jointly with remote sensing data, has brought a good opportunity to consider the Chl *a* concentration variability analysis at short time scales and in particular due to strong wind episodes and freshwater flow peaks.

The observations in Fangar Bay have shown an increase of the Chl *a* concentration after wind episodes. Proportionality of wind intensity and Chl *a* concentration increase seems consistent using *in situ* data. For instance, the increase in Chl *a* concentration during E1 was larger in comparison to E2 when the wind intensity was larger (E1 reached 15-20 $m·s^{-1}$ in comparison to E2 that was 10 $m·s^{-1}$). Nevertheless, negligible correlation between wind and *in situ* Chl *a* concentration is observed: R=-0.16 ($\rho < 0.05$) for FANGAR-III and R=-0.13 ($\rho < 0.05$) for FANGAR-IV. During FANGAR-III a time lag of 3h between wind and Chl *a* concentration reveals larger correlation than zero-lag correlation (R=0.28 and R=0.56 for satellite and *in situ* observations respectively). However, the scarce or limited data set

available suggest that further high frequency measurements are needed to conclude lag correlations which would represents a delay between the wind episodes and the Chl *a* concentration growth response within the bay. Therefore, although qualitatively correspondence between strong wind episodes and Chl *a* concentration peaks (see Figure 22), future works include intensive field campaigns to capture high frequency behavior on Chl *a* concentration evolution.

The intense wind episodes cause a mixing in the water column according to the ADCP measurements (i.e. barotropic flow during wind episodes) and CTD surveys (homogeneous profiles in density). In this sense, two responsible mechanisms that increase Chl *a* concentration during wind episodes has been may eventually occur: the resuspension of Chl *a* containing biomass and the supply of nutrients from the bottom to the water column (Delgado, 1989; Díez-Minguito & de Swart, 2020; Loureiro et al., 2009). Benthic algal (or microphytobentos) blooms may be resuspended by wind in coastal bays and estuaries (de Jonge & Van Beusekom, 1995). Chl *a* concentration is usually significantly higher in muddy substrates than in sandy substrates, as is the case in Fangar Bay (Delgado, 1989). Several authors (de Madariaga, 1995; Pinckney et al., 1998; Sondergaard et al., 1992) discuss the presence of benthic microalgae that usually live in the first centimeters of the sediment according to water samples. Recently, Díez-Minguito & de Swart (2020) demonstrated that as suspended sediment concentration increased so did Chl *a* concentration at spring-neap and tidal scales due to simultaneous resuspension of sediment and Chl *a* containing biomass induced by tidal shear stress. In this sense, Grifoll et al.

(2019), show evident relations in time-series observations in Alfacs Bay between strong wind events and increase of near bottom turbidity. Turbidity measurements in Fangar Bay (Figure 19g) have shown a relation between the increase of near-bottom turbidity and intense wind episodes making plausible the incorporation of Chl *a* containing biomass in the water column during the wind episodes. Also, several remote sensing images shown in Figure 21 indicates that the highest concentrations of Chl *a* occurs near the coastline (i.e. bay shoals) where light penetrate deeper in the water column, thereby favoring the growth of algal microorganisms at the bottom. The other mentioned mechanism of increasing Chl *a* concentration is related with the direct incorporation of nutrients from the bottom. In Ebro Delta coastal bays, several episodes of algal blooms have been reported and linked to increased nutrient concentrations (Loureiro et al., 2009; Roque et al., 2009), which were possibly triggered by resuspension mechanisms. The lack of correlation between the freshwater flow (associated at increase of nutrients) and the short term increase of Chl *a* concentration within the bay may indicates a prevalence of the first hypothesis. Unfortunately, the lack of nutrients and full water column surveys during these wind episodes cannot confirm the importance of each one of the postulated hypothesis of Chl *a* concentration growing during energetic wind events. In this sense, Sarangi et al. (2008) have also shown that high concentration of Chl *a* can be an indicator of surface water circulation driven particularly by local winds. Soriano-González et al. (2019) show that when irrigation channels are closed in Fangar Bay, the wind can play a very important role, linking at large-term scale high Chl *a* concentration increased with prolonged episodes

of strong NW winds (i.e. winter and autumn). During sea-breeze conditions, when the wind intensity is lower in comparison to NW episodes, the Chl *a* concentration does not show a noticeable increase because the stratification remains unaltered (Figure 23). The low Chl *a* concentration periods during stratification in the water column also were found by Artigas et al. (2014) in Alfacs Bay and Soriano-González et al. (2019) for both bays (i.e. Fangar and Alfacs). The larger impact of NW and E-SE wind episodes (in comparison of sea-breeze) on Chl *a* concentration is due to the characteristics of the bay, which is very shallow and micro-tidal. In this sense, winds >10 m·s^{-1} (above typical sea-breezes intensities) immediately cause mixing in water column and likely resuspension events (Cerralbo et al., 2015; F-Pedrera Balsells et al., 2020a, Grifoll et al., 2019). Also, the duration of these strong winds associated with E-SE and NW events is a few days, compared to the strong winds that may occur during sea breeze periods, which are a few hours. In consequence, there are substantial arguments to associate the wind induced resuspension (during NW and E-SE strong wind events) as a responsible mechanism of Chl *a* concentration increase fueled by the supply of nutrients or biomass from the bottom of the water column.

The analysis in Fangar Bay of Chl *a* concentration evolution at short term scales and its response to energetic wind events may be useful in similar domains. In particular, to small bays, estuaries and lagoons in the Mediterranean Sea where the tide-induced hydrodynamics used to be limited and stratification in water column tends to occurs. However, coastal bays may show substantial differences due to the influence of the geometry and bathymetry in the

hydrodynamics among other factors. For instance, Artigas et al. (2014) observed substantial heterogeneity in the distribution of Chl *a* concentration in the Alfacs Bay, finding higher concentrations in the innermost area of the bay. Our observations have shown that the distribution of Chl *a* concentration in the Fangar Bay is more homogeneous throughout the bay during NW and E-SE wind episodes in comparison to Alfacs Bay. The small size of Fangar Bay (in comparison to Alfacs Bay; 56 km^2 vs 12 km^2) may contribute to these differences on spatial variability in Chl *a* concentration. The small-size suggest a short temporal scale to homogenize the water properties within the bay (F-Pedrera Balsells et al., 2020a; Llebot et al., 2014). F-Pedrera Balsells et al. (2020a) used both ADCP data and numerical modelling to investigate the water circulation patterns in Fangar Bay. They found that the bathymetry effects may produce an axially symmetrical transverse structure with outflow on the axis of the central channel, opposite to the wind direction, alongside inflow in shallow lateral areas (see Figure 19d and Figure 20d). These water circulation patterns induce horizontal mixing within the bay due to the effectiveness of wind forcing in the shallowest areas of the bay. In this sense, the water circulation pattern within the bay may favor the increase of Chl *a* concentration during the wind episodes due to the redistribution of nutrients within the bay (not only from the resuspension events but also from the irrigation channels). Also during intense NW wind episode, satellite data shown a sharp transition of Chl *a* concentration near the mouth (see images from 30 October and 27 November in Figure 21) likely induced by a pushing effect of NW wind on surface waters near the mouth. These water

circulation patterns also may favor the increase of Chl *a* concentration during and after intense NW wind episodes.

Inspired on the previous analysis of the wind episodes on Chl *a* concentration distribution, the increase of freshwater flow as a source of nutrients might be associated to an increase of Chl *a* concentration as has been suggested by several authors in a long-term analysis (see Artigas et al., 2014; Llebot et al., 2011; Soriano-González et al., 2019). However, both *in situ* data and satellite images do not show an evident relation between Chl *a* concentration increase and freshwater peaks at short-term. The variability shown by the freshwater inflow from the irrigation channels is low compared with the mean values (see Figure 19f and Figure 20f). Neither, hydrodynamic variables (i.e. water currents) does not show correlation with the freshwater peaks. Probably the effect of irrigation is relevant at long-term scale (linked with the Chl *a* seasonal cycle reported) in comparison to short-term variability of Chl *a* concentration which the effect seems negligible.

From a methodological perspective satellite images have provided a valuable source of information of the spatial distribution of Chl *a* concentration in Fangar Bay. Sentinel-2 images show that during FANGAR-III Chl *a* concentrations are higher than during FANGAR-IV. Also satellite data during FANGAR-III campaign tends to overestimate *in situ* data being likely the satellite sensor capturing more suspended matter during autumn in comparison during summer. The Chl *a* increasing is presumably linked to the increase of turbidity within the bay during the autumn due to the intense wind episodes (mainly NW wind episodes) increasing the resuspension events (Grifoll et al., 2019)**.**

Fangar Bay as example of coastal and very shallow estuary shows limitations from the remote sensor to distinguish between Chl *a* concentration and suspended matter, in addition the increased reflectance might be also related to bottom reflectance (Soriano-González et al., 2019). Another plausible effect on Chl *a* variability may be associated at the presence of mussels during summer in Fangar Bay that act as phytoplankton filter feeders. Mussel farming cycle begins at the end of the year and harvest ends in August-September (Ramón et al., 2007), so in October-November the presence of these filter feeders is scarce, allowing the phytoplankton to grow in greater numbers. In addition, high water advection rates typical of an estuary can lead to low productivity, even under conditions of high nutrient concentrations (i.e. open channels), if dilution rates are higher than phytoplankton growth rates (Llebot et al., 2011). In this case, the combined effect of resuspension events favored by horizontal water transport within the bay during the autumn (which NW episodes occurs) may be co-responsible of larger concentrations of Chl *a* during autumn in Fangar Bay.

The pattern of these two different situations of water circulation and their effects on Chl *a* concentration in Fangar Bay are shown in Figure 24. According to the results, when the wind blows from the NW and from the E-SE, with an intensity of 10 m·s^{-1} or more, there is a modification in the estuarine circulation, causing mixing throughout the water column and along the whole bay. This implies a homogenisation of the water column and an increase in Chl *a* concentration. When the sea breeze blows, the situation reinforces the stratification in the bay, causing a decrease in the concentration of Chl *a*.
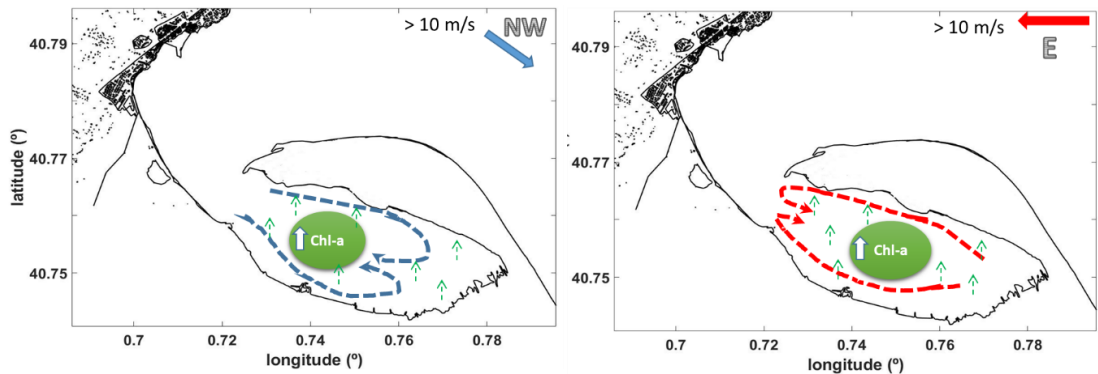
Figure 24. Water circulation and Chl a *concentration patterns in Fangar Bay. The dashed lines show the water circulation within the bay and the blue and red arrow shows the wind direction including the wind intensity minimum value (aprox.) for stratification breakage and consequently an increase of the Chl* a *concentration. The small green arrows show the resuspension of matter (nutrients or Chl* a*-containing biomass) from the bottom, caused by winds.*

The mussel and oyster farms in Fangar Bay has economic relevance in the Ebro Delta region. In this sense, it is important to know the distribution and dynamics of Chl *a* in Fangar Bay. This investigation may support decision making strategies for local shellfish producers, regulating entities and stakeholders. Eventual relocation of mussels rafts or optimizing harvesting period activity may be benefited from an improved understanding of Chl *a* concentration evolution from episodic wind and freshwater discharge events for forecasting purposes (Artigas et al., 2014; Llebot et al., 2011, 2014).

5. Conclusions

Results based on intense field campaigns and Sentinel-2 images reveals that intense winds from both NW (offshore) and E-SE (onshore) cause an increase in the concentration of Chl *a* at surface in Fangar Bay. Data have shown that there is substantial correlation with wind peaks (e.g. NW wind episodes E3, E4 or E7) alternating negligible correlations periods. However, there are not enough Chl *a* data for outright affirmations. Even that the satellite data not always coincide with the *in situ* data (sometimes overestimating and sometimes underestimating), both patterns were similar. The algorithm used for image satellite (i.e. NDCI), still uncertain for shallow coastal bays, provides feasible results. It remains for future work to compare various existing methods for the processing of this type of images for the Fangar Bay. The responsible mechanisms of Chl *a* increase during the wind episodes are the horizontal mixing and the bottom resuspension (linked also to the breakage of the stratification) that presumably resuspends Chl *a* containing biomass and/or incorporates nutrients in the water column. On the other hand, sea-breeze is not capable of breaking up the stratification, so the Chl *a* concentration does not change significantly during sea-breeze events. It has been concluded that the mixing produced by the strong winds favours an accumulation of Chl *a* concentration, while the stratification, that causes a positive estuarine circulation, reduces this accumulation. From our analysis the freshwater peaks, even that it is a relevant factor on Chl *a* concentration evolution at large-term (i.e. intra-annual cycle), its variability is not correlated with the Chl *a* concentration evolution at short-term. However, the biological and hydrodynamic linked processes

are very complex and would require additional field sampling focused on improving the spatio-temporal frequency of sampling during wind and freshwater peak episodes. In addition to the use of a coupled hydro-ecological numerical model could also help to understand these processes.

4. Biological response to hydrodynamic factors in estuarine-coastal systems: a numerical analysis in a micro-tidal bay.

C h a p t e r   4

BIOLOGICAL RESPONSE TO HYDRODYNAMIC FACTORS IN ESTUARINE-COASTAL SYSTEMS: A NUMERICAL ANALYSIS IN A MICRO-TIDAL BAY.

Abstract

Phytoplankton primary production in coastal bays and estuaries is influenced by multiple physical variables, such as wind, tides, freshwater inputs or light availability. In a short-term perspective these factors may influence the composition of biological variables such as phytoplankton biomass, as well as the amount of nutrients within the waterbody. Observations in Fangar Bay, a small, shallow, stratified and micro-tidal bay in the Ebro Delta (NW Mediterranean Sea), have shown that during wind episodes the biological variables undergo sudden variations in terms of concentration and distribution within the bay. The Regional Ocean Model System (ROMS) coupled with a nitrogen-based nutrient, phytoplankton, zooplankton, and detritus (NPZD) model has been applied to understand this spatio-temporal variability of phytoplankton biomass in Fangar Bay. Idealised simulations prove that during weak wind events (< 6 m·s^{-1}), the stratification is maintained and therefore there is not dynamic connection between surface and bottom layers, penalizing phytoplankton growth in the whole water column. Conversely, during intense wind events (>10 m·s^{-1}) water column mixing occurs,

homogenising the concentration of nutrients throughout the column, and increasing phytoplankton biomass in the bottom layers. In addition, shifts in the wind direction generate different phytoplankton biomass distributions within the bay, in accordance with the dispersion of freshwater plumes from existing irrigation canals. Thus, the numerical results prove the influence of the freshwater plume evolution on the phytoplankton biomass distribution, which is consistent with remote sensing observations. The complexity of the wind-driven circulation due to the bathymetric characteristics and the modulation of the stratification implies that the phytoplankton biomass differs depending on the prevailing wind direction, leading to sharp Chl *a* gradients and complex patterns.

Keywords: phytoplankton biomass, ROMS-NPZD model, wind, biological parameters, physical parameters, Fangar Bay.

1. Introduction

The intense biological activity of estuaries and coastal bays and their importance as a source of resources and socio-economic services is well known. The use of these areas as aquaculture zones has provided great benefits as well as great problems (Ramón et al., 2007; Llebot et al., 2010, 2011; Soriano-González et al., 2019). The influence of the terrestrial environment and human activity in these domains provide the nutrients necessary to create ecosystemic value (Lohrenz et al., 1997). The biological evolution of these waterbodies is strongly affected by physical factors. For instance, strong winds may controls the inner water circulation (Geyer, 1997; Alekseenko et al., 2013; Cerralbo et al., 2015) and, together with topographic effects, can even cause the current to flow against the wind direction in the central channels (Xie & Li, 2018; F-Pedrera Balsells et al., 2020a). Freshwater inputs can also have a considerable effect on the water circulation (Cerralbo et al., 2014) and, acting as fluvial nutrient suppliers, can determine the temporal and spatial variability of phytoplankton biomass (Geyer et al., 2018; Jiang et al., 2020). In this sense, the use of coupled physico-biological numerical models as a tool to understand the complexity of the phytoplankton regulatory mechanism in estuaries has increased in recent years, complementing *in situ* data and satellite imagery (Llebot et al., 2010; Artigas et al., 2014; Jiang et al., 2020). These numerical models can provide information on the current state of the estuary, create hypotheses and numerical experimentation, and predict certain events and ecosystem responses (Stow et al., 2009; Llebot et al., 2010).

In small and shallow estuaries, the effects of both the physical and biological mechanisms become more complex due to the geometry of the basin itself. Moreover, in the bays of the Ebro Delta (i.e. Alfacs in the southern hemidelta and Fangar in the northern hemidelta), freshwater discharges from rice field irrigation channels also play an important role, together with aquifer contributions, being an important source of nutrients for the coastal areas (Jou et al., 2019), both inorganic and organic. In a small-scale coastal bay such as Fangar Bay, where depths are only of a few metres, chlorophyll a (Chl *a*) concentrations tend to show a high variability on a seasonal scale rather than on an interannual scale (Llebot et al., 2011), with higher concentrations found during the summer (Ramón et al., 2007b). In this sense, Chl *a* concentrations in Fangar Bay tend to show a larger variability as compared to other coastal domains such as the Ría de Arousa (Ramón et al., 2007b) or Alfacs Bay (Artigas et al., 2014).

Previous investigations in Fangar Bay revealed that, during wind episodes, the biological variables undergo sudden variations in terms of concentration and distribution within the bay (F-Pedrera Balsells et al., 2021). *In situ* measurements obtained during specific field campaigns and remote sensing observations suggested a link between the breaking of the stratification during these episodes and the Chl *a* distribution in the bay, with intense winds causing an increase in the Chl *a* concentration values. The role of the discharges from the irrigation canals remained unclear because the freshwater outflow was constant during the field campaigns. However, the spatial-temporal variability of the Chl *a* concentration observed in the

field campaigns was quite complex due to the many factors involved, and deserved additional modelling efforts. The purpose of the present study is to further this first assessment by investigating the biological response of the bay to wind episodes and freshwater inputs through the combination of idealised numerical simulations and observations. For this, a biological model is embedded into a validated hydrodynamic model to reproduce the dynamics within the bay. Extensive field data and previous hydrodynamic knowledge converts Fangar Bay in a unique study area to investigate the biological response in an area with large spatio-temporal variability on Chl *a* evolution.

The chapter is organised as follows: Section 2 presents a detailed description of the model used, as well as a brief description of the pre-processing satellite images. Section 3 presents the results of the numerical simulations concerning the evolution phytoplankton, salinity and nutrients, as well as a comparison with satellite images. Section 4 discusses the effects of the wind and freshwater plume on the biological variables comparing with sites. Finally, section 5 summarises the main conclusions and suggests future works to be carried out.

2. Material and Methods

Remember that Fangar Bay (Figure 25) is micro tidal, with a tidal range smaller than 2 m, which accentuates the action of the wind, and is stratified most of the year mainly due to the freshwater flows. Because of its bathymetry and complex geometry there is a strong transverse variability of the water flows, particularly for prevalent up-bay wind episodes (NW winds), during which up-bay flow occurs in the lateral shoals and down-bay flow in the central channel for up-bay wind pulses.
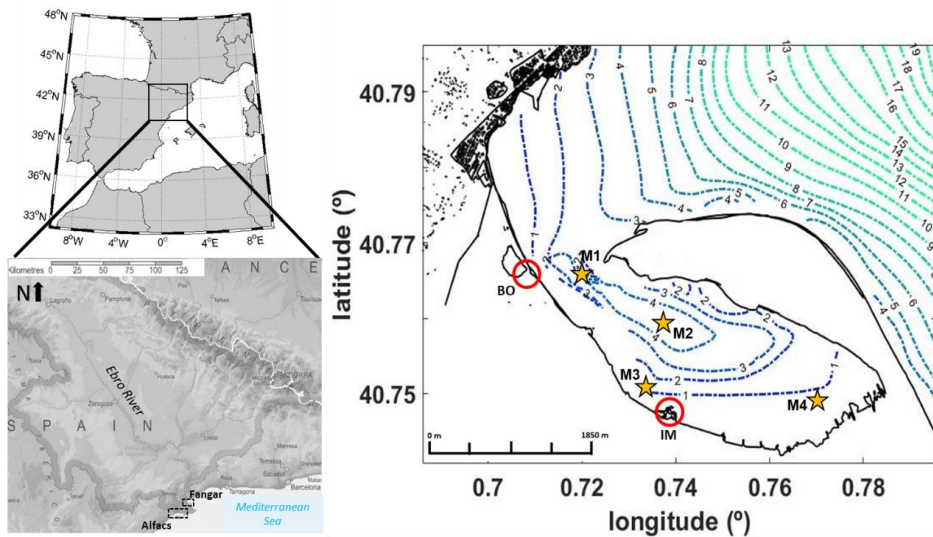
Figure 25. Location of the study area. The red circles show the two main points of freshwater discharges (Bassa de les Olles (BO) and Illa de Mar (IM). The yellow stars show the location of the control points used for the numerical model results. The bathymetry is also shown in the figure.

These winds also cause homogenisation of the whole water column. On the other hand, during calm periods the water circulation is complex: current velocities are very small and lack a clear pattern, and the bay is strongly stratified due to the freshwater inputs from the drainage channels (F-Pedrera Balsells et al., 2020a).

2.2. Numerical model and experiments design

A set of numerical experiments were conducted using the Regional Ocean Model System (ROMS) to analyse the link between the hydrodynamic and Chl *a* response to the wind in small and shallow estuaries. The ROMS numerical model is a 3D, free-surface, terrain-following numerical model that solves the Reynolds-Averaged Navier-Stokes equations using hydrostatic and Boussinesq assumptions (Shchepetkin & McWilliams, 2005). ROMS uses the Arakawa-C differentiation scheme to discretize the horizontal grid in curvilinear orthogonal coordinates and finite difference approximations on vertical stretched coordinates (Haidvogel et al., 2007). The numerical details of ROMS are described extensively in Shchepetkin & McWilliams (2005). This model has been used and validated in similar bays and estuaries, such as Alfacs Bay located south of the Ebro Delta (e.g. (Cerralbo et al., 2014, 2015, 2019)) and in the Fangar Bay (see Annex A). The domain used for the experiments consists of a regular 107x147 grid with a horizontal resolution of about 70 m and 10 sigma levels in the vertical direction. The model boundary is located 10 points away of the mouth entrance to avoid boundary noise. The hydrodynamic bottom boundary layer was parametrised with a logarithmic profile using a characteristic

bottom roughness height of 0.2 m. The turbulence closure scheme for the vertical mixing was the generic length scale (GLS) tuned to behave as a k-ε (Warner et al., 2005). Horizontal harmonic mixing of momentum was defined with constant values of 5 $m^2 \cdot s^{-1}$.

The NPZD numerical model coupled with ROMS model includes dissolved inorganic nitrogen, phytoplankton, zooplankton and detritus (Franks, 2002). The initial nitrate concentration was taken from field data collected by IRTA between the years 2009-2012 (ACA, 2012), and the initial phytoplankton concentrations were collected from observation data during the year 2019, whereas the initial zooplankton concentration was estimated from the literature (Rico, 2015; Powell et al. 2006). The units in which these data were collected were $mg \cdot m^{-3}$. The NPZD model uses $mmol \cdot m^{-3}$ units, so a conversion has been made using the mole fraction of Chl *a* (see Table 4). The rest of input variables for the ROMS-NPZD model were acquired from Llebot et al. (2010), and are detailed in Appendix B (Table B1), together with the model equations. Short-term simulations (5 days each) were carried out to analyse the response of biological variables to the wind. This simulation length exemplifies the typical wind events in the area, lasting from 3 to 5 days (except the daily sea breeze during spring and summer). Six experiments were designed, varying the wind direction and intensity, as well as the freshwater from the channels. The wind parameters are based on wind measurements in the Fangar area (F-Pedrera Balsells et al., 2020a), with weaker down-bay winds (associated to daily sea breeze, DW6 simulation), NW up-bay winds (UW10 simulation), strong NW up-bay winds (UW12 simulation) and SE down-bay winds (DW8 simulation).

For theoretical comparison, a simulation was also carried out with 0 m·s-1 wind intensity (CALM simulation). All simulations are summarized in Table 4. Temperature and salinity conditions were in accordance with those measured within the bay (see field campaign description in F-Pedrera Balsells et al., 2021). Freshwater inputs were activated to monitorize the evolution of nutrient inputs from the irrigation channels. Both channels (BO and IM, Figure 25) provides nutrients that will be presumably dispersed within the bay due to the combined action of currents and wind.

Table 4. Summary of the idealized numerical simulations using the ROMS-NPZD model for Fangar Bay.

Simulation	Wind direction	Intensity wind (m·s^{-1})	Channel flow (m^3·s^{-1} each channel)	Initial nitrate concentration (mmol·m^{-3})	Initial phytoplankton biomass (mmol·m^{-3})	Initial zooplankton biomass (mmol·m^{-3})
CALM	-	0	7.5	2.73	0.27	0.08
DW6	Down-bay wind	6	7.5	2.73	0.27	0.08
UW10	Up-bay wind	10	7.5	2.73	0.27	0.08
DW8	Down-bay wind	8	7.5	2.73	0.27	0.08
UW12	Up-bay wind	12	7.5	2.73	0.27	0.08
UW12fr	Up-bay wind	12	3	2.73	0.27	0.08

2.3. Satellite image processing

To qualitatively compare the numerical modelling results with real observations, satellite images from Sentinel-2, level 1-C, are used. These satellites carry a single optical instrument, the MultiSpectral Imager (MSI), and its swath width (290 km) and high revisit time (10 days at the equator with one satellite and 2–3 days at mid-latitudes) support monitoring of Earth's surface changes. Chlorophyll *a* concentrations were computed automatically by the Sentinel Application Platform (SNAP) (https://step.esa.int/main/toolboxes/snap/, accessed on 25 February 2021). The MSI sensor has had an atmospheric correction applied to it with a C2RCC processor (Case 2 Regional CoastColour, Brockmann et al., 2016) to obtain the Chl *a* images. The images correspond to remote sensing obtained after intense wind episodes (see details in F-Pedrera Balsells et al., 2021).

3. Results

Four points within the bay have been chosen to investigate the temporal evolution of the biological variables obtained from the NPZD model: in the mouth area (M1), in the centre of the bay (M2), in a coastal area in front of the IM discharge point (M3) and in the innermost part of the bay (M4) (Figure 25). Both channels (BO and IM, Figure 25) provide nutrients which increase the concentration of phytoplankton biomass within the bay. Figure 26 shows the time series of the numerical simulation in terms of nitrates and phytoplankton at the four control points. The nitrate concentration tends to decrease gently during the simulation, consistently with the increase in phytoplankton biomass and zooplankton. All simulations show larger concentrations of phytoplankton biomass at the surface due to the freshwater fluxes, as will be discussed later. Substantial differences of phytoplankton biomass between surface and bottom layers are evident in M1, where the stratification tends to be larger in contrast to the shallowest point (M4). The inner point M4 also shows a clear correlation of the wind intensity and the phytoplankton biomass values: as the up-bay wind intensity increases (i.e. UW12, larger than UW10) the phytoplankton biomass also increases. In all cases the numerical simulations suggest large temporal and spatial variability within the bay.
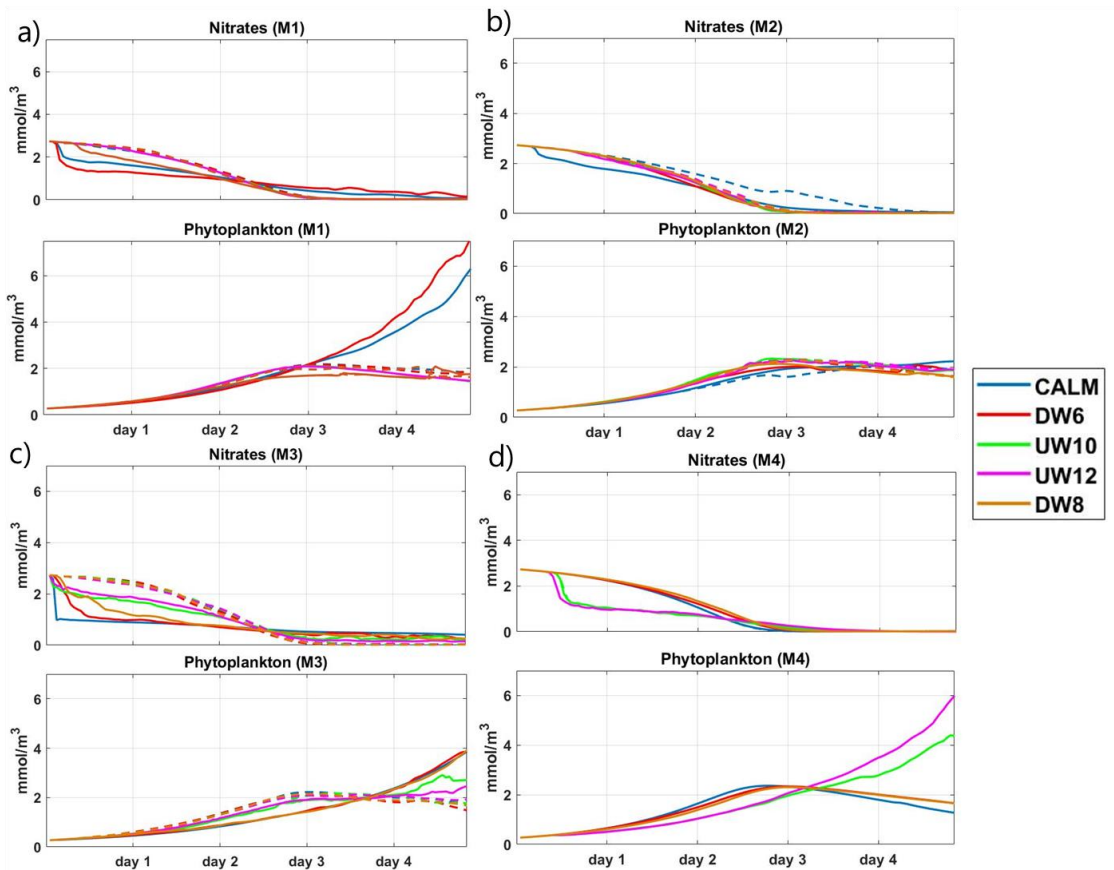
Figure 26. Time series of the nitrates and phytoplankton biomass at different points of the bay: (a) M1, (b) M2, (c) M3 and (d) M4. The different colours show the different simulations with in function of the wind. Solid line shows surface numerical results, dashed line shows bottom numerical results.

Intense wind was associated to the homogenisation of the initially stratified water column for strong wind episodes. In particular, for the UW10 and UW12 simulations (moderate and strong up-bay

wind), both surface and bottom phytoplankton time series coincide at all control points. Figure 27 shows the vertical profiles of phytoplankton biomass and salinity after three days simulation at the four points mentioned above for the DW6 (weak down-bay wind), DW8 (SE down-bay wind) and UW12 (NW up-bay wind) simulations. These profiles show homogeneous concentrations of phytoplankton biomass and salinity in the water column after strong wind episodes (DW8 and UW12). In contrast, during weaker winds (DW6) the saline stratification tends to remain in M1 and M3, leading to larger presence of phytoplankton biomass in the surface layers. At the innermost point of the bay (i.e., M4), the phytoplankton biomass is homogeneous in all simulations since, due to the shallowness of the area (lesser than 1 m deep), even weaker winds are able to mix the water column. The comparison of profiles at M3 shows a high variability of phytoplankton biomass values: DW8 shows larger values of phytoplankton biomass as compared to DW6. This means that the mixing mechanism can favour the increase of phytoplankton biomass. Finally, the comparison in M3 between DW8 and UW12 also suggests the effect of the freshwater plume on the phytoplankton biomass, which will be discussed later.

Differences in growth rates between phytoplankton and zooplankton biomass are observed in the time series. While phytoplankton can multiply rapidly under favourable concentrations of light and nutrients, increases in zooplankton numbers often lag considerably behind due to their slower generation times. Consequently, when phytoplankton biomass peaks and nutrients decline, zooplankton biomass may remain low as they begin to grow

in response to the high food supply (Figure not shown). These relations are consistent with the diagram shown in the Appendix B (B1).
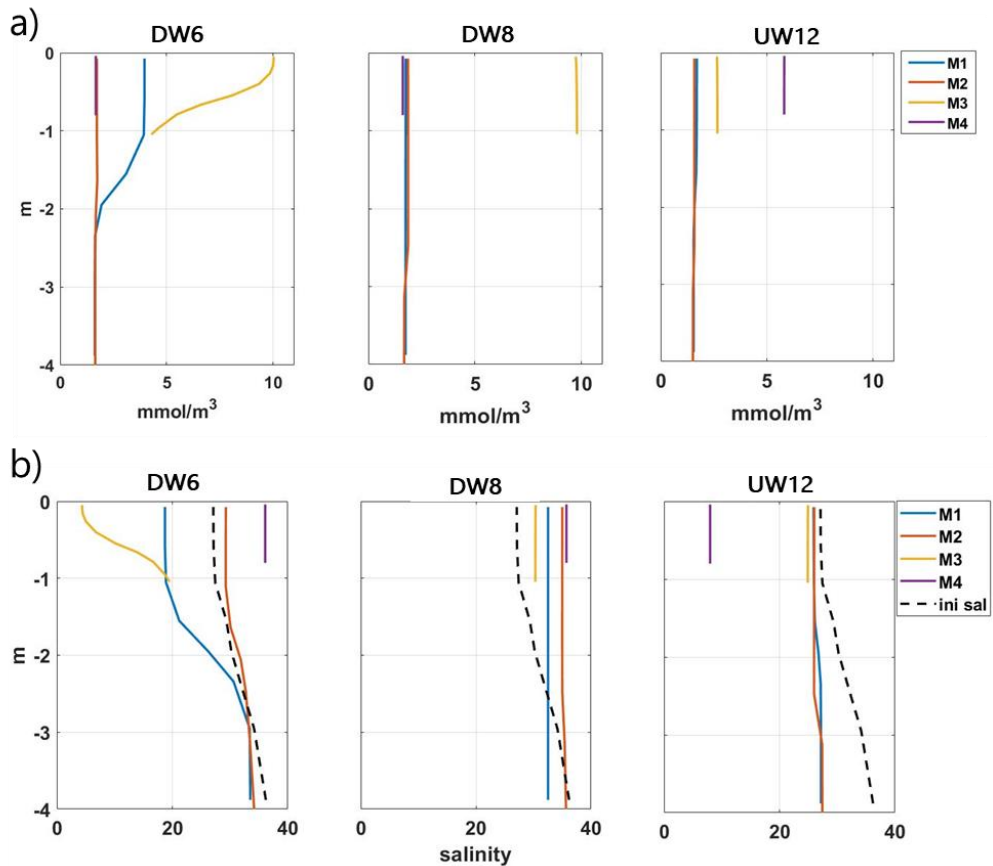
Figure 27. Vertical Chl a profiles (a) and vertical salinity profiles (b) as a function of wind events simulations at the four sampling points: M1 (blue), M2 (orange), M3 (yellow) and M4 (purple). Dashed black line shows the initial salinity.

Differences in the horizontal distribution of phytoplankton biomass are also observed in Figure 27a. During calm winds, the highest biomass value is found in front of the freshwater discharge points (M1 and M3). During strong NW up-bay winds (UW12), the highest biomass values are found in the innermost area of the bay (M4), while during strong SE down-bay winds (DW8) the largest biomass concentration is observed at the coastal point inside the bay (i.e., M3), with higher values than during the DW12 simulation.

In order to examine the spatial variability, Figure 28a shows the differences in phytoplankton biomass at the end of the simulation in comparison to the initial concentration values. Surface and bottom values are displayed according to the terrain following sigma coordinates of the numerical model. All the simulations present positive values, indicating an increase of phytoplankton biomass due to the nutrients provided by the freshwater. During up-bay winds (simulations UW12 and UW12fr), the phytoplankton biomass increases in the inner zone, both at the surface and at the bottom, with concentrations larger than 5 mmol·m^{-3}. This coincides with vertical mixing of the water column, as shown by the salinity distributions (Figure 28b). In contrast, during no wind and weak (DW6) winds, the highest phytoplankton biomass (4 mmol·m^{-3}) is located in front of the discharge points, with the largest values obtained at the point inside the bay (M3, 10 mmol·m^{-3} at the surface). For no wind simulation (CALM simulation) stratified conditions remain. In this case, bottom concentrations are small (1 mmol·m^{-3}) in comparison to other cases, highlighting the positive effect of strong winds on the vertical distribution of phytoplankton biomass. During the DW8 simulation, the highest concentrations are also

observed near the discharge points (M1 and M3), with the highest values found towards the mouth, consistent with the presence of a low-salinity plume. Overall, there is a correspondence between the freshwater plume and the phytoplankton biomass. Therefore, the wind-driven evolution of the plume has a very important impact on the final distribution of Chl *a*. In the same way, it can be seen in Figure 27 that winds of similar intensities but different directions (DW8 vs. UW10) lead to very different results in terms of the horizontal distribution of phytoplankton biomass. Finally, the results of an additional simulation similar to UW12 but with half the canals' outflow rates (UW12fr) revealed a horizontal distribution similar to UW12, but with smaller phytoplankton biomass concentrations associated to a lower nutrient input.

a)

b)
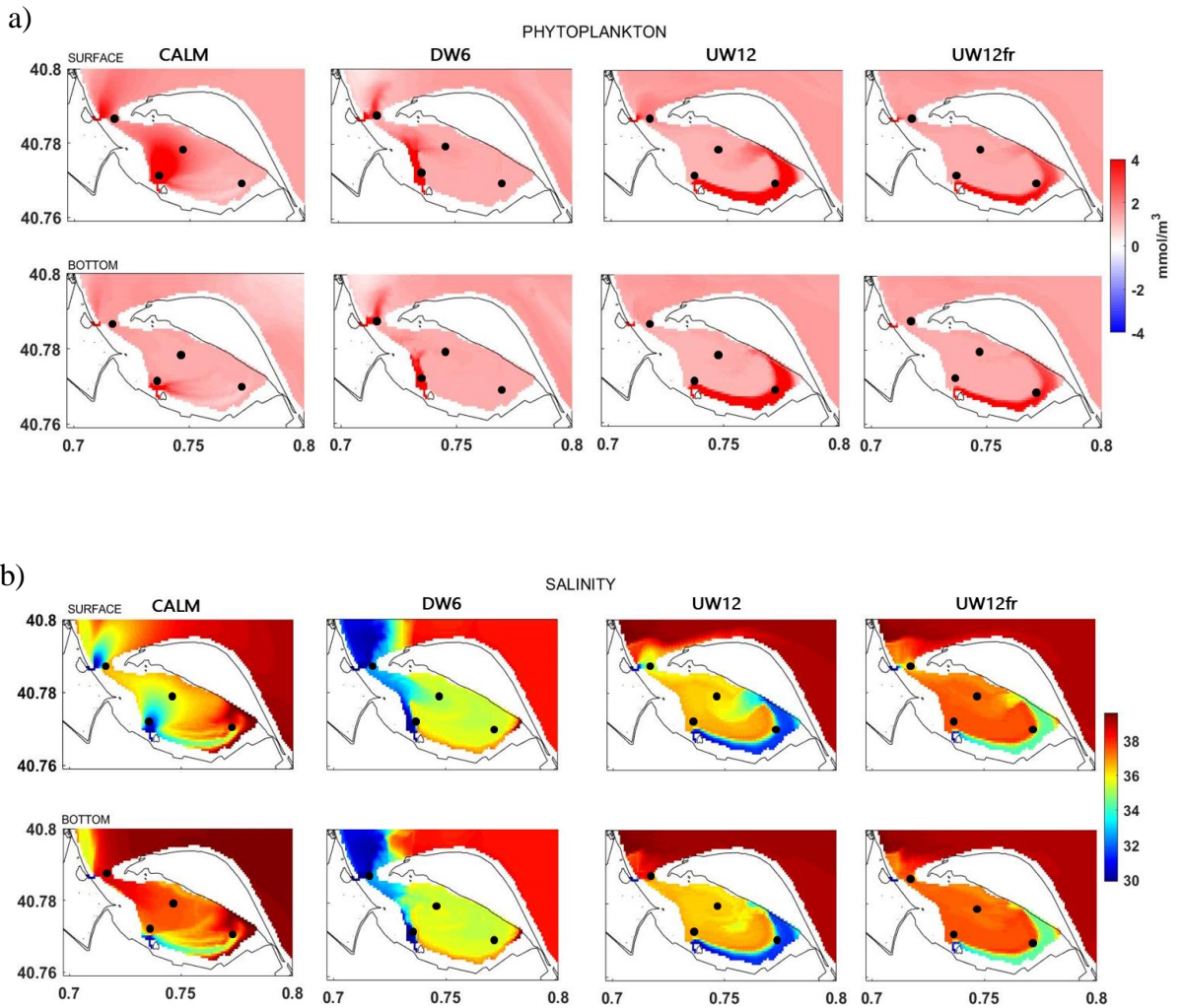
Figure 28. Differences in phytoplankton biomass (surface and bottom) at the end of the simulation in comparison to the to the initial concentration values (a) and surface and bottom salinity (b) according to different numerical simulations. The numerical control points are also marked with black dots.

Figure 29 shows a comparison between the model results and the Sentinel-2 satellite images, in periods of calm or weak wind, and strong wind which produces mixing (NW up-bay wind). The satellite images correspond to 15-Jul-2019 (Figure 29d) and 11-Aug-2019 (Figure 29c), one day after an up-bay wind episode occurred on 14-Jul-2019, and during a sea-breeze period (weak winds) between 30 July and 12 August, respectively. Note that the satellite image of the up-bay wind episode is from a few days after the wind has blown, while the model results correspond to the blowing of a steady wind. In spite of this, there is an identifiable correlation between model and images. For calm or weak down-bay wind (sea breeze), the phytoplankton biomass is relatively low, only present in the areas close to the discharge channels following the coastline consistent with the wind-driven currents due to sea breeze. During NW up-bay winds, phytoplankton biomass increases in the inner zone and is later dispersed within the bay. In any case, it should also be taken into account that the satellite, being such a shallow area, does not only show data on phytoplankton chlorophyll but also on macrophytes, which are very present in this bay (Soriano-González et al. 2019).
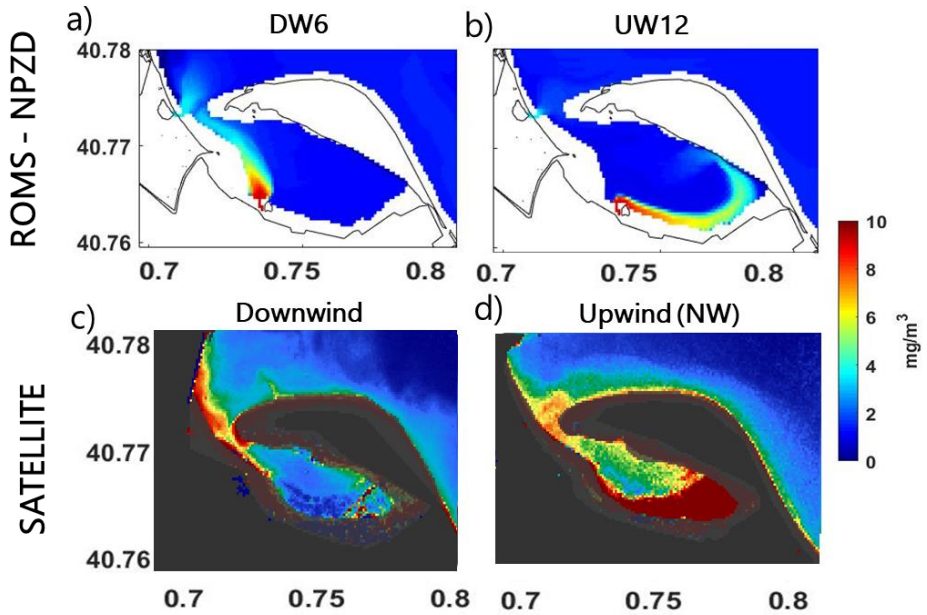
Figure 29. Comparison of surface model results with Sentinel 2 satellite images. (a) and (b) show model results during breezes and strong NW winds, respectively. (c) and (d) show corresponding satellite images with the same wind episodes.

4. Discussion

The phytoplankton distribution is controlled by turbulent mixing and advection factors, which are affected by physical forcings such as wind, tides and continental freshwater input. In tidally dominated estuaries or upwelling areas, phytoplankton biomass is distributed according to spring blooms, where algal blooms generated during upwelling events are transported to the bays through various physical mechanisms (tidal stirring, and gravitational and wind-driven circulation (Hickey and Banas, 2003; Martin et al., 2007)), as occurs in the Eastern Scheldt Bay (The Netherlands) (Jiang et al., 2020) or the Rías Baixas of Galicia (Reguera et al., 1993). On the other hand, in estuaries where the tide is practically non-existent and the depth is small, phytoplankton growth is limited by nutrients and the turbidity of the water due to large inputs of sediment from rivers and channels, such as in the Chilika lagoon, in India (Srichandan et al., 2015) or our study area, the Fangar Bay.

From a hydrodynamic point of view Fangar Bay is complex due to its shallowness and intricate bathymetry (Llebot, 2010; F-Pedrera Balsells et al., 2020a). Llebot et al. (2010) implemented a numerical model in Fangar Bay to determine the temporal distribution of phytoplankton and nutrients throughout the year. They determined that the highest concentration of phytoplankton occurred during the first months of the year with open irrigation channels, i.e., in the spring and early summer, but the role of episodic wind events remained unclear. The present study is centred on the phytoplankton distribution resulting from different short-term wind episodes typical of

the Ebro Delta area, and focuses on the summer months for which the bio-hydrodynamics are well defined (F-Pedrera Balsells et al., 2021). The numerical results have proved that the wind affects the direction and magnitude of surface currents, disperses or reinforces fronts, and induces vertical mixing, in accordance with other investigations (Geyer, 1997; Llebot et al., 2014; F-Pedrera Balsells et al., 2020a). The distribution of phytoplankton biomass in Fangar Bay agrees with water currents driven by the local winds and modulated by the complex bathymetry of the basin (F-Pedrera Balsells et al., 2020a) and the evolution of the freshwater plume of the drainage channels (Figure 28b).

The model results have shown the combined effect of the wind on phytoplankton biomass distribution within the bay from two perspectives. On the one hand, intense wind episodes are able to break the stratification, mixing the water column and leading to an increase of phytoplankton biomass in the deeper levels of the bay. Simulations with no wind (CALM), in which the bay remains stratified, are characterized by the presence of a physical barrier that prevents nutrient vertical transfer, so the phytoplankton biomass remains in the surface layers. This case shows how the absence of wind (or even the presence of sea breezes) causes the phytoplankton biomass dispersion to be governed by the estuarine circulation of the bay, with phytoplankton biomass decreasing in the seaward direction. A similar seaward negative gradient of phytoplankton is found in other estuaries and coastal systems in which the nutrient gradients control the phytoplankton distribution (Soetaert et al., 2006; Gomez et al., 2018). When strong NW up-bay winds blow in Fangar Bay, the water

column homogenises, making nutrients available throughout the column, both at the surface and at the bottom (i.e., UPW10 and UW12 simulations). The phytoplankton biomass is advected towards the inner part of the bay, following the water currents induced by the NW winds, not only at the surface but throughout the water column. With strong SE down-bay winds (DW8 simulation), phytoplankton biomass increases near the discharge channels and the phytoplankton biomass distribution follows the water circulation driven by SE winds: seaward flow in the lateral shoals (F-Pedrera Balsells et al., 2020a). The strong winds episodes suggest a non-uniformly distribution of phytoplankton biomass with irregular patterns and patches attributed to a dominant source factor (see examples in Ahel et al., 1996; Geyer et al., 2018; Jiang et al., 2020), which in the case of Fangar Bay is a role played by the discharge channels. In consequence, following the categorization exposed by Jiang et al. (2020) in terms of spatial patterns of phytoplankton biomass in estuaries and coastal bays, Fangar Bay may be included in different typologies depending on the wind configuration from a short-term perspective.

The second effect of the wind is related to the wind-driven plume dispersion. Freshwater discharges from the irrigation channels are the dominant driver of salinity and nutrient gradients. In Fangar Bay there is a colimitation of nitrogen and phosphorus, with the most limiting nutrient changing throughout the year, depending on the variability of sources and sinks of both nutrients (Llebot et al., 2010). The NPZD model considers nitrogen only and assumes no phosphorus limitation in phytoplankton growth. This sets a limit on the

full understanding of Fangar Bay's dynamics, but our analysis provides a first interpretation of the data. Freshwater discharges also vary over the year, depending on whether these irrigation channels are closed (January to March), open (April to November) or semi-open (November and December). In F-Pedrera Balsells et al. (2021) it was observed that after strong NW up-bay wind episodes in the bay, phytoplankton biomass tends to increase within the bay, but it could not be determined whether this behaviour extended to the entire water column as the simulations presented herein suggest. As described in other works (Simpson & Bowers, 1981; Horsburgh et al., 2000) vertical density stratification is an important determinant of ecosystem characteristics.

Ultimately, as a small, shallow, micro-tidal bay, wind generates very complex currents and causes large spatial and temporal variability in the distribution of phytoplankton biomass. Chl *a* peaks usually form at the front of the river plume, either by rapid nutrient assimilation and growth or by aggregation along the strong salinity gradient of this transition (Geyer et al., 2018). This explains why the highest biomass levels can be found following the river plume, as shown in Figure 28. Therefore, the same simulations were performed by halving the channel outflow and the results on phytoplankton biomass distribution were the same, only lower, due to lower nutrient input. Some studies have shown that Chl *a* concentration is higher in the freshwater areas of the bay and decreases as salinity increases. This leads to high phytoplankton biomass in the plume formed by freshwater tributaries, which discharge high levels of nutrients, as can

happen in the Scheldt River and Western Scheldt Estuary in Belgium (Soetaert et al., 2006).

Freshwater discharges from irrigation channels also control water residence times within the bay. Prolonged residence times generally facilitate the growth and accumulation of phytoplankton biomass (Wan et al., 2013). The location and magnitude of phytoplankton biomass can be partly explained by residence time, although phytoplankton productivity may be affected by other factors such as nutrient availability, light, temperature and zooplankton grazing (Wan et al., 2013). In Fangar Bay, residence time is in the range of about 20 days in the middle zone and about 40 days in the innermost quasi-stagnant zone (F-Pedrera Balsells et al., 2020b). This work also shows that an increase in freshwater discharge through the inner channel (IM) helps to decrease the residence time in the innermost zone (F-Pedrera Balsells et al., 2020b). In turn, therefore, a reduction in river discharge increases residence time and may allow a higher concentration of phytoplankton to accumulate within the estuary. Our results show a higher concentration of phytoplankton biomass in the innermost zone consistent with the larger residence time.

5. Conclusions and future works

Results based on *in situ* and remote observations and numerical models conclude that the biological variables in small-scale, shallow and micro-tidal bays (such as Fangar Bay) shows strong gradients due to the influence of the wind and the freshwater plume evolution. Strong winds have a double impact: i) breaking down the stratification and mixing the water column, leading to an increase of phytoplankton biomass at the bottom, and ii) distributing the canal-borne nutrients within the bay, resulting in an irregular pattern of phytoplankton biomass. Due to the predominance of the wind forcing on the bay's water circulation, different wind directions and/or intensities may have a completely different effect on phytoplankton biomass distribution. In this sense, wind variability explains the complex pattern of phytoplankton biomass observed in the *in situ* measurements and remote sensing, characterized by sharp horizontal gradients. In particular, the link between the hydrodynamics and the phytoplankton evolution in Fangar Bay can be summarized as shown in Figure 30. The distribution of these nutrients is further influenced by the surface currents induced by the different winds in the area. With weak down-bay winds (i.e. sea-breeze), stratification is maintained within the estuary, so higher phytoplankton biomass near the discharge points and at the surface layer are found. During strong up-bay and down-bay winds (i.e. North-westerlies, and South-easterlies, respectively), the stratification is broken, so the nutrients discharged from the channels are distributed homogeneously throughout the water column, facilitating phytoplankton growth in the deeper layers. This growth expands horizontally according to the wind-driven currents:

towards the inner zone through the lateral shoals, in the case of up-bay winds, or towards the mouth zone, in the case of down-bay winds.
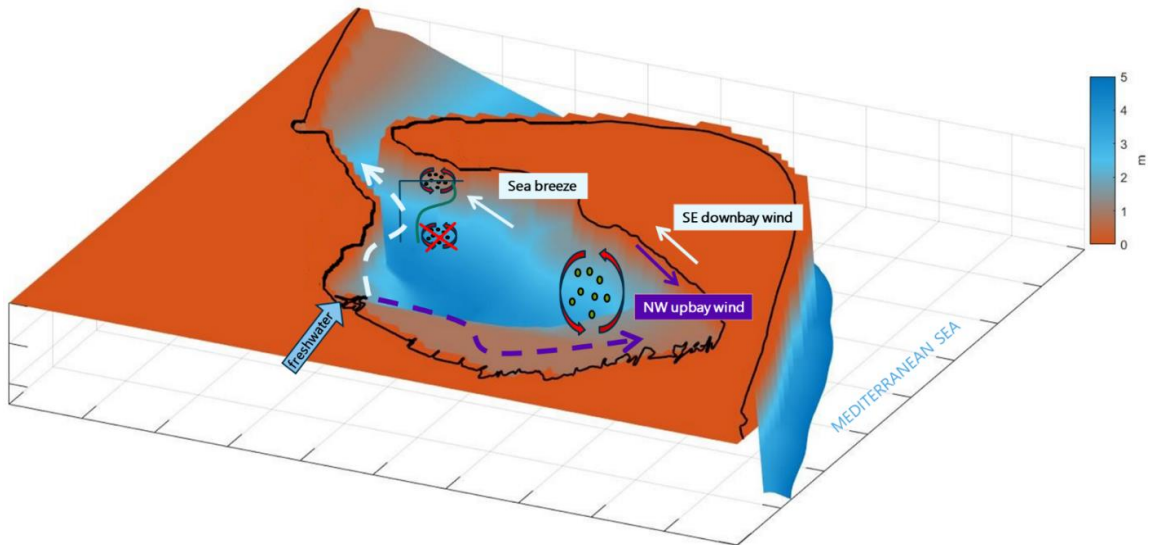
Figure 30. Conceptual diagram of estuarine processes affecting phytoplankton distribution in Fangar Bay. Strong NW up-bay winds cause mixing of the water column and the freshwater plume to move inland. Strong SE down-bay winds also cause mixing, but the freshwater plume moves seaward. Sea breezes also cause a seaward displacement of the freshwater plume, but does not break the vertical stratification, so there is a difference between phytoplankton biomass at the surface and at the bottom.

Fangar Bay is complex from both a hydrodynamic and biological standpoint. Different phytoplankton patterns are identified depending on the meteorological conditions and, to account for this, different idealised simulations were designed in order to approach

each scenario separately. Even so, there are processes that remain unexplored such as the resuspension of Chl *a* containing biomass or the effect of long-duration wind episodes, as well as the change in limiting nutrients that often occurs in such environments, affecting phytoplankton biomass, composition and seasonal cycling (D'Elia et al., 1986; Fisher et al., 1992). The availability of N or P inside the bay also influences the biochemical composition of phytoplankton (Estrada et al., 2008). These topics remain to be studied in future work, as does the analysis of the impact of these dynamics on zooplankton and detritus, which are two variables also taken into account by the ROMS-NPZD model. In any case, the combined analysis of observations and numerical models has provided compelling results and opens new perspectives to understand the short term dynamics of shallow and micro-tidal bays to meteorological events from a combined hydro-biological point of view.

6. **Appendix A.** Model validation.

The numerical implementation in Fangar Bay consists of a telescopic three-grid two-way nested ROMS scheme, with a finer bay grid (resolution of about 23 m) embedded within a cascade of coarser grids (see Figure A1). The model has been validated by comparing modelled surface velocities from the coastal domain (~ 350 m) with HFR (High Frequency Radar) data, and modelled currents from the finest domain (~ 23 m) with vertical current profiles measured inside Fangar Bay during an October-November, 2017 field campaign. The observational data were, amongst others, current velocity and direction obtained every 10 min in 25 cm thick layers distributed from the bottom to the surface.
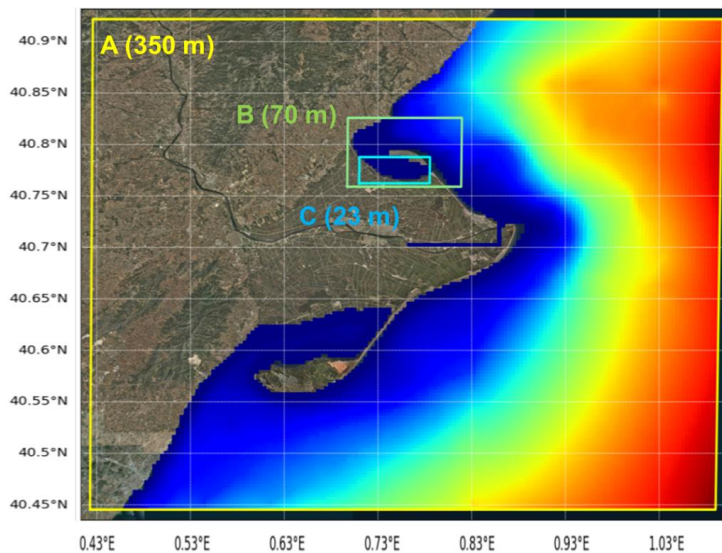
Figure A1. Ebro Delta and the Fangar Bay, with the telescoping domains used in the system. Conditions for ROMS at the A domain are obtained either from CMEMS-IBI or CMEMS-MED. Map from Google Earth, Image Landsat/Copernicus © 2018 Google.
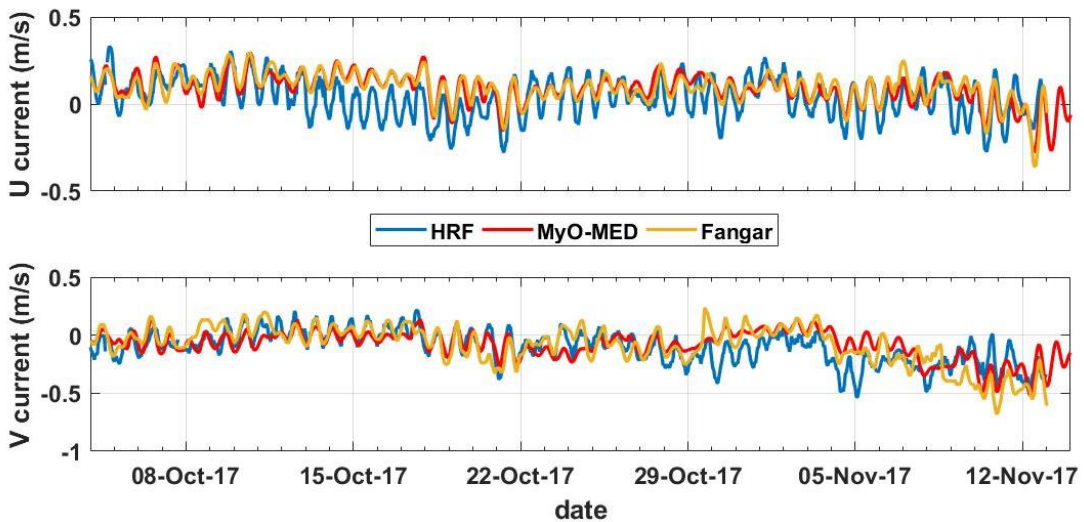
Figure A2. Surface current components U (east-west) and V (north-south) measured by the HRF radar (blue line) and modelled my CMEMS-MED (red) and the Fangar nested suite (yellow) off the Ebro Delta for domain A (350 m).

The initial and boundary conditions for the coastal domains were obtained from two different CMEMS products (IBI and MED). For the hydrodynamic module, hourly barotropic currents and sea levels are consistently accommodated to the open boundaries with Chapman and Flather algorithms, whereas the variability of currents along the water column (baroclinic component), temperature and salinity are imposed from the CMEMS-IBI daily average values (or hourly data from CMEMS-MED) with clamped conditions. The initial state of the smaller domains is obtained by interpolation from the larger domain conditions.

The comparison between the HFR and modelled eastward and northward components of the surface currents (Figure A2) revealed good agreement and correlation between both datasets, both in intensity and phase, and for both spatial components. The daily oscillations correspond to the inertial period in the region (~19h) and are well reproduced by the model. Some intensifications of the currents -probably related with energetic wind events- are also well described by the model. For comparison, Figure A2 also plots the current components predicted by CMEMS-MED. For this particular period, the correlation between measured and modelled data shows an $r^2 = 0.63$, slightly larger than the correlation between CMEMS-MED data and measured values.

Regarding the currents within the bay, the fit between the modelled and measured values is shown in Figure A3. Here, the general trend of the water flow is well captured by the model, which adequately reproduces the main events, in spite of the very low energy of the system. This is a characteristic of both Ebro Delta bays, Fangar and Alfacs (Cerralbo et al., 2014, 2019) although in Fangar it is enhanced by the bay's shallowness and narrow connection with the open sea. For these verification numerical exercises, the 6-hourly ECMWF data has been used for the atmospheric forcing. For the hydro-biological simulations shown in this contribution, the 70 m grid has been used because encompasses both the bay and part of the outer area.
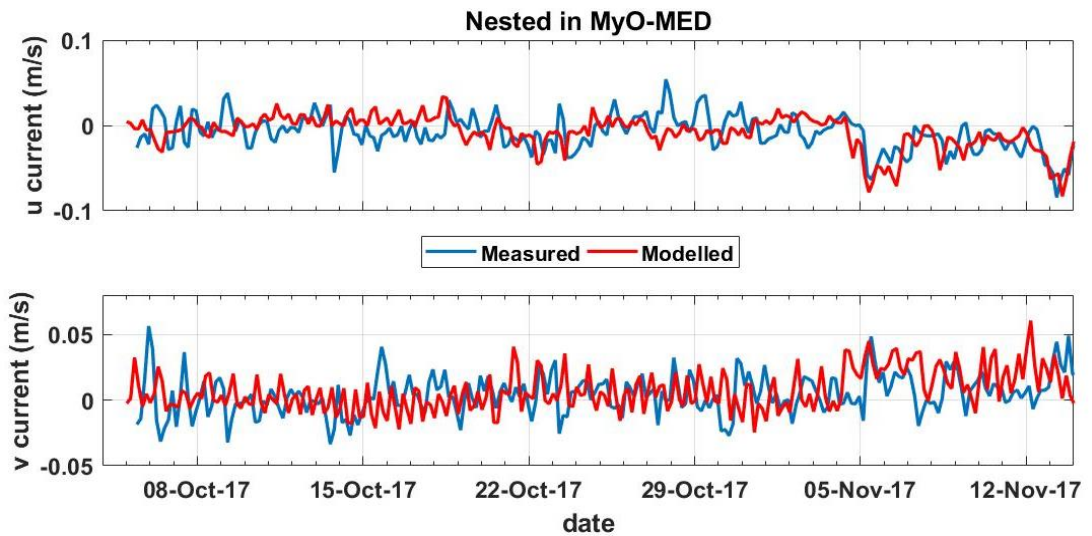
Figure A3. Surface current components U (east-west) and V (north-south) measured inside the bay (blue) and modelled by the Fangar Bay nested scheme (red) during the 2017 autumn field campaign for domain C (23 m). Correspond to boundary forcing provided by CMEMS-MED.

7. **Appendix B.** NPZD Model embedded in ROMS model.

The NPZD model follows a simple nitrogen-based scheme in order to simulate the interactions of the four variables: nutrients (N), phytoplankton (P), zooplankton (Z) and detritus (D) (Figure B1). The mathematical formulation of the internal fluxes varies in kind and complexity (see review Heinle & Slawig, 2013). This annex presents the equations used by the ROMS-NPZD model, as well as the values used for the different parameters, based on Llebot et al. (2010), in the numerical simulations (Table B1).
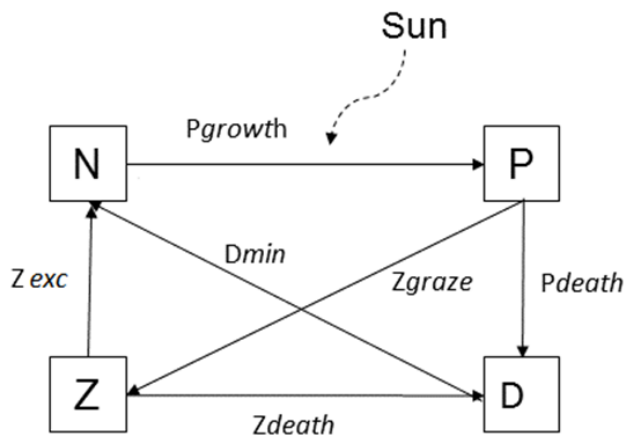
Figure B1. ROMS-NPZD model scheme including the transfer functions of the different components. N (nutrients), P (phytoplankton), Z (zooplankton) and D (detritus); Pdeath and Zdeath is phytoplankton and zooplankton mortality respectively; Pgrowth is phytoplankton growth; Zexc is zooplankton exudation; Zgraze is zooplankton grazing and Dmin is remineralization.

Nutrients

$$\frac{\partial N}{\partial t} + \mathbf{u} \cdot \nabla N = \delta D + \gamma_n GZ - UP + \frac{\partial}{\partial z}\left(k_v \frac{\partial N}{\partial z}\right), \qquad \text{(B1)}$$

U = photosynthetic growth and uptake of nitrogen by phytoplankton

P = phototrophic phytoplankton

Z = herbivorous zooplankton

G = grazing on phytoplankton by zooplankton

$\gamma_{n=}$ some proportion of the consumed phytoplankton being lost directly to the nitrate pool as a function of "sloppy feeding" and metabolic processes.

Phytoplankton

$$\frac{\partial P}{\partial t} + \mathbf{u} \cdot \nabla P = UP - GZ - \sigma_d P + \frac{\partial}{\partial z}\left(k_v \frac{\partial P}{\partial z}\right), \qquad \text{(B2)}$$

U = photosynthetic growth and uptake of nitrogen by phytoplankton

P = phototrophic phytoplankton

Z = herbivorous zooplankton

G = grazing on phytoplankton by zooplankton

σ_d = phytoplankton mortality

Zooplankton

$$\frac{\partial Z}{\partial t} + \mathbf{u} \cdot \nabla Z = (1 - \gamma_n)GZ - \zeta_d Z + \frac{\partial}{\partial z}\left(k_v \frac{\partial Z}{\partial z}\right), \qquad \text{(B3)}$$

Z = herbivorous zooplankton

G = grazing on phytoplankton by zooplankton

ζ_d = zooplankton mortality

γ_n = some proportion of the consumed phytoplankton being lost directly to the nitrate pool as a function of "sloppy feeding" and metabolic processes.

Detritus

$$\frac{\partial D}{\partial t} + \mathbf{u} \cdot \nabla D = \sigma_d P + \zeta_d Z - \delta D + w_d \frac{\partial D}{\partial z} + \frac{\partial}{\partial z}\left(k_v \frac{\partial D}{\partial z}\right), \quad \text{(B4)}$$

Grazing
$$G = R_m\left(1 - e^{-\Lambda P}\right), \quad \text{(B5)}$$

Uptake
$$U = \frac{V_m N}{k_N + N} \frac{\alpha I}{\sqrt{V_m^2 + \alpha^2 I^2}}. \quad \text{(B6)}$$

Irradiance
$$I = I_0 \exp\left(k_z z + k_p \int_0^z P(z')dz'\right), \quad \text{(B7)}$$

K_z = light extinction coefficient

k_p = self-shading coefficient

Table B1. Parameters.

PARAMETER NAME	SYMBOL	VALUE	DIMENSION
Light extinction coefficient	k_z	0.067	m^{-1}
Self-shading coefficient	k_p	0.08	m^2/ mmol-N
Initial slope of P-I curve	α	0.025	m^2 W^{-1}
Surface irradiance	I_o	158.075	W m^{-2}
Nitrate uptake rate	V_m	1.5	d^{-1}
Phytoplankton mortality rate (senescence)	Σ_d	0.15	d^{-1}
Uptake half saturation	k_N	0.8	mmol-N $\cdot$ m^{-3}
Zooplankton excretion efficiency	Γ_n	0.03	-
Zooplankton mortality rate	Z_d	0.08	d^{-1}
Ivlev constant	Λ	0.06	m^3 mmol$\cdot$N^{-1}
Zooplankton grazing rate	R_m	1.0	d^{-1}
Detritus remineralization rate	Δ	0.1	d^{-1}
Detrital sinking rate	w_d	5.0	md^{-1}

5. General conclusions
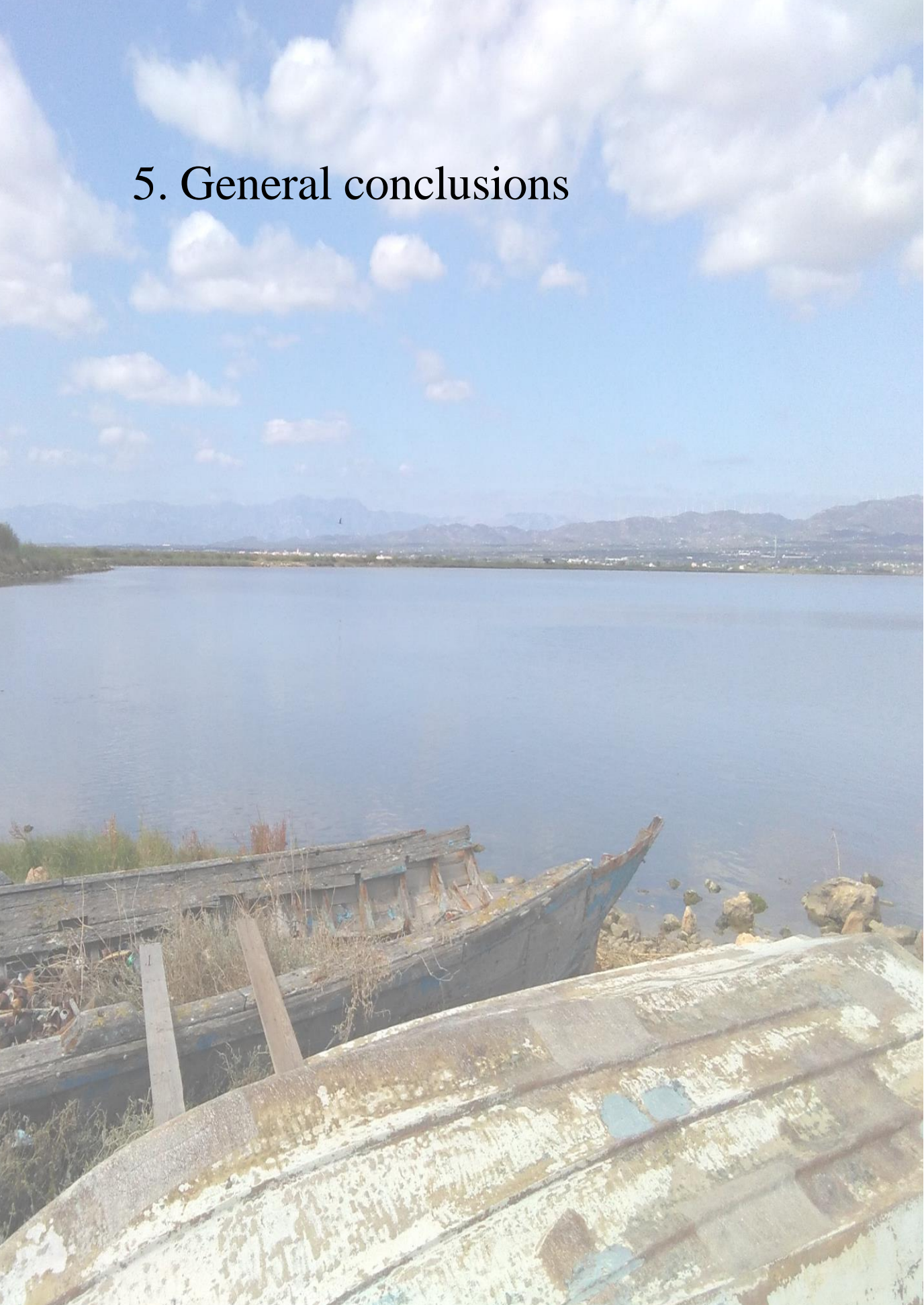
C h a p t e r   5

GENERAL CONCLUSIONS

This thesis has focussed on the analysis of the relationship between hydrodynamic and biological variables in a shallow and micro-tidal coastal bay (i.e., Fangar Bay). For the analysis, *in situ* observational data, numerical modelling, and satellite images have been used for this purpose.

The observations obtained from the field campaigns showed that Fangar Bay presents a stratified estuarine system in the water column, with less saline water leaving the surface and more saline water entering from the bottom. However, it was observed that during episodes of strong NW and SE winds, the current direction was opposite to the wind direction. Using results of the implementation of the numerical model ROMS, we proved that the dynamics in small-scale, shallow, micro-tidal estuaries, such as Fangar Bay, are characterised by a very complex circulation in the inner part. The observational results also showed that there is a tendency towards stratification due to freshwater inflows, which is broken during episodes of strong winds lasting a few hours, causing a homogenisation of the entire water column. During these episodes of strong winds, the numerical results showed that the bathymetry can produce an axially symmetrical transverse structure, with outflows in the axis of the central

channel, in the opposite direction to the wind direction together with inflows in the shallow lateral zones (for NW winds). The opposite is true for SE winds.

Once the hydrodynamics of Fangar Bay has been clarified, we proceeded to examine the primary production evolution within the bay, linking the physical process and the Chlorophyll a (Chl a) observations. The results are based on intensive field campaigns and Sentinel-2 images revealed that strong winds from both the NW (offshore) and E-SE (onshore) caused an increase in the concentration of Chl a on the surface of Fangar Bay. The mechanisms responsible for the increase in Chl a during wind episodes were horizontal mixing and bottom resuspension (also related to the breakdown of stratification) which presumably resuspends Chl a-containing biomass and/or incorporates nutrients into the water column. The mixing produced by strong winds favours the accumulation of Chl a concentration, while stratification reduces this accumulation.

However, questions from the previous analysis arise in the description of the primary production evolution. In particular, the specific mechanisms that are induced cause an increase of Chl a within the bay during windstorms. This increase was restricted to the surface layers, or whether, as the strong winds were able to homogenise the water column, they also favoured the increase of Chl a throughout the column. In this sense, a biological NPZD model coupled with ROMS was implemented within the bay. The numerical results of idealized simulations, together with results based on *in situ* and remote

observations, concluded that biological variables in small-scale, shallow, micro-tidal bays (such as Fangar Bay) showed strong gradients due to the influence of wind and the evolution of the freshwater plume. In consequence, strong winds had a double impact: i) stratification broke mixing within the water column and increased the phytoplankton biomass especially at the bottom, and ii) distribution of the nutrients transported by the land fluxes within the bay resulting in an irregular pattern of phytoplankton biomass. Furthermore, the results revealed that due to the dominance of wind force in the water circulation of the bay, a different wind direction and/or intensity could have a completely different effect on the distribution of phytoplankton biomass.

The analysis shown in the previous chapters has allowed us to understand the link between the physical and biological processes in a small, shallow, and micro-tidal estuary. However, there are still processes that remain unsolved, such as the resuspension of Chl *a*-containing biomass or the effect of long-lasting wind events, as well as the change in limiting nutrients that often occurs in these environments, affecting phytoplankton biomass, composition, and seasonal cycling. An analysis of the impact of these dynamics on zooplankton and detritus, which are two variables also taken into account by the ROMS-NPZD model, are also scientifically interesting. These issues are therefore left for future work, which would encompass additional intensive field campaign and more realistic numerical models.

In any case, the combined analysis of observations and numerical models has provided convincing results and opens new perspectives for understanding the short-term dynamics of shallow and micro-tidal bays and the effect of meteorological events from a combined hydro-biological point of view. The conclusions of this thesis might have a relevant managerial issues in the aquaculture of the Bay providing skills for contingency plans, pre-operational exercises for early warning system, and support tools for decision-making agents. Although the work is focussed on Fangar Bay, the obtained results and methodology could be translated to similar domains.

Bibliography

ACA (2012) State of water bodies in Catalonia http://aca-web.gencat.cat/WDMA

Ahel, M., Barlow, R. G., and Mantoura, R. F. C. (1996). Effect of salinity gradients on the distribution of phytoplankton pigments in a stratified estuary. *Mar. Ecol.-Prog. Ser.*, *143*, 289–295. https://doi.org/https://doi.org/10.3354/meps143289

Alekseenko, E., Roux, B., Sukhinov, A., Kotarba, R., & Fougere, D. (2013). Nonlinear hydrodynamics in a mediterranean lagoon. *Nonlinear Processes in Geophysics*, *20*(2), 189–198. https://doi.org/10.5194/npg-20-189-2013

Archetti, G., Bernia, S., & Salvà-Catarineu, M. (2010). Análisis de los vectores ambientales que afectan la calidad del medio en la bahía del Fangar (Delta del Ebro) mediante herramientas SIG. *Revista Internacional de Ciencia y Tecnologia de La Información Geográfica*, *10*(1578–5157), 252–279.

Artigas, M. L., Llebot, C., Ross, O. N., Neszi, N. Z., Rodellas, V., Garcia-Orellana, J., Masqué, P., Piera, J., Estrada, M., & Berdalet, E. (2014). Understanding the spatio-temporal variability of phytoplankton biomass distribution in a microtidal Mediterranean estuary. *Deep-Sea Research Part II: Topical Studies in Oceanography*, *101*, 180–192. https://doi.org/10.1016/j.dsr2.2014.01.006

Automatic Water Quality Information System, DEL EBRO, CHE-Hydrographic Confederation, Quality Alert Network, SAICA Project, 2013. Available online: https://www.saica.co.za/ (accessed on 30 January 2020).

Bolaños, R, Jorda, G., Cateura, J., Lopez, J., Puigdefabregas, J., Gomez, J., & Espino, M. (2009). The XIOM: 20 years of a regional coastal observatory in the Spanish Catalan coast. *Journal of Marine Systems*, *77*(3), 237–260. https://doi.org/10.1016/j.jmarsys.2007.12.018

Bolaños, R., Brown, J. M., Amoudry, L. O., Souza, A. J., & Bolaños, R. , Brown, Jennifer M. ; Amoudry, Laurent O. ; Souza, A. J. (2013). Tidal , Riverine , and Wind Influences on the Circulation of a Macrotidal Estuary. *Journal of Physical Oceanography*, *43*(1), 29–50. https://doi.org/10.1175/JPO-D-11-0156.1

Brockmann, C., Doerffer, R., Peters, M., Stelzer, K., Embacher, S., & Ruescas, A. (2016). *Evolution of the c2rcc neural network for sentinel 2 and 3 for the retrieval of ocean colour products in normal and extreme optically complex waters* (p. Living Planet Symposium, 740, 54).

Cameron, W. M., & Pritchard, D. W. (1963). Estuaries. In M. N. Hill (Ed.), *The Sea, vol 2* (pp. 306–324). John Wiley and Sons.

Camp, J., & Delgado, M. (1987). Hidrogafia de las bahías del delta del Ebro. *Inv.Pesq.*, *51 (3)*, 351–369.

Carter, G. S., & Merrifield, M. A. (2007). Open boundary conditions for regional tidal simulations. *Ocean Modelling*, *18*, 194–209. https://doi.org/10.1016/j.ocemod.2007.04.003

Cerralbo, P., Grifoll, M., Valle-Levinson, A., & Espino, M. (2014). Tidal transformation and resonance in a short, microtidal Mediterranean estuary (Alfacs Bay in Ebre delta). *Estuarine, Coastal and Shelf Science*, *145*, 57–68. https://doi.org/10.1016/j.ecss.2014.04.020

Cerralbo, P., Grifoll, M., Moré, J., Sairouní Afif, A., Espino, M., & Bravo, M. (2015). Wind variability in a coastal area (Alfacs Bay, Ebro River delta). *Advances in Science and Research*, *12*(1), 11–21. https://doi.org/10.5194/asr-12-11-2015

Cerralbo, P., Grifoll, M., & Espino, M. (2015). Hydrodynamic response in a microtidal and shallow bay under energetic wind and seiche episodes. *Journal of Marine Systems*, *149*(Septembre), 1–13. https://doi.org/10.1016/j.jmarsys.2015.04.003

Cerralbo, P., Espino, M., & and Grifoll, M. (2016). Modeling circulation patterns induced by spatial cross-shore wind variability in a small-size coastal embayment. *Ocean Modelling*, *104*, 84–98

Cerralbo, P., F.-Pedrera Balsells, M., Mestres, M., Fernandez, M., Espino, M., Grifoll, M., & Sanchez-Arcilla, A. (2019). Use of a hydrodynamic model for the management of water renovation in a coastal system. *Ocean Science*, *15*(2), 215–226. https://doi.org/10.5194/os-15-215-2019

Cloern, J. E. & Nichols, F. H. (1985). Time scales and mechanisms of estuarine variability, a synthesis from studies of San Francisco Bay. *Hydrobiologia*, *29*, 229–237.

Coogan, J., Dzwonkowski, B., Park, K., & Webb, B. (2019). Observations of Restratification after a Wind Mixing Event in a Shallow Highly Stratified Estuary. *Estuaries and Coasts*. https://doi.org/10.1007/s12237-019-00689-w

Csanady, G. T. (1973). Wind-Induced Barotropic Motions in Long Lakes. *Journal of Physical Oceanography*, *3*, 429–483.

Curcó, A. (2006). El Delta De l 'Ebre. Síntesi del medi físic d'una zona humida litoral. In *T.S.C.B..* (Vol. 14). http://publicacions.iec.cat/repository/pdf/00000097%5C00000022.pdf

D'Elia, C.F., Sanders, J.G., Boynton, W. R. (1986). Nutrient enrichment studies in a coastal plain estuary: phytoplankton growth in large-scale continuous cultures. *Can. J. Fish. Aquat. Sci.*, *43*, 397–406.

D'Ortenzio, F., d'Alcalà, M.R. (2009). On the trophic regimes of the Mediterranean Sea: a satellite analysis. *Biogeoscience*, *6*, 139–148.

de Jonge, V. N., & van Beusekom, J. E. E. (1995). Wind- and tide- induced resuspension of sediment and microphytobenthos from tidal flats in the Ems estuary. *Limnology and Oceanography*, *40*(4), 776–778. https://doi.org/10.4319/lo.1995.40.4.0776

de Madariaga, I. (1995). Photosynthetic Characteristics of Phytoplankton During the Development of a Summer Bloom in the Urdaibai Estuary, Bay of Biscay. *Estuarine, Coastal and Shelf Science*, *40*(5), 559–575. https://doi.org/10.1006/ecss.1995.0038

Delgado, M. (1989). Abundance and distribution of microphytobenthos in the bays of Ebro Delta (Spain). *Estuarine, Coastal and Shelf Science*, *29*(2), 183–194. https://doi.org/10.1016/0272-7714(89)90007-3

Delgado, M., & Camp, J. (1987). Abundancia y distribución de nutrientes inorgánicos disueltos en las bahías del delta del Ero. *Inv.Pesq.*, *51 (3)*, 427–441.

Demers, S., Lafleur, P. E., Legendre, L., & Trump, C. L. (1979). Short-Term Covariability of Chlorophyll and Temperature in the St. Lawrence Estuary. *Journal of the Fisheries Research Board of Canada*, *36*(5), 568–573. https://doi.org/10.1139/f79-081

Díez-Minguito, M., & de Swart, H. E. (2020). Relationships Between Chlorophyll-a and Suspended Sediment Concentration in a High-Nutrient Load Estuary: An Observational and Idealized Modeling Approach. *Journal of Geophysical Research: Oceans*, *125*(3), no. https://doi.org/10.1029/2019JC015188

Duchon, C. E. (1979). Lanczos filtering in one and two dimensions. *Journal of Applied Meteorology*, *18*, 1016–1022.

Dyer, K. R. (1973). *Estuaries: a physical introduction* (J. W. & Sons

(Ed.)).

ESA. (2015). *SENTINEL-2 User Handbook*. https://doi.org/GMES-S1OP-EOPG-TN-13-0001

Estrada, M., Sala, M.M., van Lenning, K., Alcaraz, M., Felipe, J., Veldhuis, M. J. W. (2008). Biological interactions in enclosed plankton communities including Alexandrium catenella and copepods: role of phosphorus. *J. Exp. Mar. Biol. Ecol.*, *355*, 1–11.

F-Pedrera Balsells, M., Grifoll, M., Espino, M., Cerralbo, P., & Sánchez-Arcilla, A. (2020a). Wind-Driven Hydrodynamics in the Shallow, Micro-Tidal Estuary at the Fangar Bay (Ebro Delta, NW Mediterranean Sea). *Applied Sciences*, *10*(19), 6952. https://doi.org/10.3390/app10196952

F-Pedrera Balsells, M., Mestres, M., Fernández, M., Cerralbo, P., Espino, M., Grifoll, M., & Sánchez-Arcilla, A. (2020b). Assessing Nature Based Solutions for Managing Coastal Bays. *Journal of Coastal Research*, *95*(sp1), 1083–1087. https://doi.org/10.2112/SI95-211.1

F-Pedrera Balsells, M., Grifoll, M., Fernández-Tejedor, M., & Espino, M. (2021). Short-term response of chlorophyll a concentration due to intense wind and freshwater peak episodes in estuaries: The case of Fangar bay (Ebro delta). *Water*, *13*(5), 701. https://doi.org/10.3390/w13050701

Fisher, T. R., Harding Jr, L. W., Stanley, D. W., and Ward, L. G. (1988).

Phytoplankton, nutrients, and turbidity in the Chesapeake, Delaware, and Hudson estuaries,. *Estuar. Coast. Shelf S.*, *27*, 61–93. https://doi.org/https://doi.org/10.1016/0272-7714(88)90032-7

Fisher, T.R., Peele, E.R., Ammerman, J.W., Harding, L. W. (1992). Nutrient limitation of phytoplankton in Chesapeake Bay. *Mar. Ecol. Prog. Ser.*, *82*, 51–63.

Franks, P. J. S. (2002). NPZ models of plankton dynamics: Their construction, coupling to physics, and application. *Journal of Oceanography*, *58*(2), 379–387. https://doi.org/10.1023/A:1015874028196

Garcia, M. A., & Ballester, A. (1984). Notas acerca de la meteorología y la circulación local en la región del delta del Ebro. *Inv.Pesq.*, 469–493.

Garcia, M. A., Ballester, A., & Garcia, M and Ballester, A. (1984). Notas acerca de la meteorología y la circulación local en la región del delta del Ebro. *Inv.Pesq.*, *48*, 469–493.

Garvine, R. W. (1985). A simple model of estuarine subtidal fluctuations forced by local and remote wind stress. *Journal of Geophysical Research*, *90*(C6), 11945. https://doi.org/10.1029/jc090ic06p11945

Geyer, N. L., Huettel, M., & Wetz, M. S. (2018a). Phytoplankton Spatial Variability in the River-Dominated Estuary, Apalachicola Bay, Florida. *Estuaries and Coasts*, *41*(7), 2024–2038.

https://doi.org/10.1007/s12237-018-0402-y

Geyer, N. L., Huettel, M., & Wetz, M. S. (2018b). Phytoplankton Spatial Variability in the River-Dominated Estuary, Apalachicola Bay, Florida. *Estuaries and Coasts*, *41*(7), 2024–2038. https://doi.org/10.1007/s12237-018-0402-y

Geyer, W R. (1997). Influence of wind on dynamics and flushing of shallow estuaries. *Estuarine, Coastal and Shelf Science*, *44*(6), 713–722. https://doi.org/10.1006/ecss.1996.0140

Geyer, W Rockwell, & MacCready, P. (2014). The Estuarine Circulation. *Annual Review of Fluid Mechanics*, *46*(1), 175–197. https://doi.org/10.1146/annurev-fluid-010313-141302

Gomez, F. A., Lee, S.-K., Liu, Y., Hernandez Jr., F. J., M.-, & Karger, F. E., and Lamkin, J. T. (2018). Seasonal patterns in phytoplankton biomass across the northern and deep Gulf of Mexico: a numerical model study. *Biogeosciences*, *15*, 3561–3576. https://doi.org/https://doi.org/10.5194/bg-15-3561-2018

Grangeré, K., Lefebvre, S., Bacher, C., Cugier, P., & Ménesguen, A. (2010). Modelling the spatial heterogeneity of ecological processes in an intertidal estuarine bay: dynamic interactions between bivalves and phytoplankton. *Marine Ecology Progress Series*, *415*, 141–158. https://doi.org/10.3354/meps08659

Grifoll, M., Cerralbo, P., Guillén, J., Espino, M., Boye Hansen, L., & Sánchez-Arcilla, A. (2019). Characterization of bottom sediment

resuspension events observed in a micro-tidal bay. *Ocean Science*, *15*(2), 307–319. https://doi.org/10.5194/os-15-307-2019

Grifoll, M., Navarro, J., Pallares, E., Ràfols, L., Espino, M., & Palomares, A. (2016). Ocean-atmosphere-wave characterisation of a wind jet (Ebro shelf, nw mediterranean sea). *Nonlinear Processes in Geophysics*, *23*(3), 143–158. https://doi.org/10.5194/npg-23-143-2016

Haidvogel, D. B., Arango, H., Budgell, W. P., Cornuelle, B. D., Curchitser, E., Shchepetkin, A. F., Sherwood, C. R., Signell, R. P., Warner, J. C., & Wilkin, J. (2007). Ocean forecasting in terrain-following coordinates : Formulation and skill assessment of the Regional Ocean Modeling System. *Journal of Computational Physics*, 1–30. https://doi.org/10.1016/j.jcp.2007.06.016

Heinle, A., & Slawig, T. (2013). Internal dynamics of NPZD type ecosystem models. *Ecological Modelling*, *254*, 33–42. https://doi.org/10.1016/j.ecolmodel.2013.01.012

Hickey, B. M. and Banas, N. S. . (2003). Oceanography of the U.S. Pacific Northwest coastal ocean and estuaries with application to coastal ecology. *Estuaries*, *26*, 1010–1031. https://doi.org/https://doi.org/10.1007/BF02803360

Horsburgh, K. J., Hill, A. E., Brown, J., Fernand, L., Garvine, R. W., & Angelico, M. M. P. (2000). Seasonal evolution of the cold pool gyre in the western Irish Sea. *Progress in Oceanography*, *46*(1), 1–58. https://doi.org/10.1016/S0079-6611(99)00054-3

Ibàñez, C., Rodrigues-Capítulo, A. & Prat, N. (1995). The combined impacts of river regulation and eutrophication on the dynamics of the salt wedge and the ecology of the lower Ebro River. *The Ecological Basis for River Management*, *In: Harper*, *D.* & *Ferguson*, *A. (eds.). John Wiley & Sons, Chichester.*, 105–114.

Ibàñez, C., Canicio, A., Day, J. W., & Curcó, A. (1997). Morphologic development, relative sea level rise and sustainable management of water and sediment in the Ebre Delta, Spain. *Journal of Coastal Conservation*, *3*(1), 191–202. https://doi.org/10.1007/BF02908194

Jiang, L. and Xia, M. (2017). Wind effects on the spring phytoplankton dynamics in the middle reach of the Chesapeake Bay,. *Ecol. Model.*, *363*, 68–80. https://doi.org/https://doi.org/10.1016/j.ecolmodel.2017.08.026

Jiang, L. and Xia, M. (2018). Modeling investigation of the nutrient and phytoplankton variability in the Chesapeake Bay outflow plume. *Prog. Oceanogr.*, *162*, 290–302. https://doi.org/https://doi.org/10.1016/j.pocean.2018.03.004

Jiang, L., Gerkema, T., C. Kromkamp, J., Van Der Wal, D., Manuel Carrasco De La Cruz, P., & Soetaert, K. (2020). Drivers of the spatial phytoplankton gradient in estuarine-coastal systems: Generic implications of a case study in a Dutch tidal bay. *Biogeosciences*, *17*(16), 4135–4152. https://doi.org/10.5194/bg-17-4135-2020

Jou, S., Folch, A., Garcia-Orellana, J., Carreño, F. (2019). Using freely

available satellite thermal infrared data from Landsat 8 to identify groundwater discharge in coastal areas. *Geophysical Research Abstracts*, *21*, p1-1. 1p.

Lalli, C. M., & Parsons, T. R. (1993). *Biological oceanography: an introduction* (Elsevier Butterworth-Heinemann (Ed.); First publ). https://doi.org/10.1016/0022-0981(96)02604-4

Li, Y., & Li, M. (2011). Effects of winds on stratification and circulation in a partially mixed estuary. *Journal of Geophysical Research: Oceans*, *116*(12). https://doi.org/10.1029/2010JC006893

Llebot, C. (2010). *Interactions between physical forcing, water circulation and phytoplankton dynamics in a microtidal estuary*. PhD thesis. http://digital.csic.es/handle/10261/100958?locale=es

Llebot, C., Spitz, Y. H., Solé, J., & Estrada, M. (2010). The role of inorganic nutrients and dissolved organic phosphorus in the phytoplankton dynamics of a Mediterranean bay: A modeling study. *Journal of Marine Systems*, *83*(3–4), 192–209. https://doi.org/10.1016/j.jmarsys.2010.06.009

Llebot, C., Solé, J., Delgado, M., Fernández-Tejedor, M., Camp, J., & Estrada, M. (2011). Hydrographical forcing and phytoplankton variability in two semi-enclosed estuarine bays. *Journal of Marine Systems*, *86*(3–4), 69–86. https://doi.org/10.1016/j.jmarsys.2011.01.004

Llebot, C., Rueda, F. J., Solé, J., Artigas, M. L., Estrada, M., Spitz, Y.

H., Solé, J., & Estrada, M. (2014). Hydrodynamic states in a wind-driven microtidal estuary (Alfacs Bay). *Journal of Sea Research*, *85*(3–4), 263–276. https://doi.org/10.1016/j.seares.2013.05.010

Lohrenz SE, Fahnenstiel GL, Redalje DG, Lang GA, Chen X, D. M. (1997). Variations in primary production of northern Gulf of Mexico continental shelf waters linked to nutrient inputs from the Mississippi River. *Marine Ecology Progress Series*, *155*, 45–54. https://www.int-res.com/abstracts/meps/v155/p45-54/

Lopez, J., & Arté, P. (1973). Hidrografía y fitoplancton del puerto del Fangar (delta del Ebro). *Inv.Pesq.*, 17–56.

Loureiro, S., Garcés, E., Fernández-Tejedor, M., Vaqué, D., & Camp, J. (2009). Pseudo-nitzschia spp. (Bacillariophyceae) and dissolved organic matter (DOM) dynamics in the Ebro Delta (Alfacs Bay, NW Mediterranean Sea). *Estuarine, Coastal and Shelf Science*, *83*(4), 539–549. https://doi.org/10.1016/j.ecss.2009.04.029

Martin, M. A., Fram, J. P., and Stacey, M. T. (2007). Seasonal chlorophyll a fluxes between the coastal Pacific Ocean and San Francisco Bay. *Mar. Ecol.-Prog. Ser.*, *337*, 51–61. https://doi.org/https://doi.org/10.3354/meps337051

Masson, D., & Peña, A. (2009). Chlorophyll distribution in a temperate estuary: The Strait of Georgia and Juan de Fuca Strait. *Estuarine, Coastal and Shelf Science*, *82*(1), 19–28. https://doi.org/10.1016/j.ecss.2008.12.022

Miller, W. and Harding, L. W. (2007). Climate forcing of the spring bloom in Chesapeake Bay. *Mar. Ecol.-Prog. Ser.*, *331*, 11–22,. https://doi.org/https://doi.org/10.3354/meps331011

Mishra, S.; Mishra, D. R. (2012). Normalized Difference Chlorophyll Index: A Novel Model for Remote Estimation of Chlorophyll-a Concentration in Turbid Productive Waters. *Remote Sens. Environ.*, *117*, 394–406.

Morales-Blake, A. R. (2006). *Estudio Multitemporal de la clorofila superficial en el mar Mediterráneo Noroccidental, evaluada a partir de datos SeaWIFS: Septiembre de 1997 a agosto del 2004.* University de Barcelona, Barcelona.

Muñoz, I. (1990). *Limnología de la part baixa del riu ebre i els canals de reg: els factors fisico-quimics, el fitoplancton i els macroinvertebrats bentonics. Tesis para la postulación al grado de doctor. Departamento de Ecología. Facultad.* Facultad de Biología. Universidad de Barcelona.

Narváez, D. A., & Valle-Levinson, A. (2008). Transverse structure of wind-driven flow at the entrance to an estuary: Nansemond River. *Journal of Geophysical Research: Oceans*, *113*(9), 1–9. https://doi.org/10.1029/2008JC004770

Niedda, M., & Greppi, M. (2007). Tidal, seiche and wind dynamics in a small lagoon in the Mediterranean Sea. *Estuarine, Coastal and Shelf Science*, *74*(1–2), 21–30. https://doi.org/10.1016/J.ECSS.2007.03.022

Noble, M. A., Schroeder, W. W., Jr, W. J. W., Ryan, H. F., & Gelfenbaum, G. (1996). Subtidal circulation patterns in a shallow , highly stratified estuary : Mobile Bay , Alabama At higher discharge current variability uncouples from the. *Journal of Geophysical Research: Oceans*, *101*(96), 25,625-689,703.

Ochoa, V., Riva, C., Faria, M., López, M., Alda, D., Barceló, D., Fernandez, M., Roque, A., & Barata, C. (2012). Science of the Total Environment Are pesticide residues associated to rice production affecting oyster production in Delta del Ebro , NE Spain ? *Science of the Total Environment, The*, *437*, 209–218. https://doi.org/10.1016/j.scitotenv.2012.07.058

Perez, M. & Camp, J. (1986). *Distribución espacial y biomasa de las fanerógamas marinas de las bahías del delta del Ebro. 50*, 519–530.

Pinckney, J. L., Paerl, H. W., Harrington, M. B., & Howe, K. E. (1998). Annual cycles of phytoplankton community-structure and bloom dynamics in the Neuse River Estuary, North Carolina. *Marine Biology*, *131*(2), 371–381. https://doi.org/10.1007/s002270050330

Powell, T. M., Lewis, C. V. W., Curchitser, E. N., Haidvogel, D. B., Hermann, A. J., & Dobbins, E. L. (2006). Results from a three-dimensional, nested biological-physical model of the California Current System and comparisons with statistics from satellite imagery. *Journal of Geophysical Research: Oceans*, *111*(7), 1–14. https://doi.org/10.1029/2004JC002506

Ràfols, L., Grifoll, M., Jordà, G., Espino, M., Sairouní, A., & Bravo, M. (2017). Shelf Circulation Induced by an Orographic Wind Jet. *Journal of Geophysical Research: Oceans*, *122*(10), 8225–8245. https://doi.org/10.1002/2017JC012773

Ramón, M., Fernández, M., & Galimany, E. (2007a). Development of mussel (Mytilus galloprovincialis) seed from two different origins in a semi-enclosed Mediterranean Bay (N.E. Spain). *Aquaculture*, *264*(1–4),   148–159. https://doi.org/10.1016/j.aquaculture.2006.11.014

Ramón, M., Fernández, M., & Galimany, E. (2007b). Development of mussel (Mytilus galloprovincialis) seed from two different origins in a semi-enclosed Mediterranean Bay (N.E. Spain). *Aquaculture*, *264*(1–4),   148–159. https://doi.org/10.1016/j.aquaculture.2006.11.014

Reguera, B., Bravo, I., Mariño, J., Campos, M.J., Fraga, S., Carbonell, A. (1993). Trends in the occurrence of Dinophysis spp. in Galician coastal waters. *Toxic Phytoplankton Blooms in the Sea. Elsevier*, 559–564.

Rico, J. E. C. (2015). *Análisis de la variabilidad de la clorofila en la Bahía de Todos Santos a través de un modelo numérico físico-biológico*. Centro de Investigación Científica y de Educación Superior de Ensenada, Baja California.

Roque, A., Lopez-Joven, C., Lacuesta, B., Elandaloussi, L., Wagley, S., Furones, M. D., Ruiz-Zarzuela, I., de Blas, I., Rangdale, R., &

Gomez-Gil, B. (2009). Detection and Identification of tdh- and trh-Positive Vibrio parahaemolyticus Strains from Four Species of Cultured Bivalve Molluscs on the Spanish Mediterranean Coast. *Applied and Environmental Microbiology*, *75*(23), 7574 LP – 7577. https://doi.org/10.1128/AEM.00772-09

Sanay, R., & Valle-Levinson, A. (2005). Wind-Induced Circulation in Semienclosed Homogeneous, Rotating Basins. *Journal of Physical Oceanography*, *35*(12), 2520–2531. https://doi.org/10.1175/JPO2831.1

Sarangi, R. K., Nayak, S., & Panigraphy, R. C. (2008). Monthly variability of chlorophyll and associated physical parameters in the southwest Bay of Bengal water using remote sensing data. *Indian Journal of Marine Sciences*, *37*(3), 256–266.

Scully, M. E., Friedrichs, C., & Brubaker, J. (2005). Control of estuarine stratification and mixing by wind-induced straining of the estuarine density field. *Estuaries*, *28*(3), 321–326. https://doi.org/10.1007/BF02693915

Shchepetkin, A. F., & McWilliams, J. C. (2005). The regional oceanic modeling system (ROMS): A split-explicit, free-surface, topography-following-coordinate oceanic model. *Ocean Modelling*, *9*(4), 347–404. https://doi.org/10.1016/j.ocemod.2004.08.002

Shintani, T., De La Fuente, A., Niño, Y., & Imberger, J. (2010). Generalizations of the wedderburn number: Parameterizing

upwelling in stratified lakes. *Limnology and Oceanography*, *55*(3), 1377–1389. https://doi.org/10.4319/lo.2010.55.3.1377

Simpson, J. H., & Bowers, D. (1981). Models of stratification and frontal movement in shelf seas. *Deep Sea Research Part A. Oceanographic Research Papers*, *28*(7), 727–738. https://doi.org/10.1016/0198-0149(81)90132-1

Soetaert, K., Middelburg, J. J., Heip, C., Meire, P., V. D., & S., and Maris, T. (2006). Long-term change in dissolved inorganic nutrients in the heterotrophic Scheldt estuary (Belgium, The Netherlands). *Limnol. Oceanogr.*, *51*, 409–423. https://doi.org/https://doi.org/10.4319/lo.2006.51.1_part_2.0409

Sondergaard, M., Kristensen, P., & Jeppesen, E. (1992). Phosphorus release from resuspended sediment in the shallow and wind-exposed Lake Arresø, Denmark. *Hydrobiologia*, *228*(1), 91–99. https://doi.org/10.1007/BF00006480

Soriano-González, J., Angelats, E., Fernández-Tejedor, M., Diogene, J., & Alcaraz, C. (2019). First results of phytoplankton spatial dynamics in two NW-Mediterranean bays from chlorophyll-A estimates using Sentinel 2: Potential implications for aquaculture. *Remote Sensing*, *11*(15). https://doi.org/10.3390/rs11151756

Srichandan, S., Kim, J. Y., Kumar, A., Mishra, D. R., B., & P., Muduli, P. R., Pattnaik, A. K., and Rastogi, G. (2015). Interannual and cyclone-driven variability in phytoplankton communities of a tropical coastal lagoon. *Mar. Pollut. Bull.*, *101*, 39–52.

https://doi.org/https://doi.org/10.1016/j.marpolbul.2015.11.030

Stow, C. A., Jolliff, J., McGillicuddy Jr., D. J., Doney, S. C., Allen, J. I., Friedrichs, M. A., & M., Rose, K. A., y Walhead, P. (2009). Skill assessment for coupled biological/physical models of marine systems. *Journal of Marine Systems*, *76*, 4–15.

Strayer, D. L., Pace, M. L., Caraco, N. F., Cole, J. J., and Findlay, S. E. (2008). Hydrology and grazing jointly control a large-river food web. *Ecology*, *89*, 12–18. https://doi.org/https://doi.org/10.1890/07-0979.1

Valle-Levinson, A. (2012). Classification of Estuarine Circulation. In *Treatise on Estuarine and Coastal Science* (Vol. 1, Issue May). Elsevier Inc. https://doi.org/10.1016/B978-0-12-374711-2.00106-6

Valle-Levinson, A., Delgado, J. A., & Atkinson, L. P. (2001). Reversing water exchange patterns at the entrance to a semiarid coastal lagoon. *Estuarine, Coastal and Shelf Science*, *53*(6), 825–838. https://doi.org/10.1006/ecss.2000.0813

Valle-levinson, A., Wong, K. C., & Bosley, K. T. (2001). Observations of the wind-induced exchange at the entrance to Chesapeake Bay. *Journal of Marine Research*, *59*(1978), 391–416. https://doi.org/10.1357/002224001762842253

Varas Schiavi, M. (2012). *Ecología de la bahía El Fangar (delta del Ebro): Factores físico-químicos , biológicos , sus interacciones y propuesta de un modelo*. PhD thesis. 294.

http://www.tdx.cat/bitstream/handle/10803/83339/MVS_TESIS.pdf
?sequence=1

Wan, Y., Qiu, C., Doering, P., Ashton, M., Sun, D., & Coley, T. (2013).
Modeling residence time with a three-dimensional hydrodynamic
model: Linkage with chlorophyll a in a subtropical estuary.
Ecological   Modelling,   *268*,   93–102.
https://doi.org/10.1016/j.ecolmodel.2013.08.008

Warner, J. C., Geyer, W. R., and Lerczak, J. A. . (2005). Numerical
modeling of an estuary: A comprehensive skill assessment.
Journal of Geophysical Research: Oceans, *110*(C05001).
https://doi.org/10.1029/2004JC002691,

Weaver, R. J., Johnson, J. E., & Ridler, M. (2016). Wind-Driven
Circulation in a Shallow Microtidal Estuary: The Indian River
Lagoon. *Journal of Coastal Research*, *322*, 1333–1343.
https://doi.org/10.2112/jcoastres-d-15-00046.1

Welschmeyer, N. A. (1994). Fluorometric analysis of chlorophyll a in the
presence of chlorophyll b and pheopigments. *Limnology and
Oceanography*,   *39*(8),   1985–1992.
https://doi.org/10.4319/lo.1994.39.8.1985

Wong, K.-C., & Valle-Levinson, A. (2002). On the relative importance of
the remote and local wind effects on the subtidal exchange at the
entrance to the Chesapeake Bay. *Journal of Marine Research*,
60(3), 477–498. https://doi.org/10.1357/002224002762231188

Xie, X., & Li, M. (2018). Effects of Wind Straining on Estuarine
      Stratification: A Combined Observational and Modeling Study.
      Journal of Geophysical Research: Oceans, *123*(4), 2363–2380.
      https://doi.org/10.1002/2017JC013470